UPPSALA
UNIVERSITET

UPTEC F 23047
Examensarbete 30 hp
Juni 2023

Measurements, Estimations and Calibration with a Fully Digital Array

Oscar Magnér

Civilingenjörsprogrammet i teknisk fysik

UPPSALA UNIVERSITET

Measurements, Estimations and Calibration with a Fully Digital Array

Oscar Magnér

Abstract

In modern digital communication, transmission and reception of information through electromagnetic signals requires digital devices that can process high data rates accurately despite being located in information heavy environments. One type of antenna receiver is the digital antenna array, which can steer its lobes electronically to increase or decrease sensitivity in specific directions. A rather recently developed system is the Wideband Digital Array Receiver, developed at Saab Surveillance in Järfälla and referred to as WiDAR. The implementations and possibilities of WiDAR are broad, but no matter its future applications, calibration is an essential feature to ensure truthful reception of data. Any type of electronic system risks errors due to hardware imperfections. The aim of this thesis is to explore and reduce these errors. Measurements with WiDAR were performed in a manner such that some of the intercepted signals were transmitted from a far away located FM and TV-mast. The data was then used to retrieve weights by calculating their relative transfer function, which were applied to calibrate all channels in the antenna array towards a chosen reference channel. These weights could then be on any accumulated set of data measured by WiDAR with hopes to compensate errors in both phase and magnitude. The results show that reducing errors this way was possible, working slightly better when calibrating phase than calibrating magnitude. If more advanced calibration is deemed necessary, further measurements could be performed to investigate where errors or variations occur by isolating different parts of the system. The calibration method used could be further developed by adding an online calibration procedure, meaning relative transfer functions are calculated in real time when performing measurements.

Teknisk-naturvetenskapliga fakulteten

Uppsala universitet, Utgivningsort Uppsala

Handledare: Johan Malmström, Björn Petersson Ämnesgranskare: Mikael Sternad

Examinator: Tomas Nyberg

Sammanfattning

I modern digital kommunikation kräver sändning och mottagning av information genom elektromagnetiska signaler att digitala system kan processera höga datahastigher trots att de befinner sig i informationstrafikerade miljöer. En slags antennmottagare är den digitala antenn gruppantennen, som elektroniskt kan styra sina lober för att öka eller minska känsligheten i en viss riktining. Ett ganska nyligen utvecklat system är Wideband Digital Array Receiver, utvecklad av Saab Surveillance i Järfälla och kallas WiDAR. Implementeringar och möjligheter hos WiDAR är breda, men oavsett dess framtida tillämpningar, är kalibrering en viktig del för att säkerställa sanningsenlig mottagning av data. Alla typer av elektroniska system riskerar fel på grund av hårdvarufel. Målet av denna avhandling är att utforska och minska dessa fel. Mätningar med WiDAR utfördes på ett sätt så att några av de mottagna signaler var sända från en långt bort belägen FM- och TV-mast. Den datan användes sedan för att ta fram vikter genom att beräkna deras relativa transferfunktion, som användes för att kalibrera alla kanaler i gruppantennen mot en vald referenskanal. Dessa vikter kunde då användas på någon uppsättning data som mätts av WiDAR med förhoppningar om att kompensera fel i både fas och magnitud. Resultaten visar att reducera fel på detta sätt var möjligt, och fungerade något bättre för kalibrering av fas än kalibrering av magnitud. Om mer avancerad kalibrering bedöms vara nödvändig kan ytterligare mätningar utföras för att undersöka var fel eller variationer uppstår genom att isolera olika delar av systemet. Den använda kalibreringsmetoden skulle kunna vidareutvecklas genom att lägga till en onlinekalibreringsprocedur, vilket betyder att relativa överföringsfunktioner beräknas i realtid när mätningar utförs.

Acknowledgements

I would first like to express my gratitude to Mats Järgenstedt for giving me the opportunity to write my thesis at Saab and for a warm welcome to the company. Major thanks to my supervisor Mikael Sternad at Uppsala university, and my supervisors at Saab, Johan Malmström and Björn Petersson, who were supportive and guided me with their knowledge in areas where my experience was lacking. Big thanks to the personnel working with WiDAR, who were very helpful during the experiments or whenever I had questions regarding the prototype.

I want to express a special thanks to family and friends. My family for always being supportive during these five years studying at Uppsala University and my friends for making it such a lovely time, both on and off campus. My friend Alex Söderlund in particular who also wrote his thesis at Saab, and made the days even more pleasant this final semester.

Contents

Abbreviations

AAF	Anti-Aliasing Filter
ADC	Analogue-to-Digital Converter
CT	Continuous-Time
CW	Continuous Wave
dBFS	Decibels of Full Scale
DAA	Digital Array Antenna
DDC	Digital Down-Converter
DFT	Discrete Fourier Transform
DOA	Direction of Arrival
DT	Discrete-Time
DVB-T	Digital Video Broadcasting - Terrestrial
EM	Electromagnetic
FEM	Front-end module
FFT	Fast Fourier Transform
LNA	Low Noise Amplifier
MUSIC	Multiple Signal Classification
RMSE	Root-mean-square-error
RF	Radio frequency
SNR	Signal-to-Noise Ratio
SINR	Signal to Interference Plus Noise Ratio
PCL	Passive Coherent Location
ULA	Uniform Linear Array
UPA	Uniform Planar Array
WiDAR	Wideband Digital Array Receiver

List of Figures

List of Tables

1 Introduction

Since the discovery of radio waves and their possible use as a means for wireless communication, antenna theory and design has been widely studied fields. From the first antennas built by Heinrich Hertz in 1888 to today's antennas built in the early 21st century, much progress has been made. While the layman perhaps thinks of a parabolic design when the word antenna is mentioned, there are many other different antennas with different features and uses. One type of antenna, the array antenna, contains multiple connected antenna elements in an array which work together as one. The set of multiple antenna elements can achieve a higher gain than an antenna with only one element, which often is an important property in various areas. Many versions of array antennas exist and depending on the design they can also cancel interference from specific directions, increase the sensitivity in a specific direction, determine the direction of arrival of signals and increase the communication reliability by maximising SINR.

Just as many other fields within electronics, the idea to solve problems regarding antennas by using computers emerged. In the 1960s the first so-called digital antenna array was developed. The main difference between the digital and the regular antenna array is that all element channels are converted to digital form before being processed. Meaning multiple digitised bit streams need to be processed, instead of only one. This is a feature that adds freedom and possibility when it comes to the processing of the signals, but also introduces new challenges due to hardware imperfections.

The purpose of this report and the corresponding work is to characterise what kind of errors may occur in a fully digital array and to study methods for reducing the impacts of these errors through calibration. The fully digital array used in this project is Saab's recently developed prototype of a wideband multi-channel digital array. This prototype, which is referred to as WiDAR at Saab, samples RF signals at 2 GHz and can store data without reduction. Imperfections in the hardware of the WiDAR will most likely create variations in the individual channels. These imperfections and their variations can to some extent be estimated and compensated for through calibration. Channel imperfections and how they are related to the estimation of physical quantities, such as the direction of arrival, is a thoroughly studied subject and in a previous master thesis project this relation has been simulated and explored theoretically. In this project however, the objective is to calibrate the WiDAR and confirm the calibration's level of success experimentally by comparing estimates of a physical quantity, like direction of arrival, with and without the calibration process.

2 Theory

2.1 Receiver Array Antenna

2.1.1 Definition and distinction

The definition of an antenna according to Webster's Dictionary is "a usually metallic device (as a rod or wire) for radiating or receiving radio waves". Another description could be that an antenna is a structure that transitions radio waves from free-space to a physical signal in a device, or the other way around.

To avoid confusion or misinterpretation, it is important to define a distinction between antennas and receivers. A receiver is the aforementioned device that is connected to the antenna via any type of transmission line, which receives the physical signal that the antenna converts from free-space. The receiver's task is then to process this physical signal and extract the embedded information. The term receiver antenna implies the entire system, from antenna to receiver. [3]

2.1.2 RF front-end and digital receivers

There are many different antenna receiver systems with different attributes and purposes, but some features and functions are very likely to be found in most modern devices. The WiDAR prototype that will be used is a digital receiver, and it is therefor useful to understand how a digital receiver differentiates from an analog. One common type of radio receiver is the so called heterodyne receiver, a block diagram of which is shown in Figure 1.

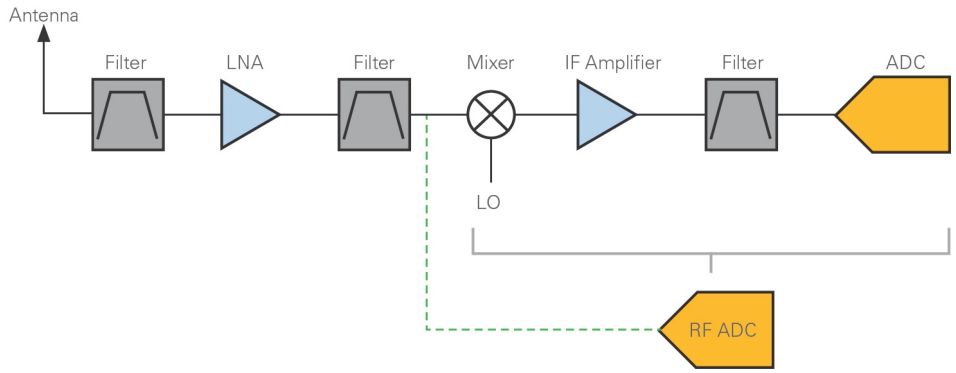

Figure 1 Example of a block diagram for a typical heterodyne receiver [1].

The signal received at the antenna first goes through a filter of some sort, most likely a band-pass filter (BPF), with the purpose of reducing the image response which may interfere with the desired signal. The filtered signal is put through an RF amplifier which amplifies the desired signal. Many systems use a low-noise amplifier (LNA) to make sure desirable signals with rather low amplitude do not get categorised as noise and filtered away later. Next step of the process is to mix the now amplified signal with a different known signal of a certain frequency, often referred to as the carrier frequency, created by a local oscillator (LO). This is done in order to convert the signal to the intermediate frequency (IF) region which is a lower frequency that traditionally has been more convenient to process than the RF.

The steps described so far constitutes the so called RF front-end which is the components up until the LO in Figure 1. The components following the RF front-end aim to further increase the frequency selectivity and to recover the message from the original signal through demodulation. As technology has improved and become cheaper, the possibility to refrain from IF-conversion has emerged in modern devices. This is becoming more common in digital receivers where demodulation occurs directly on the RF signal once it has been sampled and digitised by an Analogue-to-Digital converter (ADC). This is the case for the WiDAR and will be further explained in Section 2.4. In Figure 2 a direct RF sampling receiver is shown, which refrain from the IF-conversion steps and thereby reduces the design cost. Much of the processing and filtering can instead be done digitally.

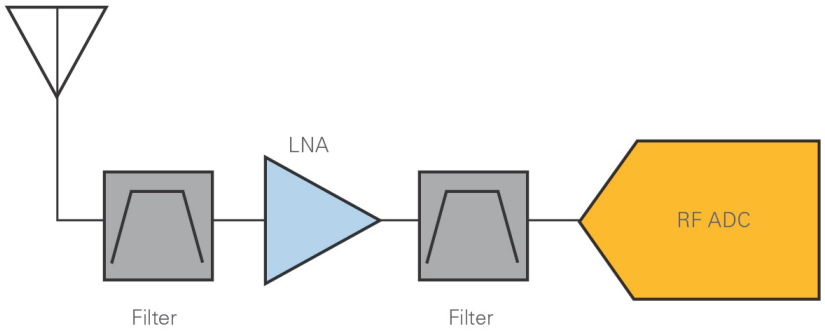

Figure 2 Example of a block diagram for a direct sampling heterodyne receiver [1].

2.1.3 Phased arrays and beamforming

It is possible and in various cases useful to mount more than a single antenna onto a receiving or transmitting radio system. This means that multiple antenna elements are

installed in a desirable geometric constellation, each connected to the receiver. Such a constellation is often referred to as a phased array or phased antenna system. A receiving antenna with a phased array takes advantage of the radiation patterns intercepted at each antenna element. With data regarding timing and phase from the intercepted signal, each element channel may be electronically manipulated to achieve constructive or destructive interference of the received signals. By performing this technique, it is possible to mimic the effect of physically steering the antenna system in a desired direction to increase the signal strength from said direction, but without actually moving the antenna and its elements at all.

This method of taking advantage of constructive and destructive interference is called beamforming, since the result of the signal gain as a function of space takes the shape of a beam pointing towards a certain direction. This beam is often referred to as the main lobe and the method and the principle of the technique can be used for transmission as well as reception. A visualisation of a system implementing beamforming is shown in Figure 3.

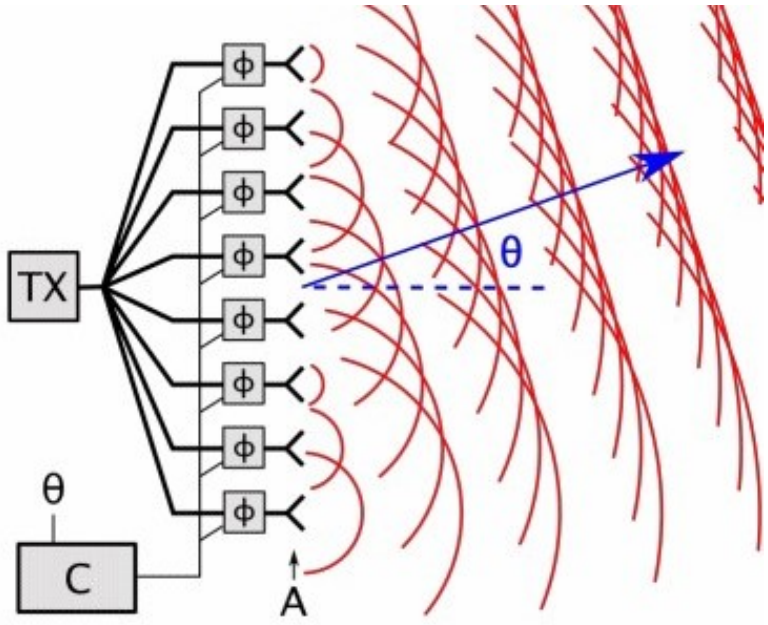

Figure 3 Phased array antenna system with a computer C which applies beamforming to steer the main lobe in the direction (θ) of the blue arrow [2]. Note that the figure illustrates a transmitting antenna system, TX, but the principle applies to receiving arrays antennas as well.

2.1.4 Fully digital array

An antenna array that is fully digital refers to the idea that every antenna element in the array is digitally converted into a individual bit stream. In other words, each antenna element has its own corresponding receiver or transmitter system. Schematics for an analogue array and a fully digital array is shown in Figure (4a) and (4b) respectively.

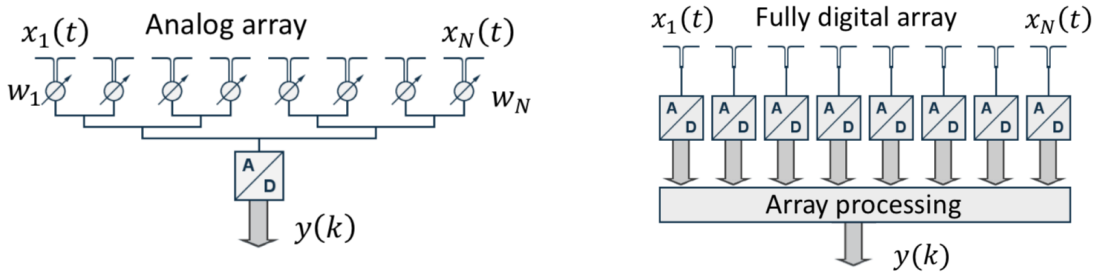

(a) **(b)**

Figure 4 An antenna array can be either analogue (a), where signals from individual elements are added before they are converted to digital form, or fully digital (b), where the signals from each individual element are converted to digital form before they are processed

They key difference between these two systems is that the access to the bit streams of each antenna element, which is provided by the fully digital array, yields new degrees of freedom when it comes to signal processing of the array, such as beamforming and attenuating interfering signals.

However, the catch with the fully digital system, besides high hardware requirements, is that hardware imperfections most likely will give notable variations between the individual channels which may decrease performance and certitude. These variations can to some extent be compensated for in a calibration procedure, which is covered in Section 2.3. This does not mean that similar variations do not exist in analogue systems, but they can not be amended for in the same way as the digital system can, since they lack multiple bit streams.

2.2 Introduction to Signal Processing

The signals intercepted by an antenna can be expressed as carriers of information with physical properties that change with time. These signals however, are most likely composed of many different frequencies. Jean-Baptiste Joseph Fourier showed, in *The Analytical Theory of Heat* [4] published in the year 1822 (translated 1878), that any arbitrary signal can be expressed as a series of sine and cosine functions, which was named Fourier Series.

In signal processing, it is often desirable to express signals in the frequency domain instead of the time domain and to decompose signals of multiple frequencies to better understand the properties of the signal. This was discovered to be possible by using an integral on the Fourier Series which is a mathematical tool now known as the Fourier transform. [5]

2.2.1 Fourier transform

There were no computers 200 years ago, and Fourier Transforming more complicated signals by hand were incredibly time consuming calculations. With the advanced computing devices available today, this is no longer much of a problem. The Discrete Fourier Transform (DFT) and the Fast Fourier Transform (FFT), which is an efficient version of the DFT, are common algorithms within engineering.

The Fourier Transform is used and implemented in plenty of areas. To to put it simple, the Discrete Fourier Transform is the algorithm that establishes a relationship between the time domain and the frequency domain of a finite length discrete data set. The Fast Fourier transform (FFT) is a version of the DFT that was developed in the 1960's and generally credited to J. W. Cooley and J. W. Tukey . It heavily reduces the computing complexity and time by limiting the amount of calculations needed from N^2 to $N \log N$, which is especially significant the larger the data set [6] [7].

The amount of data captured and recorded per time unit by the WiDAR is quite large, which is further mentioned in section 2.4, and the algorithm used when processing the data in this project will therefore be the FFT.

The Fourier Transform of a continuous-time infinite-length function $x(t)$ is defined by

$$F\{x(t)\} = \int_{t=0}^{\infty} x(t)e^{-j\omega t}dt, \tag{1}$$

where t is time, ω is the angular frequency and j is the imaginary unit. The resulting continuous $F\{x(t)\}$ is often denoted $X(f)$ and it contains information regarding the power at each frequency embedded in the signal.

The signals encountered and measured by a fully digital array instrument will be continuous in time. When capturing the data corresponding to theses signals, the signals ultimately have to be made discrete and finite. Fourier transforming a data set of uniformly spaced samples of continuous functions is often done using the discrete-time Fourier transform (DTFT)

$$X(\omega) = \sum_{n=\infty}^{\infty} x(n)e^{-j\omega n}. \tag{2}$$

In the DTFT the continuous integral in (1) is replaced with a discrete sum, however in equation (2) the sum is infinite, and most sets of data are finite. With a sampled set of finite data, $[x_n] = x_0, x_1, ..., x_{N-1}$, containing a sequence of N complex numbers, the discrete Fourier transform (DFT) transforms $[x_n]$ into another equally large sequence of complex numbers $[X_k] = X_0, X_1, ..., X_{N-1}$. This DFT sequence X_k is defined as,

$$X_k = \sum_{n=0}^{N-1} x(n)e^{-\frac{j2\pi}{N}kn}. \tag{3}$$

2.2.2 Sampling

A sample is a single piece of digital data and often large amounts of points of data are necessary for thorough analysis, regardless of field or application. In signal processing, the process of gathering many data points of some signal by measuring instantaneous values of the desired data is called sampling. In order to store data from a continuous analogue signal digitally, the physical values need to be represented by bits of ones and zeros. This is performed by components called Analogue-to-Digital converter (ADC) and the process is sometimes referred to as digitising, where the analogue signal is discretised into a limited number of data points. Sampling can therefore be defined as, ”the process of measuring the instantaneous values of continuous-time signal in a discrete form”. [8].

Since the signal has to be represented with a finite number of bits, a process called quantisation takes place in the sampling process. The continuous amplitude values need to be rounded to a discrete quantised value for each sample. The resolution of the quantised signal depend on the amount of quantisation levels, or the number of available bits. This digitised signal’s waveform is sometimes referred to as a staircase waveform, since it takes the shape of a staircase that stutters along the continuous wave when compared to it. Both quantisation and sampling will inevitably never capture all of the information regarding the original signal. However, increasing the number of quantisation levels and

sampling frequency will reduce the loss of information, perhaps to such an extent that the quantised signal may be good enough to serve its intended purpose. [9]

The rate of which the data is sampled called sampling frequency, f_s, is important to bring sufficient resolution to the sampled data and to neither lose or over-lap crucial information regarding the signal. According to the Nyquist-Shannon sampling theorem, any signal that is sampled with a frequency greater than twice that of the highest frequency component of the signal, f_{max}, can be perfectly recovered or reconstructed. Consequently, to guarantee a perfect reconstruction of a signal, the band limit, B_{limit} must be less than half the sampling frequency f_s.

$$f_{Nyquist} = 2f_{max} \qquad , \qquad f_s > f_{Nyquist} \qquad , \qquad 2B_{limit} < f_s \tag{4}$$

The frequency that is twice the maximum frequency component, f_{max} is called the Nyquist frequency, $f_{Nyquist}$ or folding frequency and if the signal is sampled with an insufficient sampling frequency, one that is equal to or lower than the Nyquist frequency, a phenomena called aliasing may occur. [8] [10]

2.2.3 Aliasing

Aliasing may present itself when a signal is reconstructed after its been sampled with a sampling frequency below the Nyquist frequency, The reconstructed signal then contains additional frequencies that were unprecedented in the original signal. A common method to prevent aliasing, other than simply guaranteeing requirements in (4) are met, is to install a anti-aliasing filter (AAF) before the ADC or sampler. The ideal purpose of this filter would be to cut off all frequencies equal and larger than the Nyquist frequency. But in practice most AAFs will not exclude distortion and aliasing entirely, which makes oversampling a common practice. Oversampling simply means sampling the signals of interest with a frequency that is higher than what would be theoretically required to ensure perfect reconstruction. [11]

2.2.4 Jitter

Another phenomena called jitter may impact the trueness of a reconstructed signal. The ADC's sampling points are steered by a clock whose signal ideally would be perfectly periodic, but which may experience deviation from this periodicity. This deviation in the clock signal leads to a displacement of the sampling point which in turn leads to an untrue value in terms of amplitude of that sampling point. The effects of jitter becomes increasingly impactful the higher the frequency of the sampled signal, since the amplitude of a higher frequency changes faster than the amplitude of a lower frequency.

2.2.5 Power and noise

Due to the often times large difference in signal strength between signals in time and frequency, logarithmic values are commonly used when visually presenting data of received signals. Known as the decibel scale with unit dB, values in sets of data differing with several orders of magnitude may be represented in graphs without causing it to look stretched. For example a value ten times larger than another is 10 dB and a magnitude difference of 100 is represented by a difference of 20 dB.

When using the dB scale it is important to understand if it is desirable to express data to a physical unit like power in watts, a reference is needed since dB is a measure of relative power. In signal processing that reference is commonly milliwatts and the formula for signal power in dBm is

$$P_{dBm} = 10\log_{10}(\frac{P}{1\text{mW}}), \tag{5}$$

where P is the power of the signal.

Another unit of measurement known is decibels of full scale, dBFS, which is commonly used when expressing amplitude values in digital systems that have a limited maximum peak. The formula to express a digitsed, or quantised, value, Q_{value}, in dBFS is given by

$$Q_{dBFS} = 20\log_{10}\frac{|Q_{value}|}{Q_{max}}, \tag{6}$$

where Q_{max} is the maximum quantised value, which is 2^{13} = 8192 for WiDAR, where the 14:th bit is sign bit. The sampled signal has a maximum digital value, which 0 dBFS corresponds to. A dBFS value of -6 therefore equals a value half the maximum level.

An important distinction to make between equations (5) and (6) is the multiplication of the factor of either 10 or 20. This depends on if the quantity linear or quadratic, such as voltage (V) and power (P) for example [12]. This is because

$$10\log_{10}\left(\frac{P_2}{P_1}\right) = 10\log_{10}\left(\frac{V_2}{V_1}\right)^2 = 20\log_{10}\left(\frac{V_2}{V_1}\right). \tag{7}$$

2.3 Calibration and errors

2.3.1 Calibration

Calibration is a term often used within electronics, or any other kind of field requiring measurements of certain systems. No measurement of a physical quantity can be said to be perfectly true. Errors in measurement systems or techniques are ever present and can only be narrowed down to a degree of certainty within an interval. Performing a calibration is often a repetitive process where the system or chain of systems being calibrated first need to be characterised. Characterisation can be described as the act of experimentally determining the so called transfer function of a given instrument or transducer.

2.3.2 Transfer function

The transfer function is as a way of expressing the ratio between a system's output versus its input. When the system has been characterised, an adjustment can be performed to tune the instruments so that the output is more in line with reality. The calibration procedure is the back and forth cycle of characterisation and adjustment to iteratively increase accuracy of the desired measurements.

The transfer function used in calibration is a way of representing the relationship between the input and the output of a system. The function is a mathematical model which captures the linear time-invariant dynamics of the system. Describing a system mathematically can be done in a number of ways and it is often helpful in order to systematically simulate, design or analyse a physical system. There are a couple of reasons it is beneficial to use the transfer function as a mathematical description of a system over other mathematical models. One of the main reasons is the finesse and simplicity of the model, even when systems get increasingly complicated. Describing systems with differential equations for example can require a lot of computing power to solve if they are rather complicated, especially when integrating multiple such systems. Converting the description of these systems using their transfer functions and combining these is forgiving in comparison.

In order to express the transfer function of a system, the conventional procedure is to first use the Laplace Transform to convert a real variable function to a complex variable function. The Laplace Transform in (8) transforms differential equations into algebraic equations where, most commonly, the real variable is time, denoted t, which is converted to the complex so called frequency domain or s-domain, denoted s.

$$\mathscr{L}\{x(t)\} = \int_{t=0}^{\infty} x(t)e^{-st}dt. \tag{8}$$

Once the function $x(t)$ has been transformed, the alternate notation $X(s)$ is common instead of $\mathscr{L}\{x(t)\}$, where $s = \sigma + j\omega$.

Now let the output and the input of a given system be denoted $y(t)$ and $u(t)$ respectively. Performing the Laplace transform from (8) on the functions for the input and output yields

$$\begin{aligned} y(t) &\rightarrow Y(s) \\ u(t) &\rightarrow U(s), \end{aligned} \tag{9}$$

and the transfer function of the system is then given by

$$G(s) = \frac{Y(s)}{U(s)}, \tag{10}$$

where $G(s)$ is the transfer function given by the ratio of the output $Y(s)$ and the input $U(s)$. [13]

Comparing (1) and (8) it can be seen that the Fourier Transform is defined as the Laplace Transform when $\sigma = 0$. Meaning the system is in steady state. In signal processing a system's steady state response is often of interest, rather than characteristics or issues caused by instability. This means the transfer function for these systems can be expressed and determined using the the Fourier Transform.

2.3.3 Potential errors

The errors that may present themselves in the data gathered through a receiving antenna system is ultimately a variation or offset in both amplitude and phase. There are plenty of contributors to these variations, all the way from the system where the signal is generated to the resolution of the FFT. These variations may be a function of time, frequency, temperature and environment for example.

Since the main interest in this thesis work is to find and amend the variations caused by imperfections in the system's hardware, it is important to mitigate variations or errors caused elsewhere. One example of mitigating such errors is by creating a environmental setting when measuring which limits the amount of signal reflections intercepted by the receiving antenna. It is assumed that while phenomenons such as aliasing and jitter will exist, their impact will be minuscule compared to the effect of imperfect hardware and measurement settings.

2.4 WiDAR - Wideband digital array receiver

Saab's developed WiDAR prototype is a receiving antenna system with the intent of discovering the possibilities of a branch within surveillance known as Passive radar. Figure 5 is a simplified overview of the entire WiDAR system.

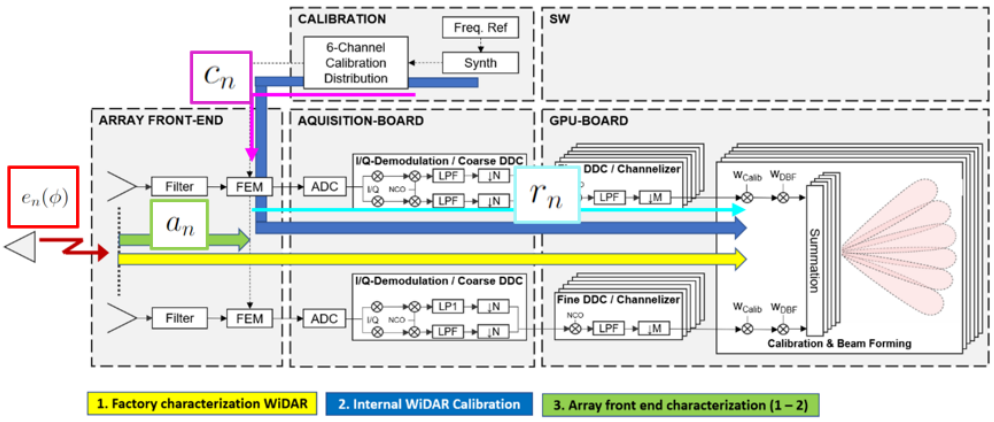

Figure 5 Block diagram overview of the WiDAR system

2.4.1 Aperture

The antenna's aperture is in contact with the RF environment and intercepts the signals. The WiDAR prototype consists of 115 antenna elements which are mounted on a metal plate with dimensions 800x500x500mm. The antennae are tapered slot antennas, also known as Vivaldi antennas, 60 of which are polarised horizontally and 55 vertically. Orthogonally arranged metal plates allow interception of polarised signals in both directions of the plane, but not simultaneously. One advantageous feature essential of the Vivaldi antennae is their broad frequency range, which is quite an essential feature for the purposes and applications of WiDAR. The ones used in the WiDAR prototype are more than capable of receiving frequencies from 450 MHz to 2200 MHz, meaning signals on the DVB-T, LRAM and Telecom band can be intercepted. The same cannot be said regarding the broadness of the band for the components following the aperture but for this prototype a broader band than the current is unnecessary since the signals of interest are within this band. If further applications of WiDAR technology requires an even broader bandwidth, the Front-End-Module (FEM) and filters will have to be replaced.

2.4.2 RF front-end module (FEM)

The FEM part of the system refers to the radio frequency front end module which is the generic term for every piece of circuitry between the antenna and the digitisation stage

where the signal is sampled. In the WiDAR this down conversion may be done digitally instead of analogically using mixers, as previously explained in Figure 1.

But before the down conversion the signal is put through one of two band-pass filters, which can be altered between manually using a python script. The frequency range of the two filters are 450-950 MHz and 1080-1900 MHz, one of which can be active at a time. The filters are designed on boards with four filters, each with its own channel connected to one of the antenna elements.

When only the signal contents of the desired frequency band remain, each channel is amplified separately. Once again each board contains four channels and thus also four amplifiers, which have been developed in-house. The amplifier gain is controlled manually and the isolation between each channel is high, at least 60 dB. To each board and channel in the system, a calibration signal may be injected to redress any error or variation.

2.4.3 Analogue-to-Digital Converter (ADC)

The ADC transforms continuous analogue signals into discrete digital signals. This is done by sampling the signal with a certain frequency and quantizing the signals real value to a digital number representing the magnitude of the value. The sampling frequency of the WiDAR is 2 GHz and each sample has the resolution of 14 bits, resulting in $2^{14} = 16384$ different values of digitised data. The length and size of each capture is controllable but with the default settings a file corresponding to 10 ms of data and each channel containing 20 000 000 samples was stored.

Since the ADCs on the boards are independent of one another, they have to be synchronised in order to not experience the similar effects as caused by the previously described phenomena known as jitter. This is done with a common clock, resulting in all samples over all channels being synchronised in time.

3 Method

3.1 Objective and assumptions

Before calibrating the WiDAR, instructions were given that the system may be thought to be divided into two parts; the antenna array and the RF-network. The shape of the beam in the beamforming will be affected by the configuration of both parts, but in this work the antenna array is assumed to be ideal, at least to begin with. In this case, it means that the calibration only covers the imperfect variations in the RF-system and not the imperfections that most likely exist in the antenna array. Further, this implies that any angle-dependent variations are excluded from the calibration and any occurring variations in phase and amplitude as a function of angle is assumed to be the responsibility of the lobe-forming algorithms.

Additional assumptions were made regarding the hardware to further frame the parameters of the work. The antenna array, the succeeding passive filter and the calibration distribution network are assumed to be fairly stable over time and temperature and can therefor most likely be characterised with just one time measurement. It should be noted that the accuracy of the characterisation may be reduced if the antenna or components of the RF-network is disassembled or adjusted after characterisation. What may vary with time, temperature and restarts however is the part of the RF-network that contains amplifiers and ADCs. This makes up the active part of the RF receiver chain and will need to be calibrated with online measurements to adjust for these variations.

The calibration will correct errors in amplitude and phase for a selected down converted frequency. It is expected that the performance of the calibration is degraded for frequencies other than the selected. The transfer function of the RF-channels relative to one another has to be determined. In other words the relative amplitude and phase-shift. Calibration measurement levels and correction factors are assumed to be independent of signal amplitude, meaning in the linear region.

3.2 Calibration methods

Two methods for calibrating the system were suggested, one slightly more advanced than the other. The methods are briefly described before being thoroughly expounded. Figure 6 illustrating the parameters and their definitions are listed below.

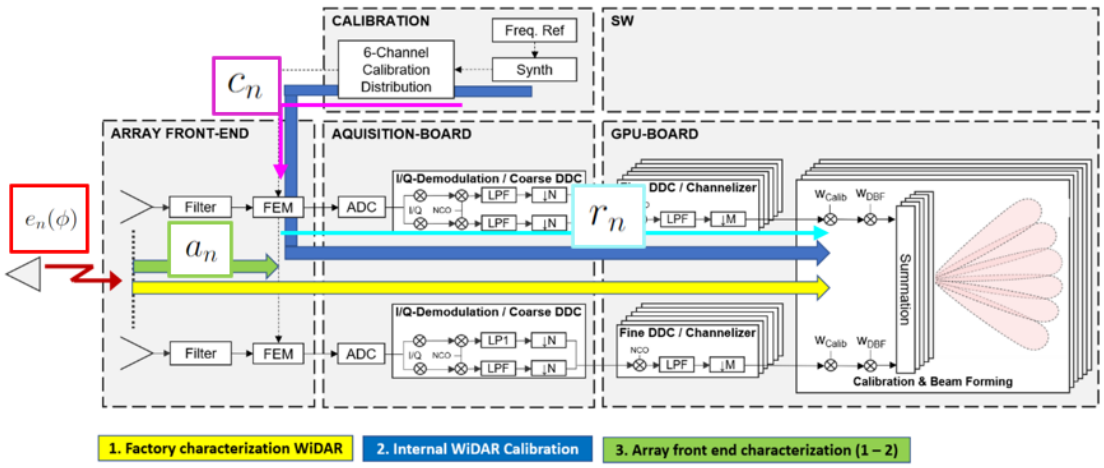

Figure 6 Transfer function and calibration paths of WiDAR

- $e_n(\phi)$, the angle dependent element factor
- a_n, transfer function of the first part (antenna) of the RX network (passive)
- r_n, transfer function of the second part (RF-system) of the RX network (active)
- c_n, transfer function of the calibration network (passive)

3.2.1 Calibration method 1

With the first method, the entire system is characterised by measurements and the characterisation values are stored in a memory. The characterisation procedure can be summarised in three steps:

1. At the array, apply a plane wave of power density D at an angle close to the mechanical broadside direction (by definition the plane wave angle will correspond to $\phi = 0$) and measure received signals in all n elements.

$$S_n = D \cdot e_n(\phi = 0) \cdot a_n \cdot r_n.$$

   Note that D is independent of element n.

2. If the power density D is known, the absolute channel gain can be calculated as

$$|G_n| = \left| \frac{S_n}{D} \right|$$

3. Calculate the relative transfer function as

$$Grel_{n,m} = \frac{G_n}{G_m} = \frac{S_n}{S_m} = \frac{|e_n(\phi = 0)| \cdot a_n \cdot r_n}{|e_m(\phi = 0)| \cdot a_m \cdot r_m}$$

and store in memory. Note that $Grel_{n,m}$ can be determined even if D is unknown.

Correction procedure: Use the inverse/conjugate of $Grel_{n,m}$ to calibrate channels n and m to each other.

3.2.2 Calibration method 2

Calibration with internal signal loop. Some characterisation values are stored in memory and used together with an additional online calibration measurement performed immediately before the start of the system function. The procedures are as follows:

Characterisation procedure:

1. Perform the measurements described in Method 1
2. Immediately after the Method 1 measurements, perform an internal calibration measurement.
3. Measure $Scal_n = Pcal \cdot c_n \cdot r_n$. $Pcal$ is the signal generator power, which has unknown amplitude and phase.
4. Calculate the relative transfer function as

$$Scal_{n,m} = \frac{Scal_n}{Scal_m} = \frac{(c_n \cdot r_n)}{c_m \cdot r_m}$$

5. Calculate

$$C_{n,m} = \frac{Grel_{n,m}}{Scal_{n,m}} = \frac{(|e_n(\phi = 0)| \cdot a_n \cdot c_m)}{(|e_m(\phi = 0)| \cdot a_m \cdot c_n)}$$

and store in memory. Note that the formula only contains factors which are considered stable (passive RF components).

Online calibration:

1. Measure $Scal'_n = Pcal' \cdot c_n \cdot r'_n$. Note that r'_n may be different from r_n due to temperature etc.
2. Calculate the relative transfer function as

$$Scal'_{n,m} = \frac{Scal'_n}{Scal'_m} = \frac{(c_n \cdot r'_n)}{c_m \cdot r'_m}$$

3. Calculate the relative transfer function

$$Grel'_{n,m} = C_{n,m} \cdot Scal'_{n,m} = \frac{(|e_n(\phi = 0)| \cdot a_n \cdot r'_n)}{(|e_m(\phi = 0)| \cdot a_m \cdot r'_m)}$$

Correction procedure: Use the inverse/conjugate of $Grel'_{n,m}$ to calibrate channels n and m to each other.

3.3 Experiments with WiDAR

In the beginning of the project, much time was spent researching and learning about the hardware of the WiDAR prototype, some knowledge regarding the start-up procedure and the available software was also acquired in the lab before the first outdoors experiment. In this section, a description of the experiments and their measurements are given. The data processing, results and discussion of which is proposed in later sections. An illustration of the measurement setup is given in Figure 7.

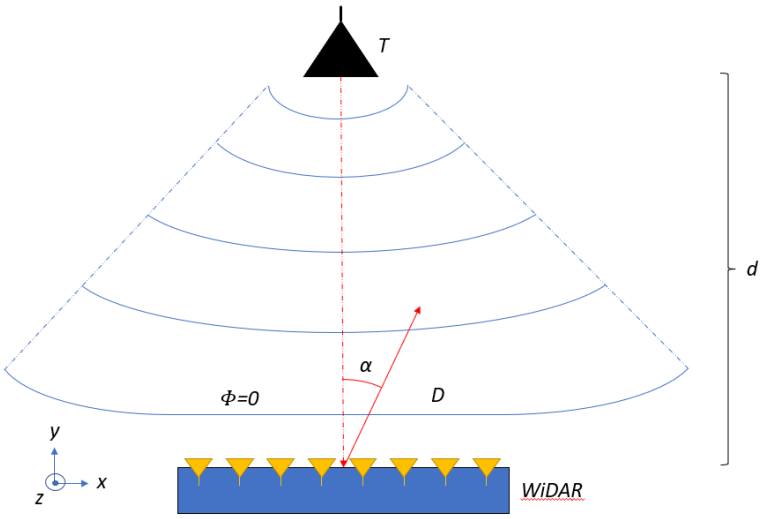

Figure 7 Illustration of the measurement setup. WiDAR being placed at a distance , d, and turned by an azimuth angle, α, from a known transmitter, T. If the transmitter is located at a sufficient distance, the plane wave with power density, D, will correspond to the mechanical broadside $\phi = 0$. This means no time delay will be experienced between the antenna elements and thus no phase shift.

3.3.1 Experiment 1

On the 24th of February 2023 the first experiment was performed on the yard outside Saab's facilities. The setup consisted of a transmitting antenna connected to a signal generator. The transmitter was placed at a distance of 40 meters from, and pointed directly towards, the WiDAR and a signal of 682 MHz was broadcasted. The WiDAR was booted and despite the cold outdoors it was ready to run almost instantly. Data from 7 measurements were downloaded by running an already existing script. The measurements were all with different angles toward the transmitting antenna, which are listed in Table 1.

Table 1: Measurements investigating variation in vertical and azimuth angle

Measurement	Local time	Vertical angle (θ)	Azimuth angle (α)
1	14:57:36	0	0
2	14:59:53	0	10
3	15:01:23	0	20
4	15:03:09	25	30
5	15:03:57	45	30
6	15:09:27	0	-10
7	15:10:58	0	-30

For this first experiment of data collection, the hopes were to see some phase variation between the channels, which should vary in a linear manner when altering the azimuth angle, α towards the transmitter, and that some initial characterisation and calibration could be performed with the gathered set of data.

3.3.2 Experiment 2

The second experiment was performed on the 5th of April 2023 but this time the WiDAR was taken to the rooftop at about a height of 20 m. The idea was to try to measure the signals transmitted by the FM/TV-stations commonly known as ”Nackamasterna”, located at a distance of 23 km from Saab’s facilities. The hopes were that placing the WiDAR as close to the edge of the roof as possible, with safety in mind, and measuring signals propagating much further than those in the first experiment, would limit the significance of constructive and destructive reflexes and better mimic a perfect plane wave scenario.

More measurements were taken at this occasion. Every setup was at least captured twice and the specifics of the setups are listed in Tables 4, 5 and 6.

3.3.3 Experiment 3

Another measurement was performed on the roof in a similar manner as the second measurement, with the goal of capturing data to use the calibration weights on. This measurement was carried out the 3rd of May 2023 and once again the target frequencies were those broadcasted by ”Nackamasterna”. Captures with different positions and azimuth angles were taken, but in addition to the previous measurement, two measurements were performed using other antenna elements and by rearranging the coupling between antenna elements and RF-channels. This was performed to investigate whether most of the variations were caused by the antenna elements or the RF-front-end.

3.4 Processing retrieved data

The standard setting of the scripts capturing data with the WiDAR prototype resulted in each capture containing 20 mega sample in a time window of 10 ms. Each saved measurement resulted in three of these files which after all measurements were done would be converted from bin-files to npy.files. These npy-files were 320 MB in size and were quite demanding to process in python.

It was therefor of interest to reduce the size of these files, but without sacrificing important information. Through some testing and iteration it was found that cutting the captures into chunks of 2^{16} = 65 536 samples were suitable and reduced processing time significantly. Meaning only about the first 0.3 μs of the captures are used, which is the case for all data from performed measurements. This means the frequency bins will be roughly 30.5 kHz since $2 \cdot 10^9/2^{16}$ = 30 517.

3.4.1 Experiment 1

The sampled data acquired from the first channel in the first measurement during the first experiment is shown in figure 8. This collection of data contains 20 mega samples which was cut of into chunks of 2^{16} = 65 536 samples. Figure 9 presents the corresponding FFT in absolute decibel values of the chunk from the first measurement, with zero degrees azimuth. Only positive frequencies are plotted which means half of the samples are discarded, resulting in 32 768 samples.

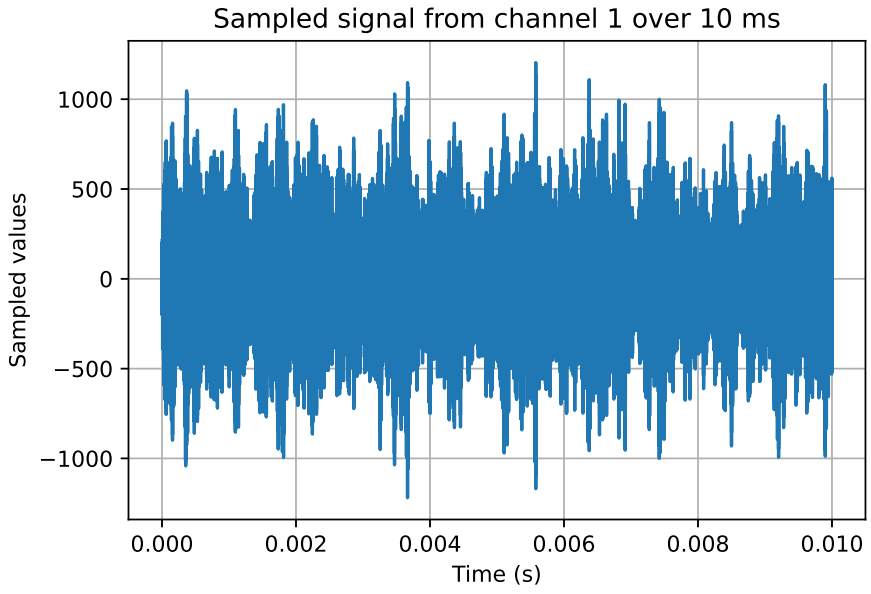

Figure 8 Experiment 1: Digitised samples of signal from the first measurement

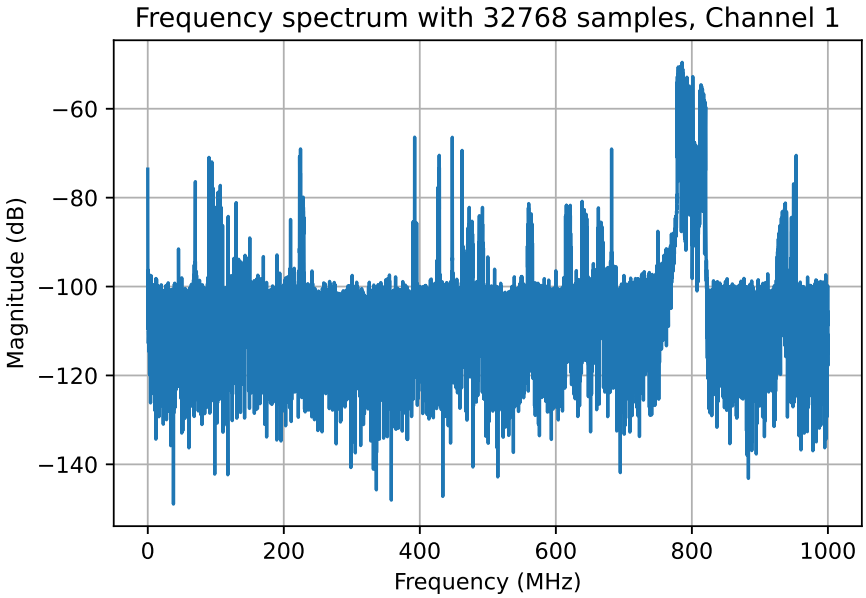

Figure 9 Experiment 1: FFT of 2^{16} chunk of sampled signal in dB

The plots for the other eight channels are as expected very similar and the resulting amplitude and phase variations between the eight channels at frequency 682 MHz are shown i figures 10a and 10b respectively. It should be noted that with the length of each frequency bin provided by the FFT is 30.5 kHz using data chunks of size 2^{16}. The spectral density of the broadcasted signal at 682 MHz was encapsulated in a single frequency bin. This clarification is provided since this is not the case for the measurements from the other experiments.

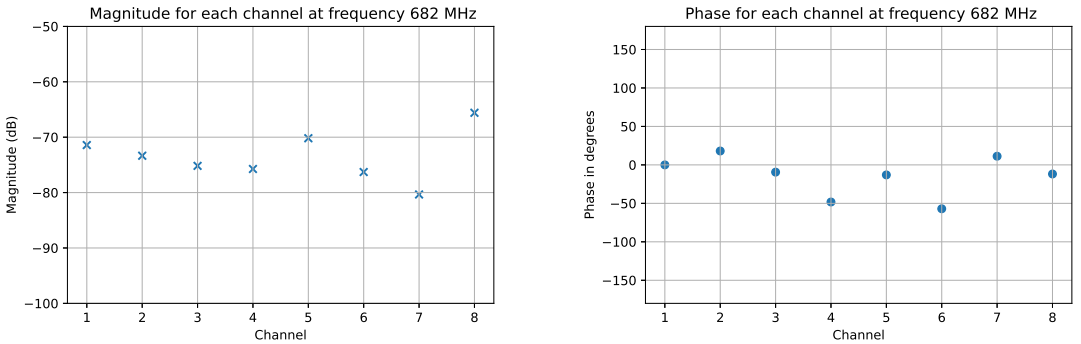

(a) Experiment 1: Magnitude **(b)** Experiment 1: Phase

Figure 10 Experiment 1: Each channel's magnitude and phase at 682 MHz. The phase being normalised around channel 1.

From the resulting figures it may be derived that there are significant variations between channels, both in received signal magnitude and phase, which is highly doubtful to be the sole responsibility of imperfections in the hardware. The significance was true for the other six measurements as well.

However, the measurements with increased vertical angle, measurement 4 and 5, resulted in less variation, and it was concluded that this was due to less ground reflections reaching the antenna elements. It was therefore decided that the measurements gathered from the first experiment would not be particularly useful to calibrate the system, and that the next experiment had to be performed in a different manner to reduce contribution by reflexes.

3.4.2 Experiment 2

The second experiment was performed on the roof at about 20 meters above ground level, with the hopes to reduce ground reflexes. From Figure 11 it can be seen that the intercepted signals magnitude levels are higher in general, apart from frequencies around 800 MHz, compared to the first measurement from the first experiment.

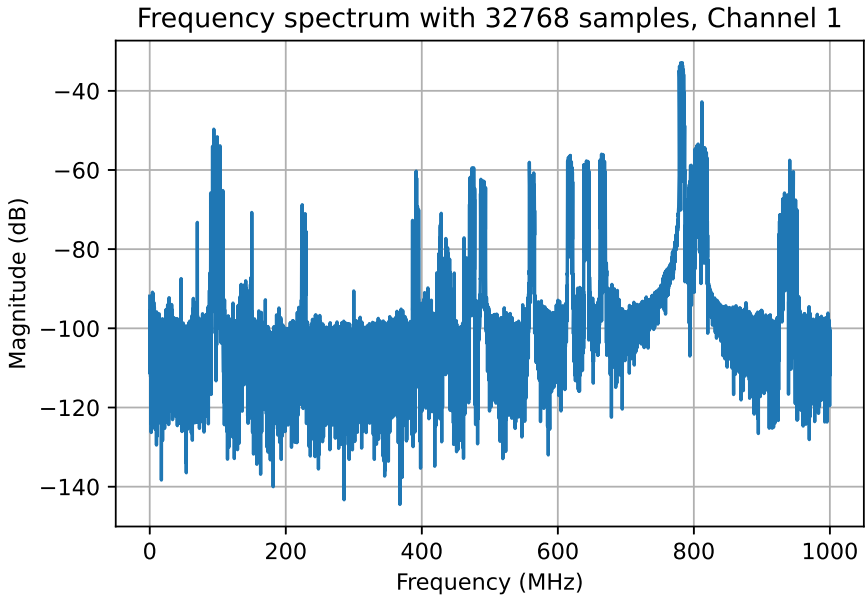

Figure 11 Experiment 2: Values converted to decibel scale after FFT on 2^{16} samples of the signal

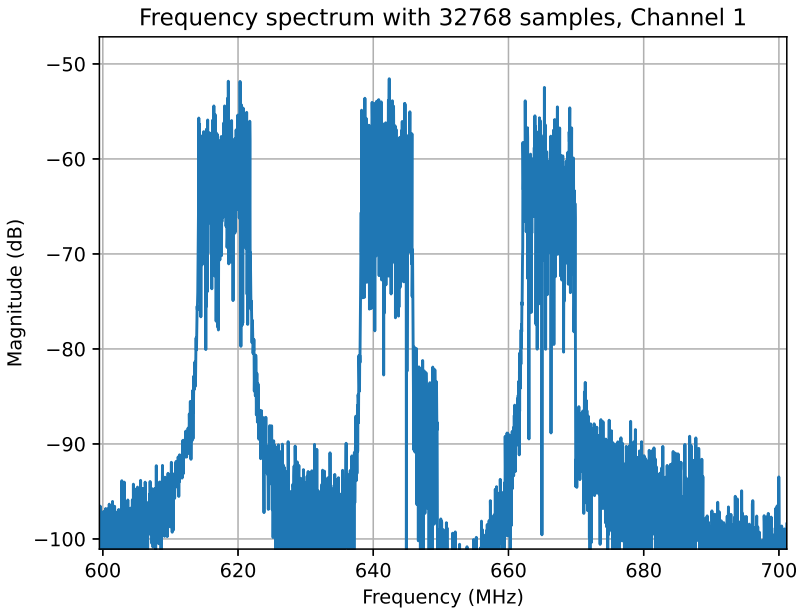

Figure 12 Experiment 2: Values converted to decibel scale after FFT on 2^{16} samples of the signal, zoomed in at 600-700 MHz

Three peaks at about 618, 642 and 666 MHz are frequencies within the UHF-band and are allocated to different TV-channels which are broadcasted from ”Nackamasten”. These frequencies were chosen to be thoroughly studied and would hopefully result in good calibration weights. Figure 12 contains the same data as 11 but is zoomed in at these frequencies. The broadcasted signals at these frequencies are intercepted within the range of -50 to -80 dBFS while the noise is below -90 dBFS, meaning the noise should have limited effects on these three frequency bands.

The plots for the other eight channels are as expected very similar. The resulting amplitude and phase variations between the eight channels at frequency 618 MHz are shown i Figures 13(a)-(b), 642 MHz in Figures 14(a)-(b) and 666 MHz in Figures 15(a)-(b). Note that in Figure 15(b) it might look like an something is erroneous, but channel 8 is wrapped to a negative value since the phase is a few degrees larger than 180.

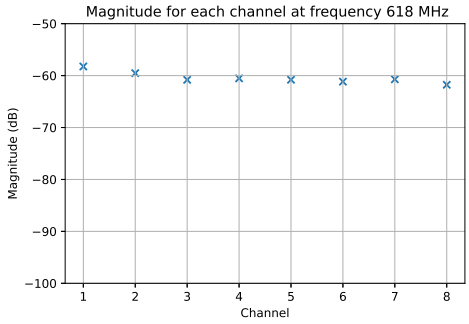

(a) Experiment 2: Magnitude

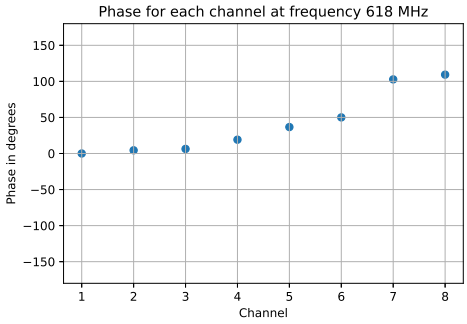

(b) Experiment 2: Phase

Figure 13 Experiment 2: Each channel's magnitude and phase at 618 MHz. The phase being normalised around channel 1.

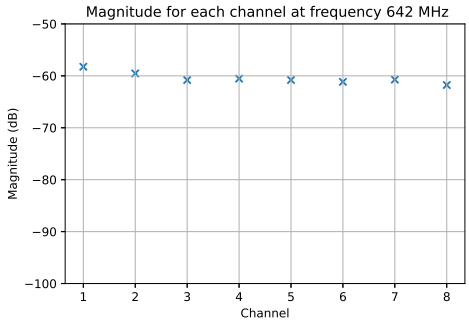

(a) Experiment 2: Magnitude

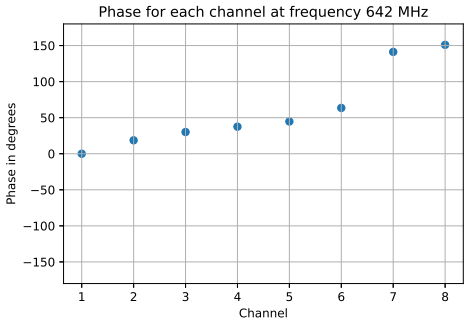

(b) Experiment 2: Phase

Figure 14 Experiment 2: Each channel's magnitude and phase at 642 MHz. The phase being normalised around channel 1.

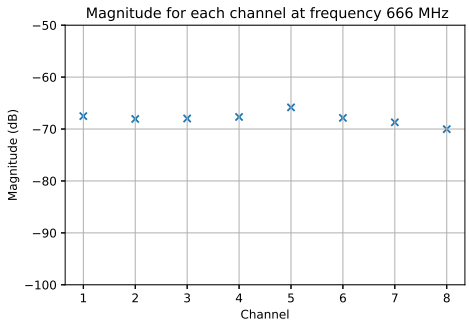

(a) Experiment 2: Magnitude

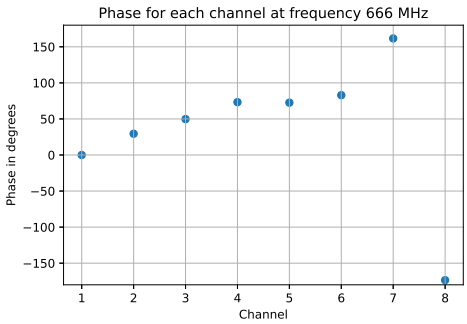

(b) Experiment 2: Phase

Figure 15 Experiment 2: Each channel's magnitude and phase at 666 MHz. The phase being normalised around channel 1.

These figures containing data of signal amplitude and phase are all retrieved from one frequency bin each. The chosen frequency bin is the ones containing the given values 618, 642 and 666 MHz, the center frequencies of the bins only varying by a couple of kHz from these values.

This could be one reason causing the difference in intercepted magnitude between the three frequency bands. Since interest lies in the variations between channels and not in total received magnitude, this may be overlooked. Nevertheless it was decided to use multiple frequency bins over the frequency bands to calculate an average value for all channels, which would hopefully reduce the risk of uncertainties or anomalies in the frequency bands.

3.4.3 Experiment 3

Since the data from the second experiment was promising, the third experiment was carried out in a manner similar to the previous measurements. This time the first measurement was captured with an azimuth angle as close to zero as possible to the human eye, since the available compass did not provide satisfying precision. The first measurement from the third experiment was meant to serve as the data from which calibration weights would be calculated. The new data was first investigated and ensured to be similar to the second experiments data. Comparing Figures 16 and 17 with the corresponding figures from the second experiment confirms that the frequency spectrum from both occasions are satisfyingly similar. Figures 18a through 20b may be compared to the corresponding figures from the second measurement, but recall that there is a azimuth difference at around -15 degrees between the first measurements from both experiments.

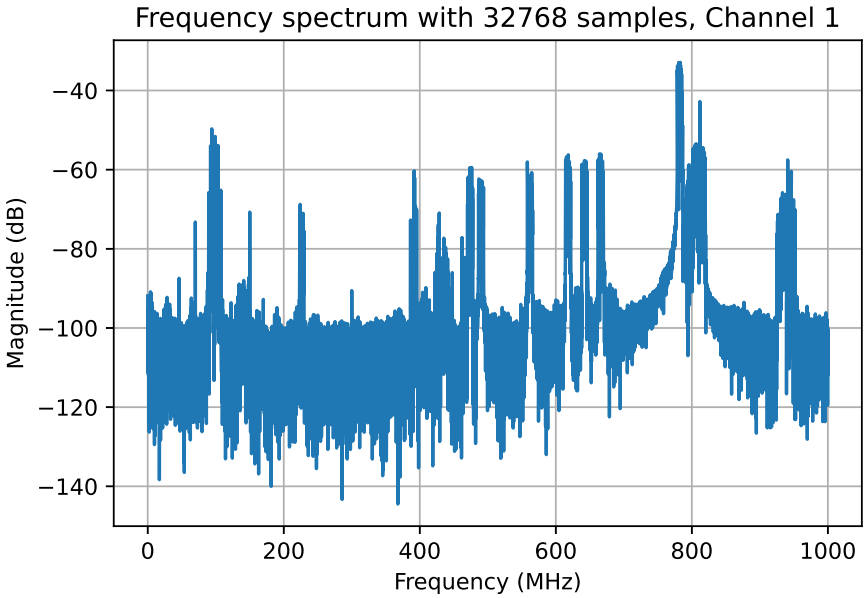

Figure 16 Experiment 3: Values converted to decibel scale after FFT on 2^{16} samples of the signal

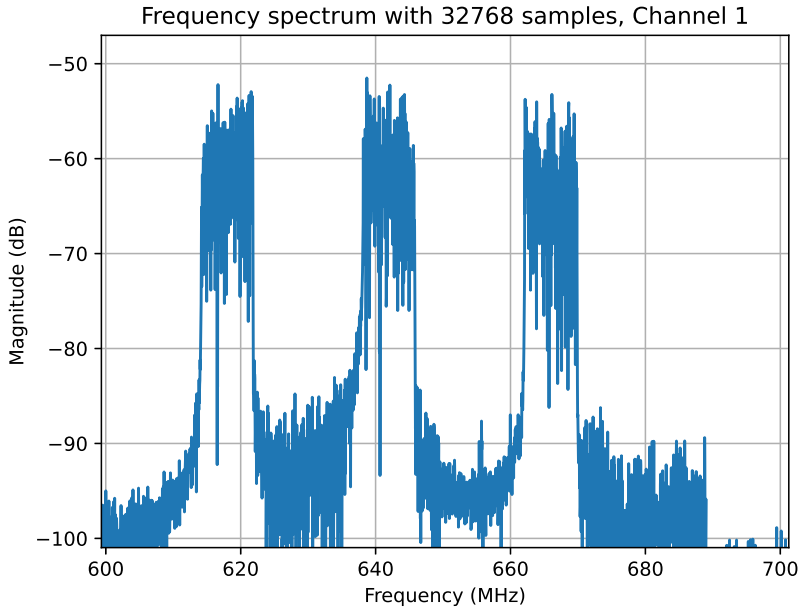

Figure 17 Experiment 3: Values converted to decibel scale after FFT on 2^{16} samples of the signal, zoomed in at 600-700 MHz

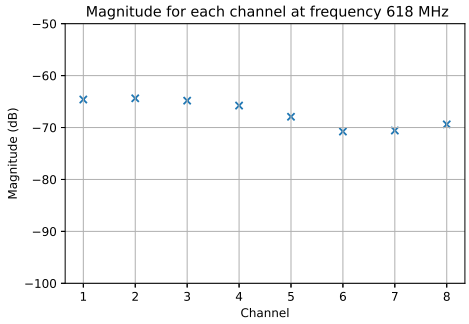

(a) Experiment 3: Magnitude

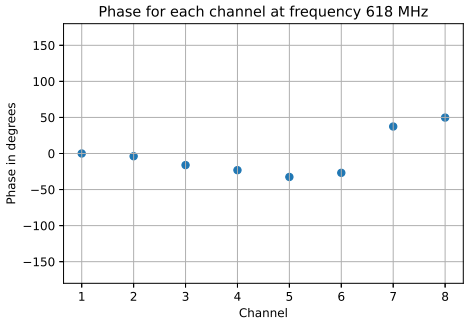

(b) Experiment 3: Phase

Figure 18 Experiment 3: Each channel's magnitude and phase at 618 MHz. The phase being normalised around channel 1.

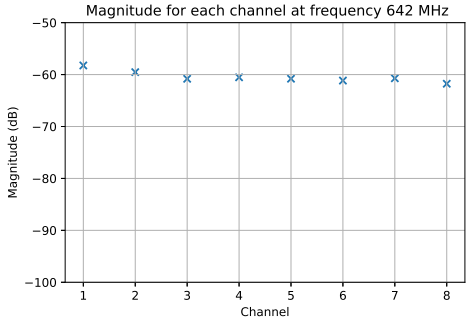

(a) Experiment 3: Magnitude

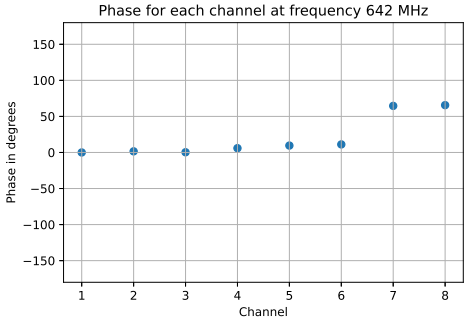

(b) Experiment 3: Phase

Figure 19 Experiment 3: Each channel's magnitude and phase at 642 MHz. The phase being normalised around channel 1.

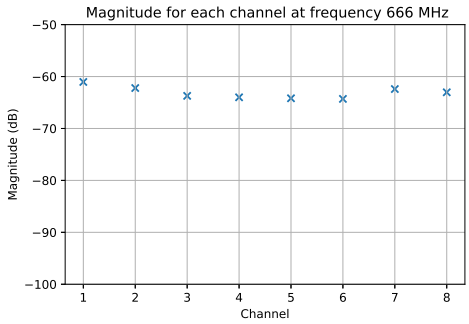

(a) Experiment 3: Magnitude

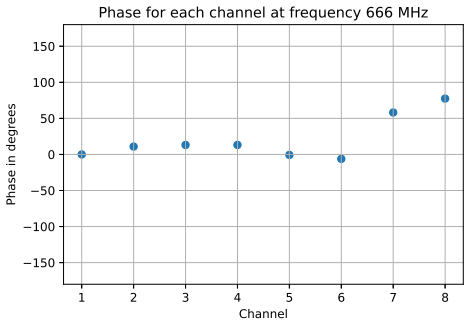

(b) Experiment 3: Phase

Figure 20 Experiment 3: Each channel's magnitude and phase at 666 MHz. The phase being normalised around channel 1.

3.5 Including multiple frequency bins

To get a better result than just taking a value from one frequency bin, multiple frequency bins over the frequency band of interest may be involved and summed to minimise errors.

Lets denote the digitised bit stream from one channel $y[k]$, y being a complex number and k the k:th sample. The difference between two channels, for example channel 1 and 2, at a given frequency can be expressed as

$$\triangle c_{1,2}[k] = \frac{F\{y_{ch1}[k]\}}{F\{y_{ch2}[k]\}}. \tag{11}$$

By summing the complex values corresponding to each frequency bin and then calculating the angle of that sum, $\phi_{diff_{1,2}}$,

$$\phi_{diff_{1,2}} = \angle \sum_{k=1} \triangle c_{1,2}[k] \tag{12}$$

a summed complex vector is retrieved. This vector is much less likely to present a deceptive phase value over the frequency band than a random frequency bin would.

The same idea is applied to produce the average magnitude. The average magnitude difference between channel 1 and 2, $M_{diff_{1,2}}$, may be calculated as

$$M_{diff_{1,2}} = 20\log_{10}\sqrt{\sum_{k=1} \frac{|\triangle c_{1,2}[k]|^2}{k}}. \tag{13}$$

Calculating the average values for phase and magnitude over a broader frequency band, as in equations 12 and 13, should yield more accurate results than just taking an arbitrary frequency bin within the band, since the sum of delta values should have a higher SNR compared to single frequency bin values.

Recall from Table 4 and Figures 15(a)-(b), in the first measurement the antenna was turned by -15 degrees azimuth towards the source. Meaning that for example channel 1 should be located further away from ”Nackamasten” and therefor the signals intercepted at antenna channel 1 have a longer propagation time than those signals received at channel 2. This means comparing a channels phase with a channel adjacent to the right, should give a negative value.

In Figures 21(a), 22(a) and 23(a), example of this are visualised. The difference in magnitude is also investigated in the same manner in Figures 21(b), 22(b) and 23(b)

but it is more difficult to draw any conclusions regarding what is more accurate when it comes to the magnitude of received signals, since it seems to vary remarkably with time and frequency bins.

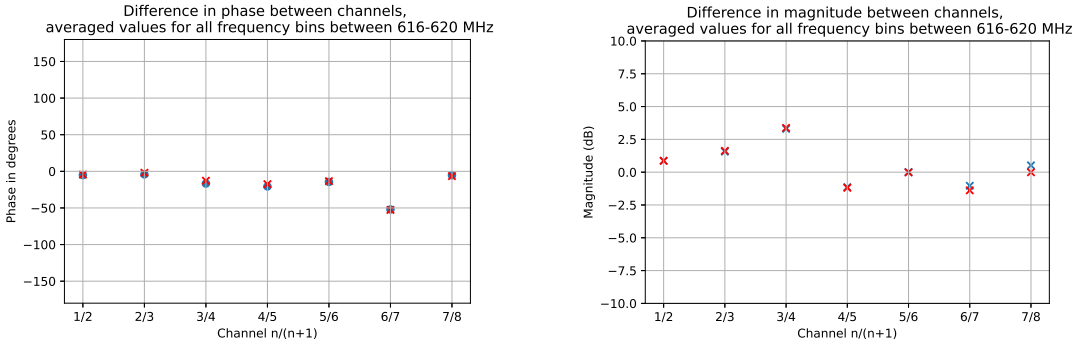

(a) Phase **(b)** Power

Figure 21 Experiment 2: Difference in phase and magnitude between adjacent channels, measured magnitude and phase at frequency bin containing 618 MHz (red) vs average magnitude and phase of all bins between 616-620 MHz (blue)

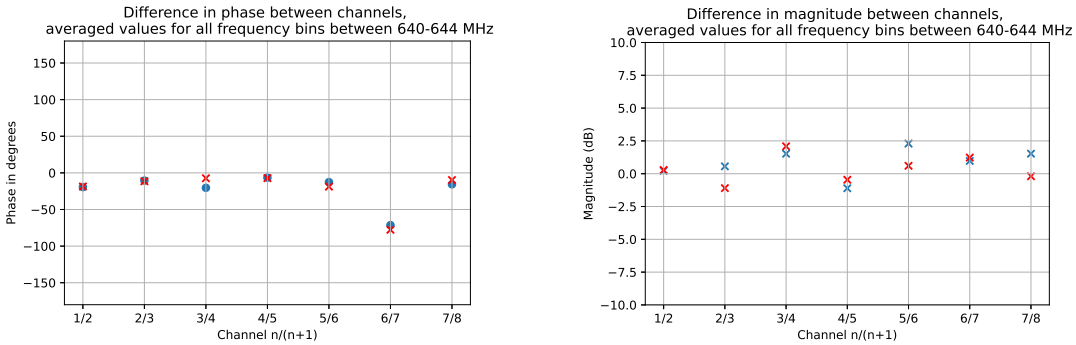

(a) Phase **(b)** Power

Figure 22 Experiment 2: Difference in phase and magnitude between adjacent channels, measured magnitude and phase at frequency bin containing 642 MHz (red) vs average magnitude and phase of all bins between 640-644 MHz (blue)

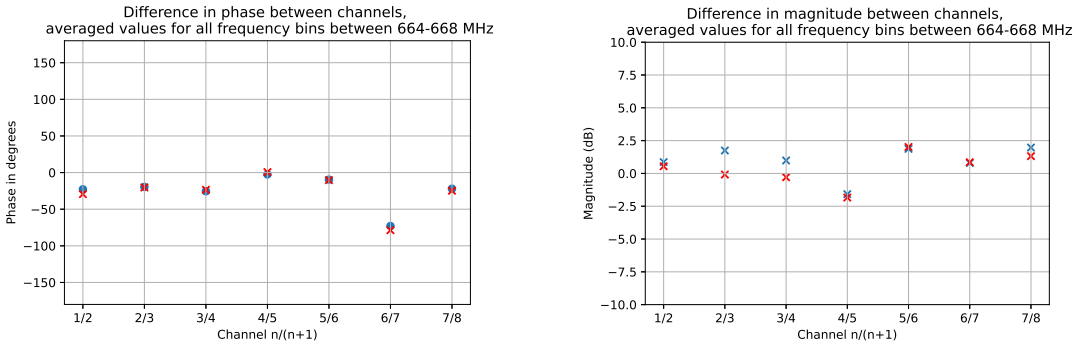

(a) Phase **(b)** Power

Figure 23 Experiment 2: Difference in phase and magnitude between adjacent channels, measured magnitude and phase at frequency bin containing 666 MHz (red) vs average magnitude and phase of all bins between 664-668 MHz (blue)

Studying figure 21(a)-(21b) it may be derived that the single frequency bin including the frequency 618 MHz gives a similar representation of the channel differences that the summation of the bins in the entire frequency bands do. This is true for both phase and magnitude.

For the frequencies 642 and 666 MHz this is true as well, but only for the phase. The magnitude difference between some of the channels vary significantly. It is assumed, but not necessarily true, that the differences retrieved by summing multiple frequency bins give a more accurate representation of the signal space that was measured. This assumption is made when calculating calibration weights for these frequency bands.

3.6 Determining the transfer functions and calibration weights

In the example from equation 11, channels 1 and 2 were compared. The reference channel, meaning the channel which the rest of the array was calibrated towards, was selected as channel 1.

For any of the other channels, x, calibration coefficients for phase and magnitude, c_f and c_m can be calculated and stored from $\triangle c_{x,1}[k]$ using equations (14) and (15).

$$c_f = \sum_{k=1} \frac{\frac{\triangle c_{x,1}[k]}{|\triangle c_{x,1}[k]|}}{k} \tag{14}$$

$$c_m = \sqrt{\sum_{k=1} \frac{|\triangle c_{x,1}[k]|^2}{k}}. \tag{15}$$

The coefficients for phase and magnitude may then be multiplied together to get a coefficient, w_{cal}, that adjusts both phase and magnitude when $\triangle c_{x,1}[k]$ is divided by that coefficient.

$$w_{cal} = c_f \cdot c_m \tag{16}$$

Note that the procedure to calculate calibration coefficients is performed for all channels in the array, which in the measurements performed in this thesis work consisted of eight channels. Resulting in seven calibration weights, w_{cal}, that may be stored for each frequency or frequency band of interest in a measurement.

3.7 Verification of calibration model

To make sure the method to calculate the calibration weights correlated with what was intended, the weights were used on the same data they were extracted from. This means values for phase and magnitude for all channels compared to the reference channel should be next to zero. The set of calibration weights from the third experiment are presented in Table 2. The calibration weights have a precision of 19 decimal values but are rounded to four decimal values in the table for convenience. Note that the presented calibration weights serve as an example, which are calculated from data between 616-620 MHz. The presented results will in addition to these values use calibration weights from the frequencies 640-644 MHz and 664-668 MHz.

Table 2: Calibration coefficients for 618 MHz

Channel	w_{cal}
1	(1+0j)
2	(0.9575-0.0985j)
3	(0.8862-0.3024j)
4	(0.8266-0.3639j)
5	(0.6572-0.3555j)
6	(0.5665-0.1932j)
7	(0.5176+0.4061j)
8	(0.4647+0.4961j)

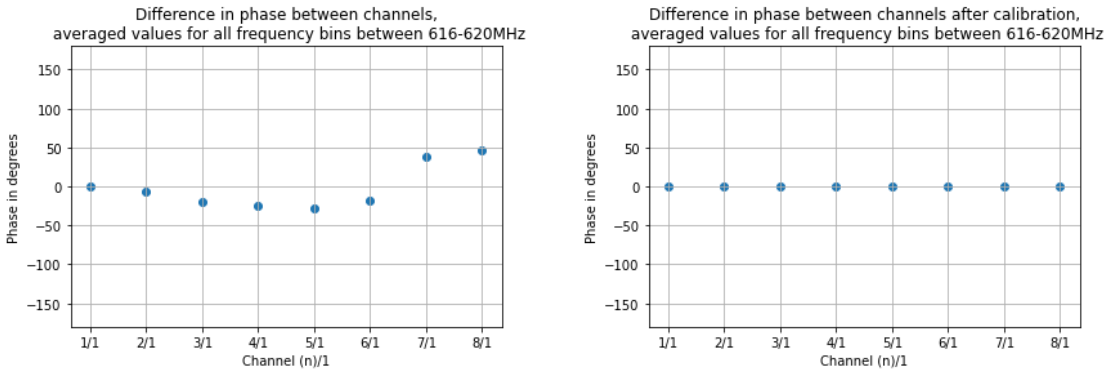

(a) Without calibration **(b)** With calibration

Figure 24 Experiment 3: Phase difference between each channel, with channel 1 as reference

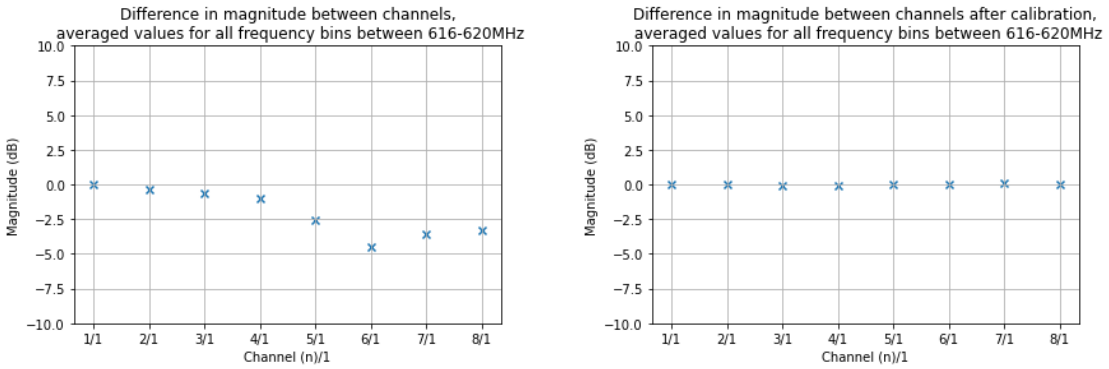

(a) Without calibration **(b)** With calibration

Figure 25 Experiment 3: Magnitude difference between each channel, with channel 1 as reference

As figures 24 and 25 illustrate, the calibration method works fairly well since all channels are in proximity to zero in both phase and magnitude after use of the calibration weights.

4 Results and Discussion

The resulting calibration weights that were used were those calculated from Experiment 3, since the first measurement from that experiment had approximately zero degrees azimuth towards ”Nackamasten”.

To see how well the set of calibration weights work beside the frequency band they were calculated from, they are also applied on the other strong nearby frequency bands. Those frequency bands are the same as previously mentioned in Figure 12, namely 618, 642 and 666 MHz. The resulting calibration weights are presented in Table 3 and are extracted from the data presented in Figures 26, 27 and 28.

Table 3: Experiment 3: Each channel's calibration weight, w_{cal} for each of the three investigated frequency bands.

	f = 618 MHz	f = 642 MHz	f = 666 MHz
Channel	w_{cal}	w_{cal}	w_{cal}
1	1 + 0j	1 + 0j	1 + 0j
2	0.9575-0.0985j	0.9083+0.0411j	0.9501+0.1494j
3	0.8862-0.3024j	0.8863-0.0429j	0.8794+0.1158j
4	0.8266-0.3639j	0.8393+0.0552j	0.9151+0.0926j
5	0.6572-0.3555j	0.9090 -0.0026j	0.8243-0.0681j
6	0.5665-0.1932j	0.8307+0.0601j	0.7140 -0.0699j
7	0.5176+0.4061j	0.4356+0.7918j	0.4008+0.7232j
8	0.4647+0.4961j	0.2796+0.6491j	0.1264+0.7686j

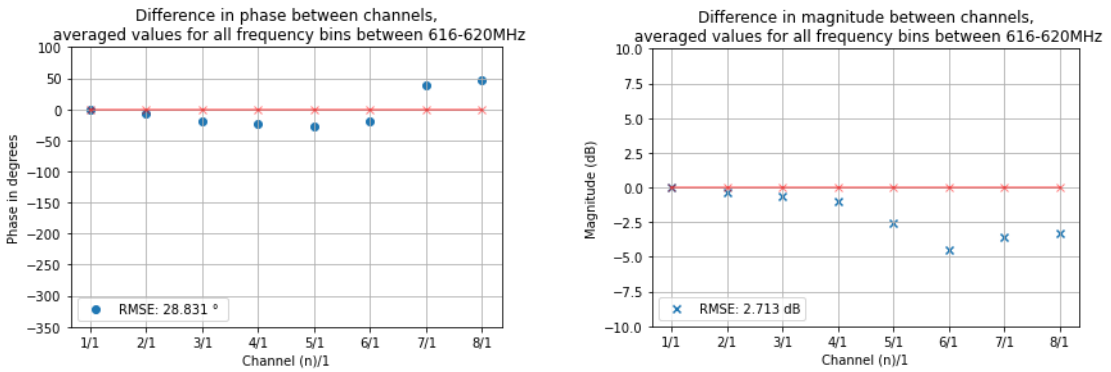

(a) Phase **(b)** Magnitude

Figure 26 Experiment 3, Measurement 1: Phase and magnitude difference between each channel and reference channel 1, $f = 618$ MHz, $\alpha = 0$.

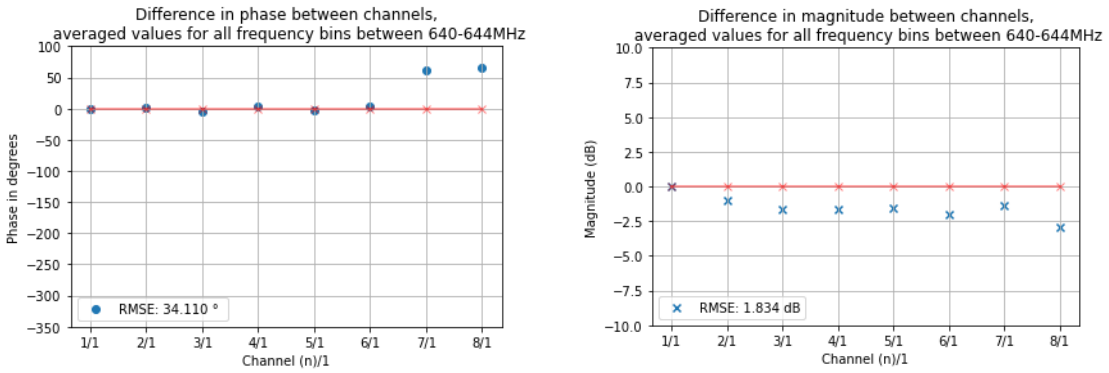

(a) Phase **(b)** Magnitude

Figure 27 Experiment 3, Measurement 1: Phase and magnitude difference between each channel and reference channel 1, $f = 642$ MHz, $\alpha = 0$.

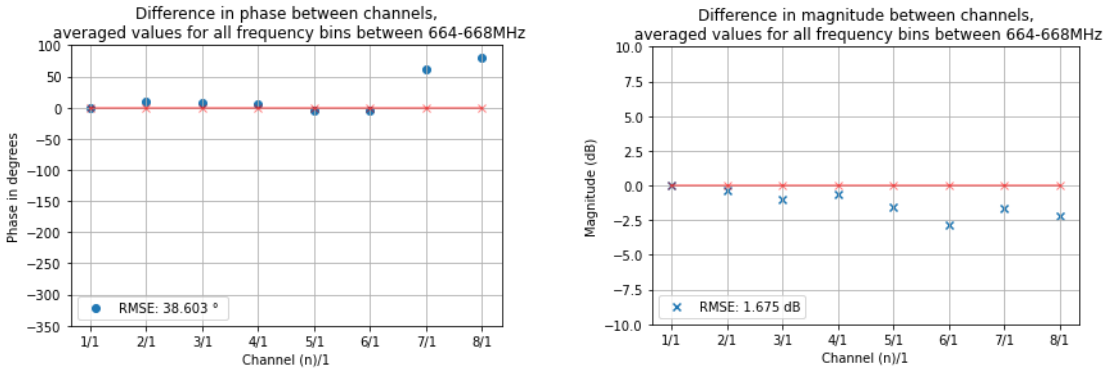

(a) Phase **(b)** Magnitude

Figure 28 Experiment 3, Measurement 1: Phase and magnitude difference between each channel and reference channel 1, $f = 666$ MHz, $\alpha = 0$.

The root-mean-square error (RMSE) is calculated from what is theoretically expected for both phase and magnitude, with and without calibration. These expected values are presented as red crosses in the figures and a lower RMSE signifies a reduction in variation between channels. It is assumed that the magnitude should be the same at each channel and the phase shift should depend on the additional transmission distance caused by altering the azimuth angle. The received signal is most likely not a perfect plane wave even in Experiment 2 and 3, meaning the theoretical values for phase and magnitude should not be the true reference, but they were determined to suffice. The figures are illustrating the expected values compared to the measured values and in the bottom left corner all channel's RMSE is presented. The rest of the measurements and

their calibration results are presented in the Appendix, so are tables with the RMSE values for the different calibration weights.

One way of illustrating the success of the calibration is to plot the RMSE with and without calibration. In Figure 29 the phase RMSE from Table 11 is presented in a plot.

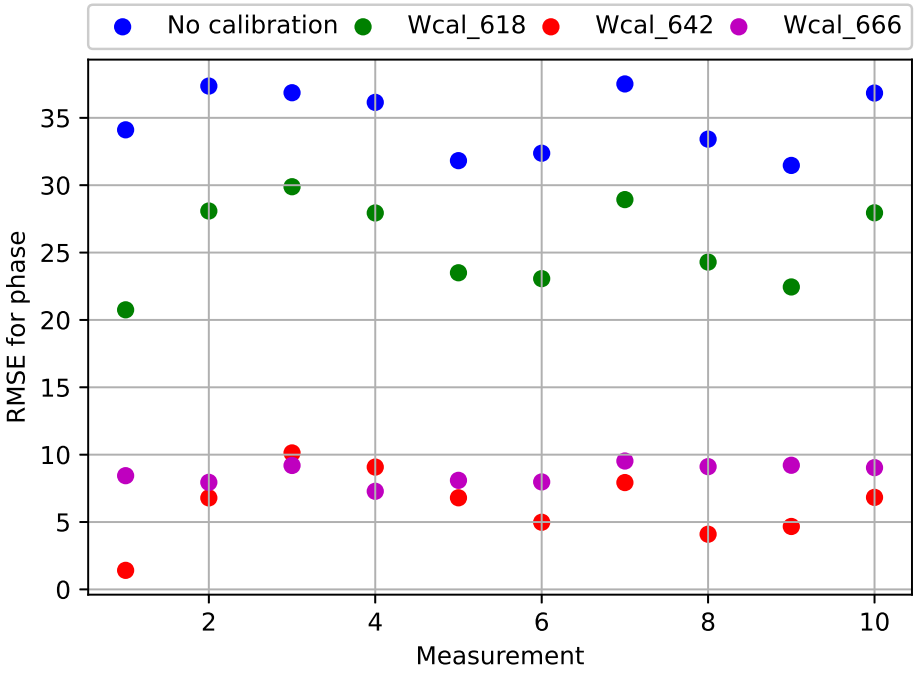

Figure 29 Resulting phase RMSE with and without calibration

The circles coloured blue, green, red and magenta in Figure 29 correspond to values without calibration and with calibration weights from 618, 642 and 666 MHz respectively. A quick study reveals that the calibration weights retrieved from frequency 642 and 666 MHz, results in values closer to zero than the calibration weight from 618 MHz do. Even so, every single measurement has a reduces RMSE after calibration was performed.

Figure 29 reflects the general results regarding phase. It is not always true that all calibration weights perform in this manner but overall, calibration reduced the RMSE. Apart from a few specific cases, the calibration weight from frequency 618 MHz performed worse than both calibration weights from 642 and 666 MHz.

The same level of success is not achieved when calibrating the magnitude. In Figure 30 a similar plot as in Figure 29 is with values from Table 17 presented with the same colour scheme but crosses instead of circles. The magnitude values after calibration

with weights from 642 MHz seems to result in highest RMSE, even though the data is from the frequency band around 642 MHz. Apart from Measurement 10, all calibration weights seem to reduce the RMSE on this set of data. It should be mentioned that this is not the general case, and occasionally the RMSE without calibration is lower than after calibration with any of the weights.

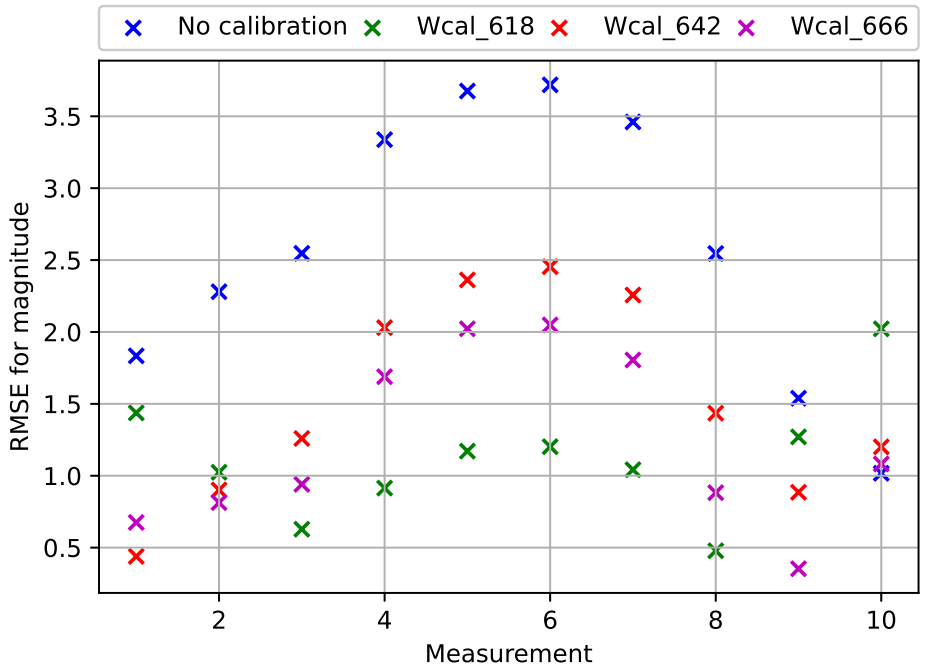

Figure 30 Resulting magnitude RMSE with and without calibration

4.1 Discussion of results

4.1.1 Phase calibration

A reoccurring pattern that may be extracted from Experiment 3 and Tables 10, 11 and 12, is that the measurements have a similar RMSE value despite altering the azimuth. This is an understandable pattern when studying Figures 31-60. Channels 7 and 8 seem to be at a similar offset throughout the ten measurements, the rest of the channels are in contrast very close to the expected phases.

Another pattern is that the calibration weights obtained from the frequency band with center frequency 618 MHz seem to generally perform worse in regards of RMSE than the calibration weights from frequency bands with center frequency 642 and 666 MHz. Apart from a few measurements, this seem to be true even when calibrating the data from the same frequency band the calibration weight was calculated from. This fact

suggest that the first measurement, which was used as a foundation for calibration, is a poor reflection of the phase of the signals. Looking at Figure 26a that assumption seems fair when comparing the relative phases measured at channels 2 through 6 in Figures 27a and 28a, which are much closer to 0.

Investigating the RMSE values from Experiment 2 at Tables 13, 14 and 15, one may once again draw the conclusion that the frequency band around 618 MHz deviates from the other two investigated frequency bands. This is at least true for measurements 1, 8 and 10, where the RMSE without calibration or with calibration weight from 618 MHz outperforms or is in proximity to the RMSE retrieved with the other two calibration weights.

Unlike the data from the frequency band at 618 MHz, applying the calibration weights seem to lower the RMSE for all measurements with data from the frequency bands at 642 and 666 MHz. While this is true for the calibration weights from 618 MHz, just like in the case for experiment 3, the RMSE is notably larger than for the other two sets of calibration weights.

One could argue that the applied calibration method generally improves the phase RMSE, at least if the measurement that is used as foundation for calibration is accurate. A lower RMSE however does not in itself guarantee a better estimation of the true signal space. It could be the case that the data from the channel which the other channels are calibrated towards, is fallacious.

4.1.2 Magnitude calibration

Unlike the phase calibration, the pattern noted regarding the calibration weight from 618 MHz does not seem to persist when calibrating the magnitude. Which calibration weight performs best in reducing the RMSE seem to be a bit more random, apart from the first few measurements which is most likely to be more similar to the reference measurement. This is a relationship that agrees with the perception gathered when measuring the magnitude, which varied greatly between measurements.

Since the calibration weights are extracted from Experiment 3, it does not seem too improbable that the RMSE should be lower in general when they are applied to measurements from Experiment 2. Other than that, calibration on Experiment 2 seem to be as random as calibration on experiment 3.

For both experiments, apart from a few measurements, the magnitude RMSE is generally reduced when calibration is done. However, studying Figures 79-108 some channels occasionally differ more from the reference channel after calibration.

4.2 Other measurements

The reason behind why the calibration weights only are applied to the azimuth measurements is because the other measurements gave insights regarding the signal space rather than quantifiable and comparable results. For example as previously mentioned in Section 3.4.1, the measurements with varying vertical angle, measurements 4 and 5 from Table 1, retrieved different results. This was no longer the case in Experiments 2 and 3 when the experiment setups better resembled a plane wave scenario.

The measurements varying the perpendicular positions by the same length as the distance between antenna elements was performed to investigate if the signal space was more or less constant or if the variations followed the antenna array. If the signal space would be constant the data would be displaced with one antenna element between measurements 11 and 12, meaning channel 1 in measurement 12 would result in the same magnitude as channel 2 did in measurement 11. It was concluded that the relative channel variation pattern was very similar despite changing the perpendicular position.

In Experiment 3, measurement 15 and 16 was performed to ascertain that the antenna elements did not affect the results significantly. By inverting the order of the channels on one of the FEM-cards the resulting measured magnitude should also be inverted. Switching antenna elements to another horizontally polarised row should result in similar measurements. Both measurements indicated that these assumptions were true.

4.3 Characterising errors and reducing their impact

First of all, it should mentioned that one source of error is the azimuth. This is because the azimuth angle throughout all measurements were estimated by hand and sight, since the available tools such as a compass was irregular and therefore unreliable. The azimuth angle is used to gain the theoretically expected values and could therefore have an impact on the resulting RMSE.

One error that is clear over all measurements is the phase shift at channels 7 and 8. This error seem to be reasonably well compensated for with all calibration weights. Looking at the imaginary parts of the channels' calibration weights in Table 3, one can identify that the weight for channels 7 and 8, unlike the other channels, are more dominated by the imaginary part. Since this phase error is consistent throughout all measurements this is most likely a variation caused by the hardware.

Comparing the results from calibrating phase and magnitude, it seems like compensating phase variations were more successful. Why this is the case for the magnitude calibration may be because, unlike the phase, difference in magnitude seem to vary much more between measurements. Parameters such as time, space and frequency seem to affect the relative magnitude between channels more than the relative phase between

channels.

A factor that should be mentioned even if the calibration theoretically should not be affected by it, is which channel is chosen as the reference. Throughout all plots presented, channel 1 has served as reference. But other channels were used to as reference channel as well. As previously stated, there is reason to believe that the first measurement is not a good reference for the other measurements when it comes to the frequency band around 618 MHz. Other channels were therefore used as reference which results in new as sets of calibration weights. When these new weights were applied to the same data, the resulting RMSE for some measurements were reduced and some were increased. Which channel serves as the best reference depends on the measurement, and this seems so be rather random.

Exactly what these errors and uncertainties stem from is difficult to be certain of. It could be anything from constructive or destructive interference of signals to hardware imperfections such as temperature fluctuations. Performing more tests and measurements to gain insight in and isolate errors would be beneficial to further improve the magnitude calibration.

5 Conclusions

The purpose of the thesis project was to explore methods to compensate for variations in a wide-band digital array receiver, a procedure often referred to as calibration. Many fields and areas need calibration to decrease the probability and magnitude of errors and better ensure that what ever data is collected is as truthful as possible. Truthful data is of great importance when applying beamforming or spatial filtering to achieve satisfying results of spatial selectivity. In the case of this thesis, the data that was calibrated were the phase and magnitude properties of electromagnetic signals which was intercepted by WiDAR.

The data was collected by measuring signals from a high power transmitter far away within the frequency band 0-1 GHz, selecting a strong frequency band to investigate, and from which calibration weights could be calculated. These calibration weights were retrieved by summing all frequency bins within the frequency band and relating each channel's transfer function to a reference channel's transfer function. The calibration weights were then applied to certain data both within and out of the frequency band, to investigate if it would reduce the phase and magnitude variations between the channels.

The results showed that the used calibration procedure did decrease variations for both phase and magnitude by comparing the root mean-square error (RMSE) between channels and the reference channel with and without applying the calibration weights. Studying the Figures and Tables in the Appendix, it became evident that the phase calibration was more consistent and successful than the calibration of the magnitude. Exactly what this depends on should be further investigated but it should be mentioned that the magnitude seemed to more randomly fluctuate across channels and measurements than the phase did before calibration was performed.

The calibration's level of success seems to be connected to the accuracy of measurement used as foundation, which is understandable. The calibration weights were applied to data from two different experiments, which took place about a month apart. Despite a time gap of one month, the calibration procedure resulted in less variations between channels for both experiments. The calibration weights were calculated and applied in an offline manner, but if an online calibration method was to be incorporated in the software connected to WiDAR, even better calibration results are to be expected.

6 Future work

Depending on what the future holds for WiDAR or a similar digital array receiver, a much higher level of certitude with regards to calibration may be of interest. In that case it would certainly be interesting to try to perform a calibration procedure as described in Section 3.2.2, introducing an online calibration with an internal signal loop that compensates for changes in the active RF-network, r_n.

Some insights regarding the signal space and errors as well as the used calibration method has been obtained. Since the received magnitude seem to be quite time and space dependent it is more difficult to compensate for with and offline procedure. Using an online calibration procedure and investigate how the resulting weights change with time and space, a better understanding of the applications and limits of the offline calibration procedure could be obtained.

One of the objectives of this thesis was to analyse the calibration errors and relate the errors to some physical quantity. Such analysis was not done and if this project was resumed, one of the first things that could be done is to implement a DoA-algorithm, such as MUSIC. Since the results are presented with RMSE values compared to what is expected theoretically, it would perhaps be more useful to investigate how the produced calibration weights would affect the prediction rate of a physical quantity such as direction of arrival.

Other than developing the online calibration procedure and the DoA-algorithm, a more thorough memory of calibration weights could be gathered to reduce the risk of anomalies in the data. Already existing weights could also be used on data gather from signals broadcasted by other sources and in other frequency bands further away from those investigated in this study.

References

[1] Advantages of direct rf sampling architectures. https://www.ni.com/en/solutions/aerospace-defense/radar-electronic-warfare-sigint/advantages-of-direct-rf-sampling-architectures.html. Accessed: 2023-06-02.

[2] Phased array antenna and beamforming. https://en.wikipedia.org/wiki/File:Phased_array_animation_with_arrow_10frames_371x400px_100ms.gif. Accessed: 2023-02-14.

[3] C. A. Balanis. *Antenna Theory - Analysis and Design*. John Wiley Sons, 2005.

[4] Jean Baptiste Joseph Fourier. *The Analytical Theory of Heat*. Cambridge University Press, 1878.

[5] The fourier transform and signal processing. https://community.sw.siemens.com/s/article/what-is-the-fourier-transform. Accessed: 2023-02-07.

[6] Difference between fft and dft. http://www.differencebetween.net/technology/difference-between-fft-and-dft/. Accessed: 2023-02-07.

[7] Gauss and the history of the fast fourier transform. https://faculty.washington.edu/seattle/physics541/%202010-Fourier-transforms/history-3.pdf. Accessed: 2023-02-14.

[8] Digital communication - sampling. https://www.tutorialspoint.com/digital_communication/digital_communication_sampling.htm. Accessed: 2023-02-14.

[9] Digital communication - quantization. https://www.tutorialspoint.com/digital_communication/digital_communication_quantization.htm. Accessed: 2023-05-30.

[10] Andrea Goldsmith. *Wireless communications*. Cambridge University Press, Cambridge, 2nd ed. edition, 2005.

[11] What is aliasing? what causes it? how to avoid it? https://thewolfsound.com/what-is-aliasing-what-causes-it-how-to-avoid-it/. Accessed: 2023-02-23.

[12] Decibel. https://learnemc.com/working-with-decibels. Accessed: 2023-06-07.

[13] Håkan Sollervall and Bo Styf. *Tranformteori för ingenjörer*. Studentlitteratur AB, 1999.

A Tables of measurements

Experiment 2: Tables of measurements

Table 4: Measurements investigating starting position and variation in vertical angle

Measurement	Local time	Vertical angle (θ)	Azimuth angle (α)	Position offset (cm)
1	11:45:54	5.1	-15	0
2	11:46:21	5.1	-15	0
3	11:46:45	5.1	-15	0
4	11:47:09	5.1	-15	0
5	11:47:35	5.1	-15	0
6	11:50:40	31.7	-15	0
7	11:51:08	31.7	-15	0
27	12:24:37	61.5	-15	0
28	12:25:04	61.5	-15	0

Table 5: Measurements investigating different azimuths towards the transmitter

Measurement	Local time	Vertical angle (θ)	Azimuth angle (α)	Position offset (cm)
8	11:54:26	5.1	-7	0
9	11:54:53	5.1	-7	0
10	12:02:19	5.1	11	0
11	12:02:49	5.1	11	0
12	12:04:30	5.1	33	0
13	12:04:57	5.1	33	0
14	12:08:10	5.1	53	0
15	12:08:37	5.1	53	0
16	12:09:07	5.1	53	0
17	12:11:00	5.1	75	0
18	12:11:24	5.1	75	0

Table 6: Measurements investigating different perpendicular positions of WiDAR

Measurement	Local time	Vertical angle (θ)	Azimuth angle (α)	Position offset (cm)
19	12:16:28	5.1	-15	7
20	12:17:32	5.1	-15	7
21	12:18:48	5.1	-15	14
22	12:19:17	5.1	-15	14
23	12:20:06	5.1	-15	21
24	12:20:34	5.1	-15	21
25	12:21:28	5.1	-15	28
26	12:22:03	5.1	-15	28

Experiment 3: Tables of measurements

Table 7: Measurements investigating different azimuth angles

Measurement	Local time	Vertical angle (θ)	Azimuth angle (α)	Position offset (cm)
1	10:46:11	5.1	0	0
2	10:48:43	5.1	5	0
3	10:51:45	5.1	10	0
4	10:52:52	5.1	15	0
5	10:55:09	5.1	20	0
6	10:56:42	5.1	25	0
7	10:57:38	5.1	30	0
8	10:59:07	5.1	35	0
9	11:00:14	5.1	40	0
10	11:01:09	5.1	45	0

Table 8: Measurements investigating different perpendicular positions

Measurement	Local time	Vertical angle (θ)	Azimuth angle (α)	Position offset (cm)
11	11:05:11	5.1	0	0
12	11:06:57	5.1	0	7
13	11:07:57	5.1	0	14
14	11:09:01	5.1	0	21

Table 9: Measurements investigating different antenna elements and RF-channels

Measurement	Local time	Vertical angle (θ)	Azimuth angle (α)	Position offset (cm)
15	11:17:57	5.1	0	21
16	11:23:56	5.1	0	21

B Calibration results

B.1 Phase calibration

B.1.1 Experiment 3: Tables with RMSE before and after calibration

Table 10: Experiment 3: Comparison of RMSE regarding phase for frequency 618 MHz without calibration and with calibration

Measurement	Azimuth	Without calibration	w_{cal} from 618 MHz	w_{cal} from 642 MHz	w_{cal} from 666 MHz
	α	RMSE °	RMSE °	RMSE °	RMSE °
1	0°	28.831	0.205	21.931	24.567
2	5°	28.430	9.740	12.310	16.271
3	10°	31.286	22.0.82	3.859	10.458
4	15°	34.107	30.117	10.705	12.918
5	20°	29.091	26.656	11.810	14.569
6	25°	29.447	27.263	11.350	13.713
7	30°	30.631	26.100	8.854	11.682
8	35°	19.524	15.425	15.927	19.844
9	40°	17.216	15.198	19.325	23.249
10	45°	26.907	22.568	9.663	13.374

Table 11: Experiment 3: Comparison of RMSE regarding phase for frequency 642 MHz without calibration and with calibration

Measurement	Azimuth	Without calibration	w_{cal} from 618 MHz	w_{cal} from 642 MHz	w_{cal} from 666 MHz
	α	RMSE °	RMSE °	RMSE °	RMSE °
1	0°	34.110	20.750	1.414	8.440
2	5°	37.358	28.085	6.792	7.946
3	10°	36.864	29.887	10.129	9.199
4	15°	36.148	27.940	9.080	7.282
5	20°	31.822	23.501	6.799	8.094
6	25°	32.373	23.064	4.983	7.976
7	30°	37.516	28.931	7.929	9.529
8	35°	33.419	24.295	4.095	9.111
9	40°	31.468	22.448	4.670	9.214
10	45°	36.840	27.952	6.830	9.036

Table 12: Experiment 3: Comparison of RMSE regarding phase for frequency 666 MHz without calibration and with calibration

Measurement	Azimuth	Without calibration	w_{cal} from 618 MHz	w_{cal} from 642 MHz	w_{cal} from 666 MHz
	α	RMSE °	RMSE °	RMSE °	RMSE °
1	0°	38.602	24.485	8.109	0.102
2	5°	44.021	30.425	11.454	6.721
3	10°	45.674	34.731	13.909	11.417
4	15°	48.532	41.779	20.184	19.156
5	20°	47.307	42.016	20.399	20.134
6	25°	50.953	46.201	24.493	24.215
7	30°	52.637	48.129	26.455	26.423
8	35°	43.321	37.201	16.030	14.923
9	40°	30.653	22.023	5.641	9.366
10	45°	33.242	25.059	5.689	9.725

B.1.2 Experiment 2: Phase RMSE before and after calibration

Table 13: Experiment 2: Comparison of RMSE regarding phase for frequency 618 MHz without calibration and with calibration

Measurement	Azimuth	Without calibration	w_{cal} from 618 MHz	w_{cal} from 642 MHz	w_{cal} from 666 MHz
	α	RMSE °	RMSE °	RMSE °	RMSE °
1	$-15°$	17.083	14.137	26.224	31.210
8	$-7°$	19.410	22.388	16.633	20.613
10	$11°$	18.672	17.656	16.384	20.587
12	$33°$	32.377	29.284	10.475	14.659
14	$53°$	42.453	39.303	18.105	19.556
17	$75°$	56.001	53.046	32.391	32.534

Table 14: Experiment 2: Comparison of RMSE regarding phase for frequency 642 MHz without calibration and with calibration

Measurement	Azimuth	Without calibration	w_{cal} from 618 MHz	w_{cal} from 642 MHz	w_{cal} from 666 MHz
	α	RMSE °	RMSE °	RMSE °	RMSE °
1	$-15°$	28.130	18.085	7.709	11.486
8	$-7°$	29.459	15.956	6.996	12.295
10	$11°$	28.126	25.426	11.656	13.725
12	$33°$	34.269	25.726	5.071	10.230
14	$53°$	43.860	38.676	17.051	18.606
17	$75°$	52.540	44.356	22.848	22.099

Table 15: Experiment 2: Comparison of RMSE regarding phase for frequency 666 MHz without calibration and with calibration

Measurement	Azimuth	Without calibration	w_{cal} from 618 MHz	w_{cal} from 642 MHz	w_{cal} from 666 MHz
	α	RMSE °	RMSE °	RMSE °	RMSE °
1	$-15°$	34.004	26.797	8.049	9.112
8	$-7°$	29.218	11.425	11.247	14.299
10	$11°$	41.190	37.783	17.412	16.858
12	$33°$	33.701	23.550	2.739	9.324
14	$53°$	43.145	34.697	13.011	14.090
17	$75°$	50.124	42.817	21.306	20.860

B.1.3 Experiment 3, Phase: Figures before and after calibration

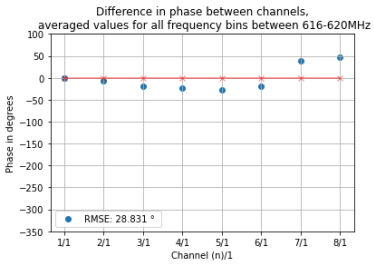

(a) No calibration

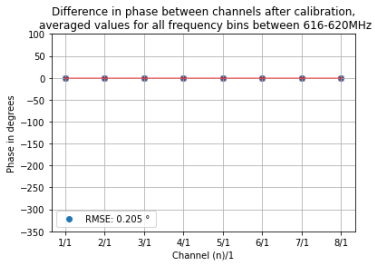

(b) Calibration with w_{cal} from 618 MHz

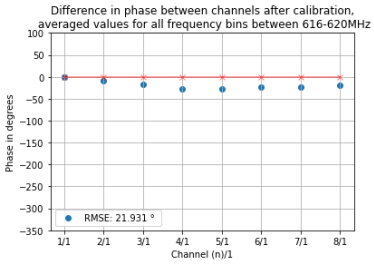

(c) Calibration with w_{cal} from 642 MHz

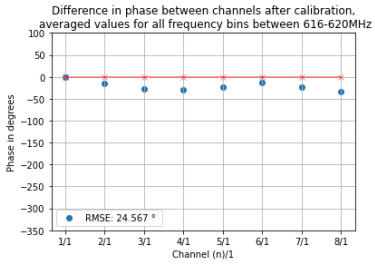

(d) Calibration with w_{cal} from 666 MHz

Figure 31 Experiment 3, Measurement 1: Phase difference between each channel and channel 1, compared with theoretical expected values. Frequency f = 618, azimuth α = 0.

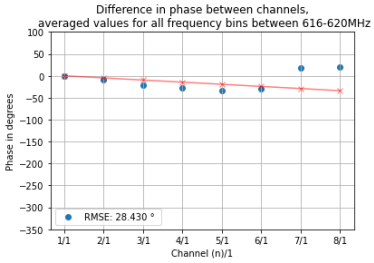

(a) No calibration

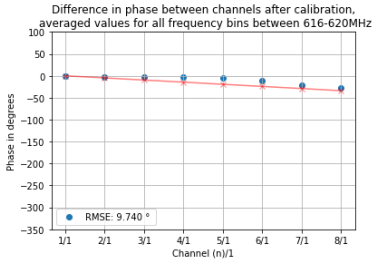

(b) Calibration with w_{cal} from 618 MHz

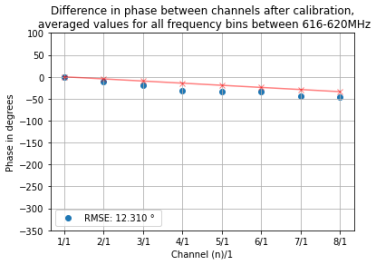

(c) Calibration with w_{cal} from 642 MHz

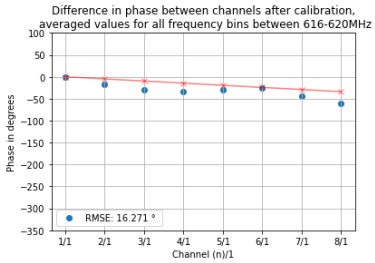

(d) Calibration with w_{cal} from 666 MHz

Figure 32 Experiment 3, Measurement 2: Phase difference between each channel and channel 1, compared with theoretical expected values. Frequency f = 618, azimuth α = 5.

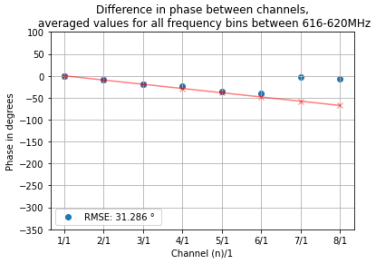

(a) No calibration

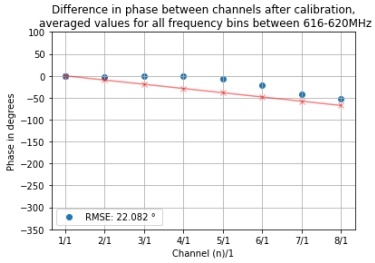

(b) Calibration with w_{cal} from 618 MHz

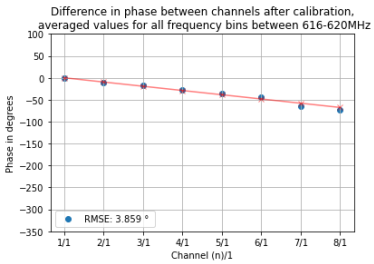

(c) Calibration with w_{cal} from 642 MHz

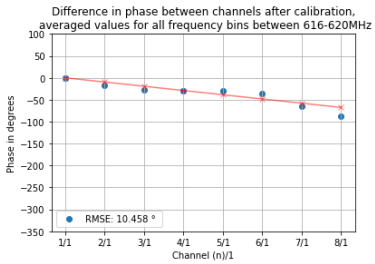

(d) Calibration with w_{cal} from 666 MHz

Figure 33 Experiment 3, Measurement 3: Phase difference between each channel and channel 1, compared with theoretical expected values. Frequency f = 618, azimuth α = 10.

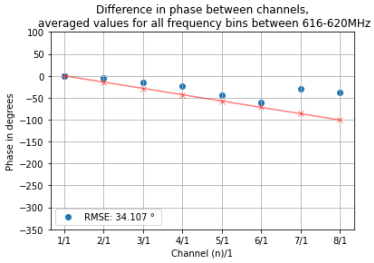

(a) No calibration

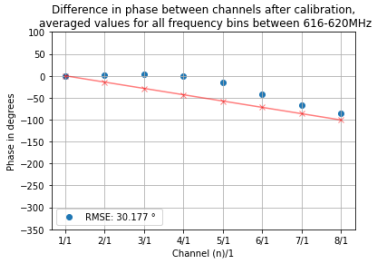

(b) Calibration with w_{cal} from 618 MHz

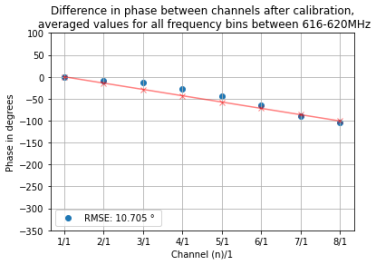

(c) Calibration with w_{cal} from 642 MHz

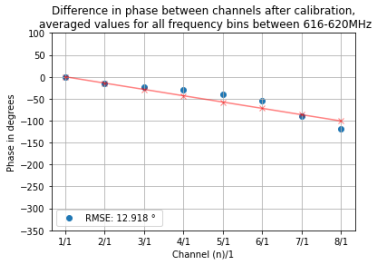

(d) Calibration with w_{cal} from 666 MHz

Figure 34 Experiment 3, Measurement 4: Phase difference between each channel and channel 1, compared with theoretical expected values. Frequency f = 618, azimuth α = 15.

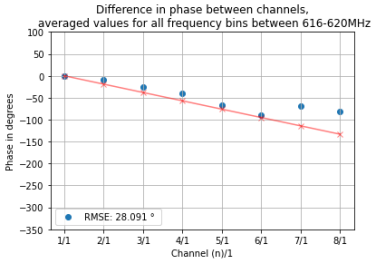

(a) No calibration

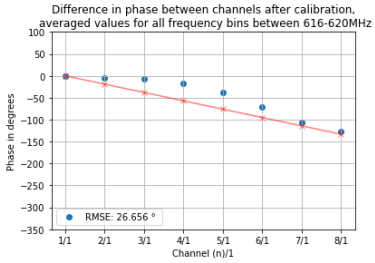

(b) Calibration with w_{cal} from 618 MHz

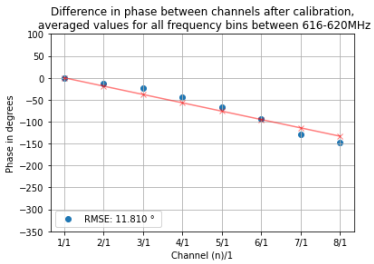

(c) Calibration with w_{cal} from 642 MHz

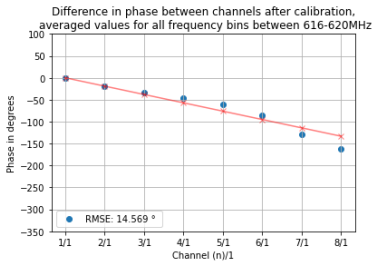

(d) Calibration with w_{cal} from 666 MHz

Figure 35 Experiment 3, Measurement 5: Phase difference between each channel and channel 1, compared with theoretical expected values. Frequency f = 618, azimuth α = 20.

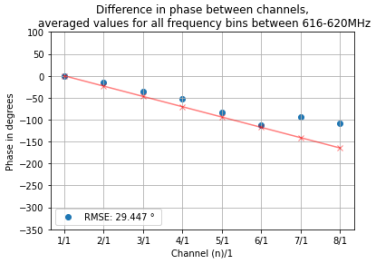

(a) No calibration

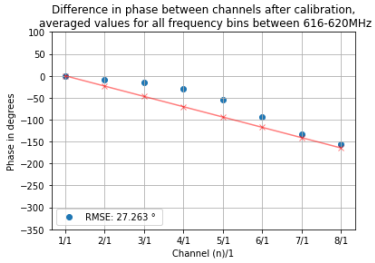

(b) Calibration with w_{cal} from 618 MHz

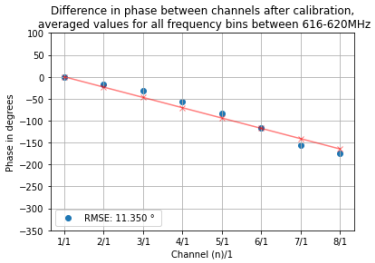

(c) Calibration with w_{cal} from 642 MHz

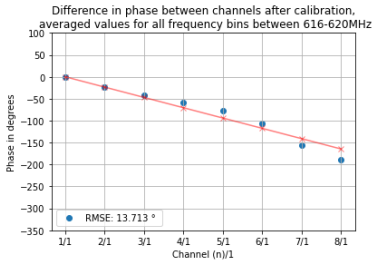

(d) Calibration with w_{cal} from 666 MHz

Figure 36 Experiment 3, Measurement 3: Phase difference between each channel and channel 1, compared with theoretical expected values. Frequency f = 618, azimuth α = 25.

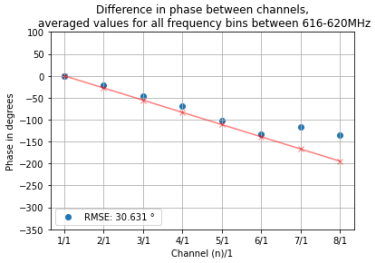

(a) No calibration

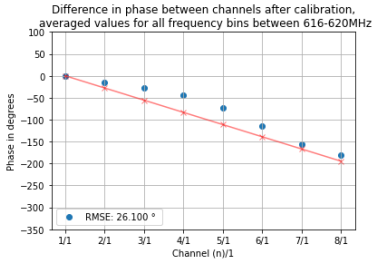

(b) Calibration with w_{cal} from 618 MHz

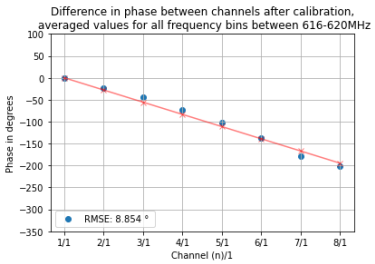

(c) Calibration with w_{cal} from 642 MHz

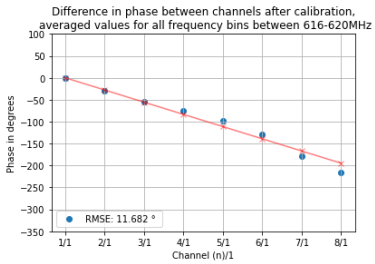

(d) Calibration with w_{cal} from 666 MHz

Figure 37 Experiment 3, Measurement 7: Phase difference between each channel and channel 1, compared with theoretical expected values. Frequency f = 618, azimuth α = 30.

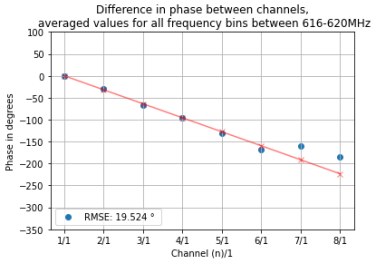

(a) No calibration

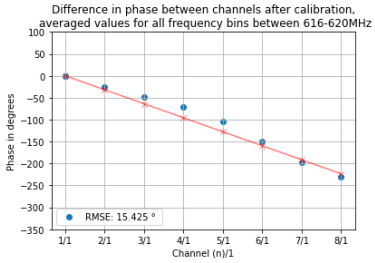

(b) Calibration with w_{cal} from 618 MHz

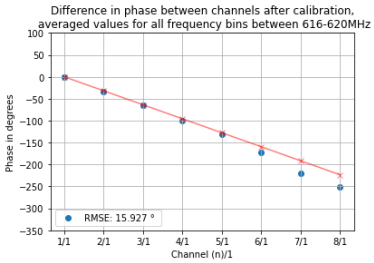

(c) Calibration with w_{cal} from 642 MHz

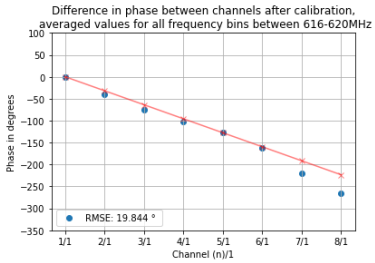

(d) Calibration with w_{cal} from 666 MHz

Figure 38 Experiment 3, Measurement 8: Phase difference between each channel and channel 1, compared with theoretical expected values. Frequency f = 618, azimuth α = 35.

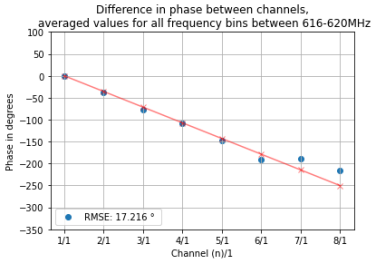

(a) No calibration

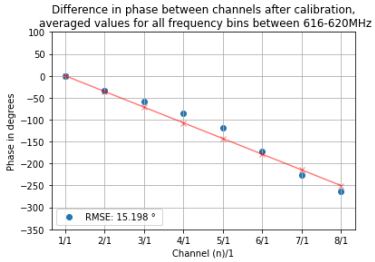

(b) Calibration with w_{cal} from 618 MHz

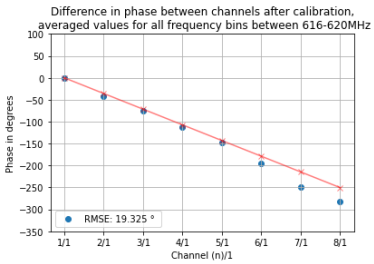

(c) Calibration with w_{cal} from 642 MHz

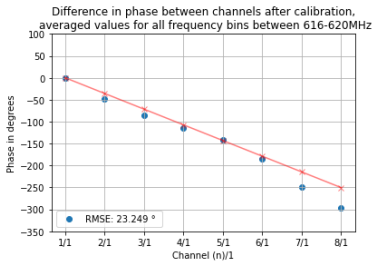

(d) Calibration with w_{cal} from 666 MHz

Figure 39 Experiment 3, Measurement 9: Phase difference between each channel and channel 1, compared with theoretical expected values. Frequency f = 618, azimuth α = 40.

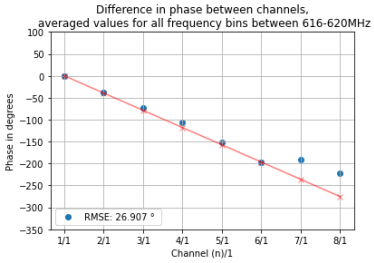

(a) No calibration

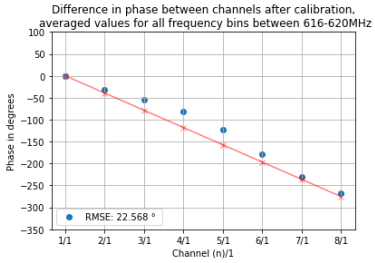

(b) Calibration with w_{cal} from 618 MHz

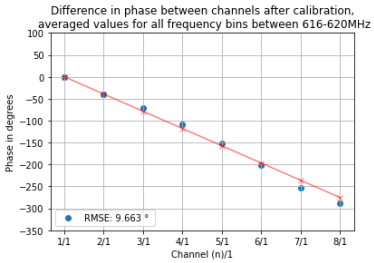

(c) Calibration with w_{cal} from 642 MHz

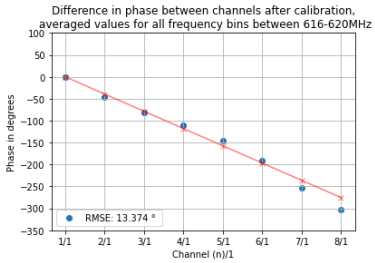

(d) Calibration with w_{cal} from 666 MHz

Figure 40 Experiment 3, Measurement 10: Phase difference between each channel and channel 1, compared with theoretical expected values. Frequency $f = 618$, azimuth $\alpha = 45$.

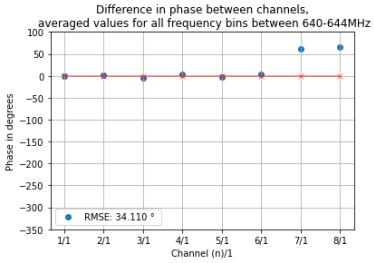

(a) No calibration

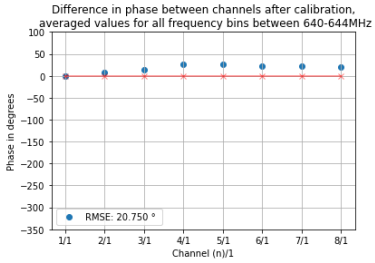

(b) Calibration with w_{cal} from 618 MHz

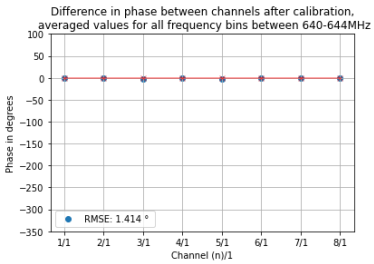

(c) Calibration with w_{cal} from 642 MHz

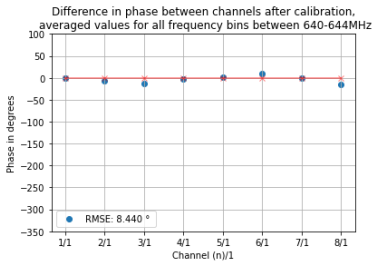

(d) Calibration with w_{cal} from 666 MHz

Figure 41 Experiment 3, Measurement 1: Phase difference between each channel and channel 1, compared with theoretical expected values. Frequency $f = 642$, azimuth $\alpha = 0$.

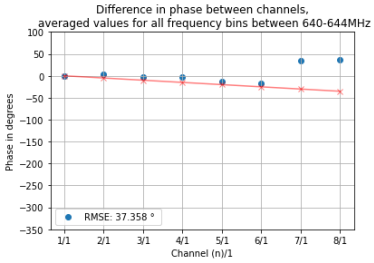

(a) No calibration

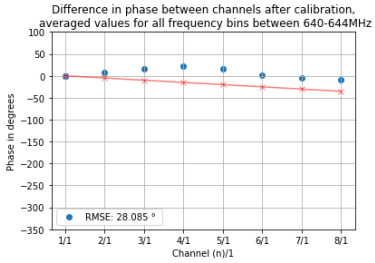

(b) Calibration with w_{cal} from 618 MHz

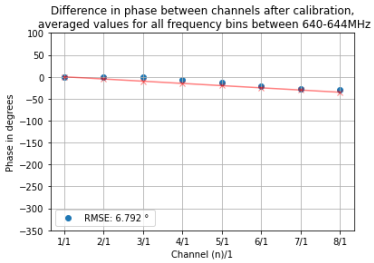

(c) Calibration with w_{cal} from 642 MHz

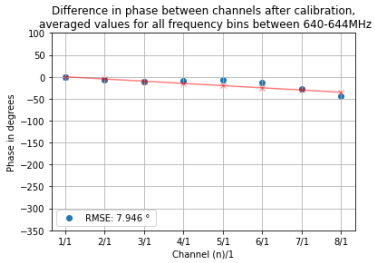

(d) Calibration with w_{cal} from 666 MHz

Figure 42 Experiment 3, Measurement 2: Phase difference between each channel and channel 1, compared with theoretical expected values. Frequency f = 642, azimuth α = 5.

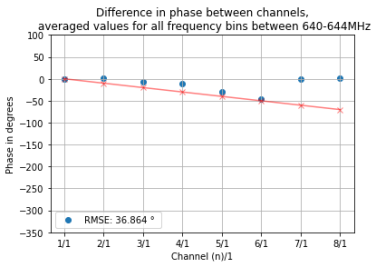

(a) No calibration

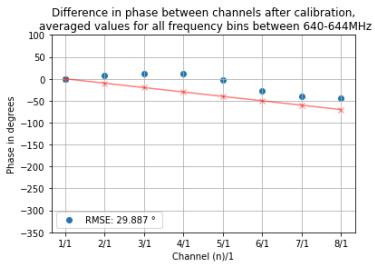

(b) Calibration with w_{cal} from 618 MHz

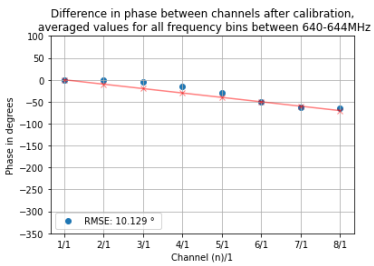

(c) Calibration with w_{cal} from 642 MHz

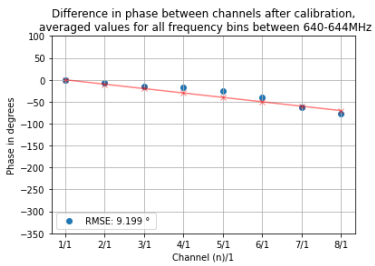

(d) Calibration with w_{cal} from 666 MHz

Figure 43 Experiment 3, Measurement 3: Phase difference between each channel and channel 1, compared with theoretical expected values. Frequency f = 642, azimuth α = 10.

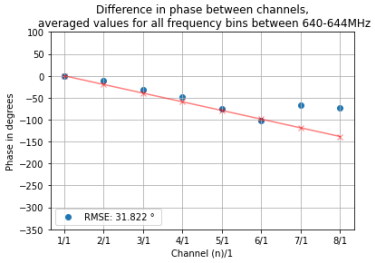

(a) No calibration

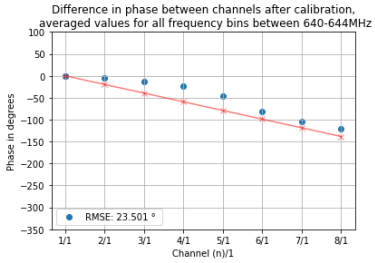

(b) Calibration with w_{cal} from 618 MHz

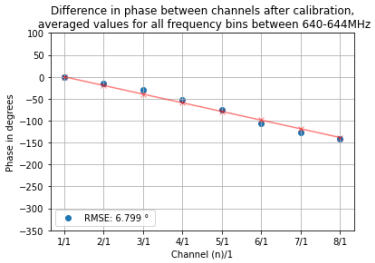

(c) Calibration with w_{cal} from 642 MHz

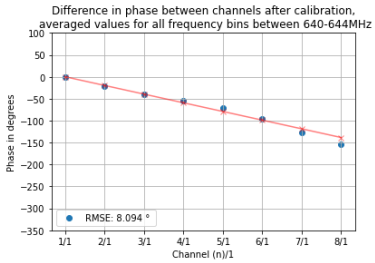

(d) Calibration with w_{cal} from 666 MHz

Figure 45 Experiment 3, Measurement 5: Phase difference between each channel and channel 1, compared with theoretical expected values. Frequency f = 642, azimuth α = 20.

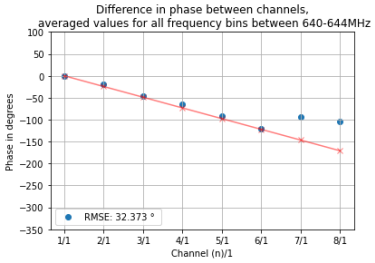

(a) No calibration

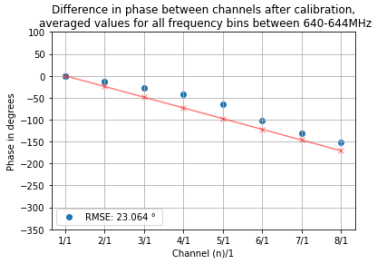

(b) Calibration with w_{cal} from 618 MHz

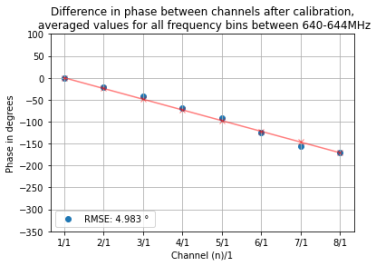

(c) Calibration with w_{cal} from 642 MHz

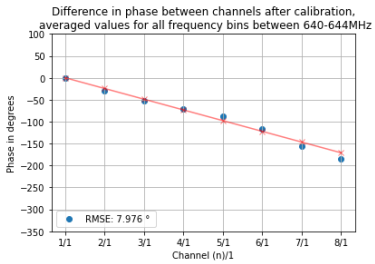

(d) Calibration with w_{cal} from 666 MHz

Figure 46 Experiment 3, Measurement 6: Phase difference between each channel and channel 1, compared with theoretical expected values. Frequency f = 642, azimuth α = 25.

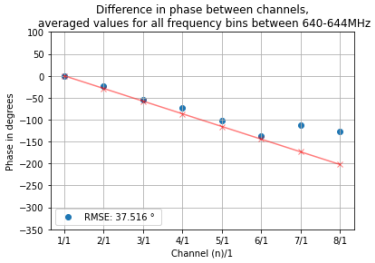

(a) No calibration

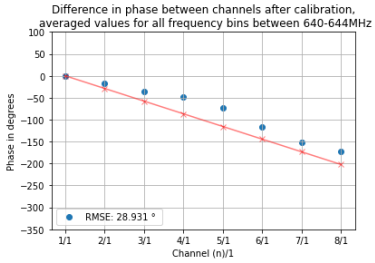

(b) Calibration with w_{cal} from 618 MHz

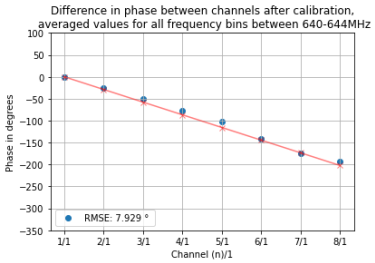

(c) Calibration with w_{cal} from 642 MHz

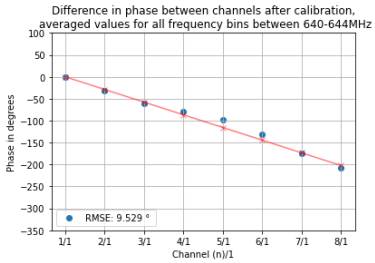

(d) Calibration with w_{cal} from 666 MHz

Figure 47 Experiment 3, Measurement 7: Phase difference between each channel and channel 1, compared with theoretical expected values. Frequency f = 642, azimuth α = 30.

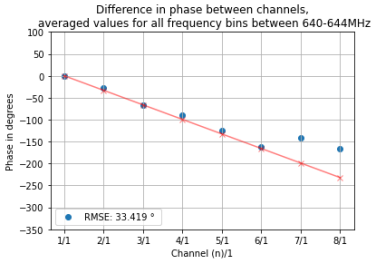

(a) No calibration

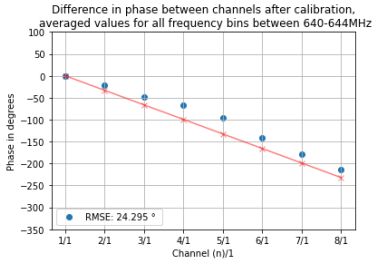

(b) Calibration with w_{cal} from 618 MHz

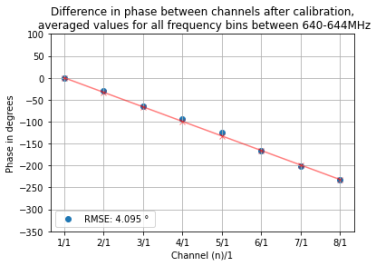

(c) Calibration with w_{cal} from 642 MHz

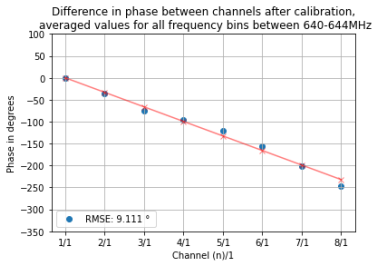

(d) Calibration with w_{cal} from 666 MHz

Figure 48 Experiment 3, Measurement 8: Phase difference between each channel and channel 1, compared with theoretical expected values. Frequency f = 642, azimuth α = 35.

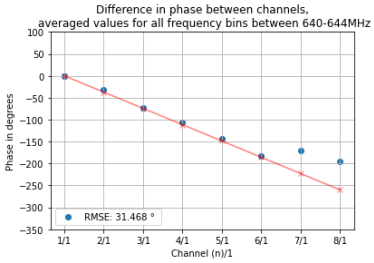

(a) No calibration

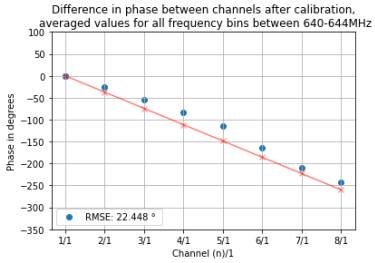

(b) Calibration with w_{cal} from 618 MHz

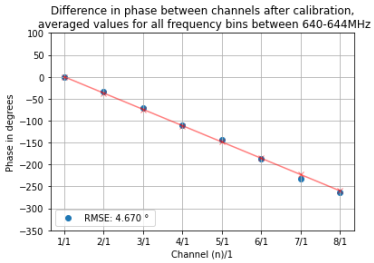

(c) Calibration with w_{cal} from 642 MHz

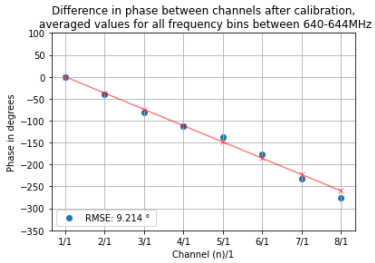

(d) Calibration with w_{cal} from 666 MHz

Figure 49 Experiment 3, Measurement 9: Phase difference between each channel and channel 1, compared with theoretical expected values. Frequency $f = 642$, azimuth $\alpha = 40$.

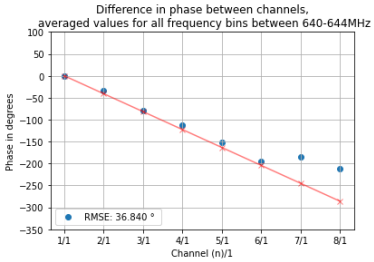

(a) No calibration

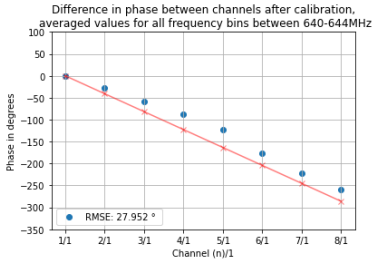

(b) Calibration with w_{cal} from 618 MHz

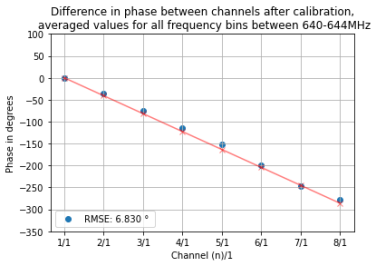

(c) Calibration with w_{cal} from 642 MHz

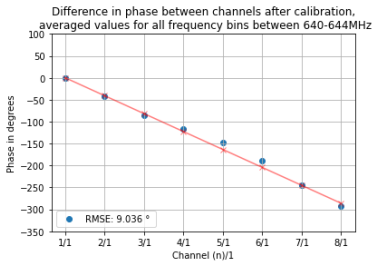

(d) Calibration with w_{cal} from 666 MHz

Figure 50 Experiment 3, Measurement 10: Phase difference between each channel and channel 1, compared with theoretical expected values. Frequency $f = 642$, azimuth $\alpha = 45$.

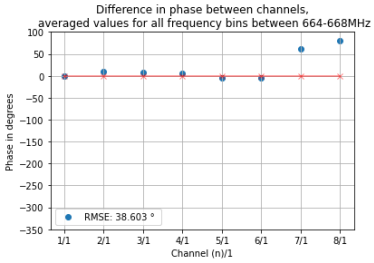

(a) No calibration

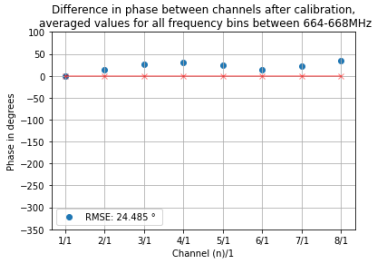

(b) Calibration with w_{cal} from 618 MHz

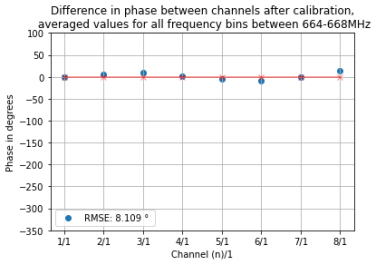

(c) Calibration with w_{cal} from 642 MHz

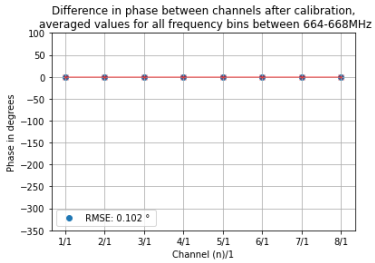

(d) Calibration with w_{cal} from 666 MHz

Figure 51 Experiment 3, Measurement 1: Phase difference between each channel and channel 1, compared with theoretical expected values. Frequency f = 666, azimuth α = 0.

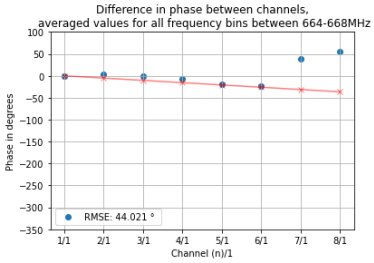

(a) No calibration

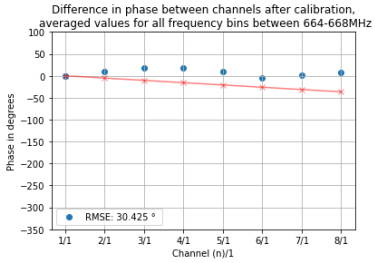

(b) Calibration with w_{cal} from 618 MHz

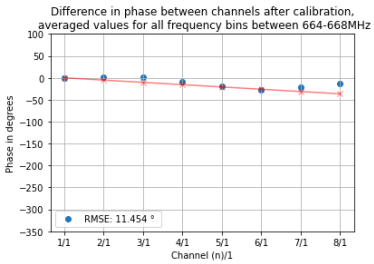

(c) Calibration with w_{cal} from 642 MHz

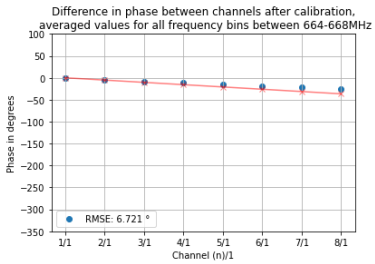

(d) Calibration with w_{cal} from 666 MHz

Figure 52 Experiment 3, Measurement 2: Phase difference between each channel and channel 1, compared with theoretical expected values. Frequency f = 666, azimuth α = 5.

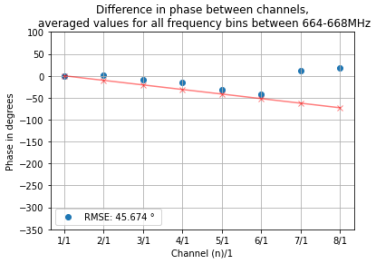

(a) No calibration

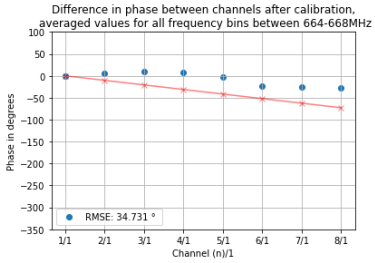

(b) Calibration with w_{cal} from 618 MHz

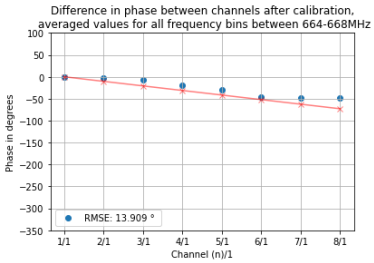

(c) Calibration with w_{cal} from 642 MHz

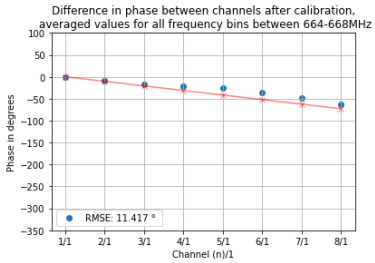

(d) Calibration with w_{cal} from 666 MHz

Figure 53 Experiment 3, Measurement 3: Phase difference between each channel and channel 1, compared with theoretical expected values. Frequency f = 666, azimuth α = 10.

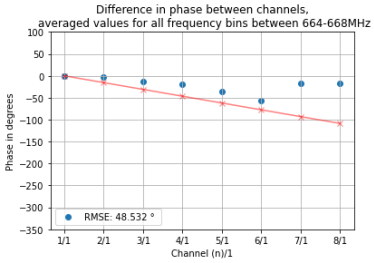

(a) No calibration

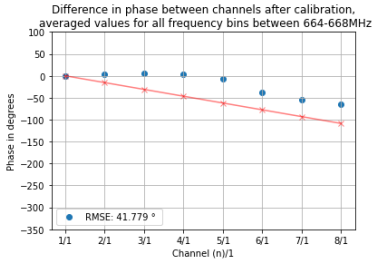

(b) Calibration with w_{cal} from 618 MHz

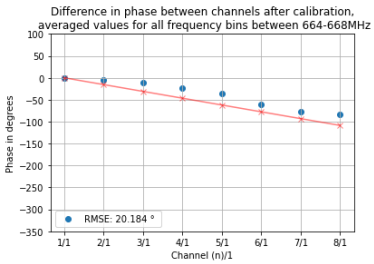

(c) Calibration with w_{cal} from 642 MHz

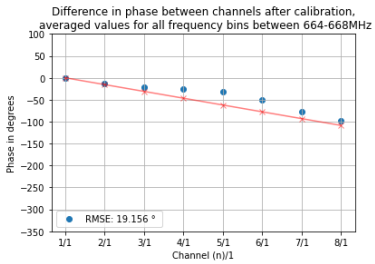

(d) Calibration with w_{cal} from 666 MHz

Figure 54 Experiment 3, Measurement 4: Phase difference between each channel and channel 1, compared with theoretical expected values. Frequency f = 666, azimuth α = 15.

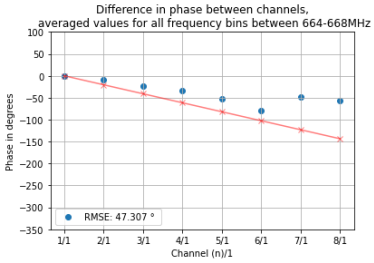

(a) No calibration

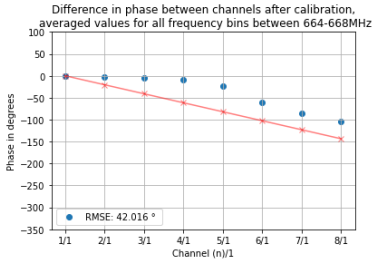

(b) Calibration with w_{cal} from 618 MHz

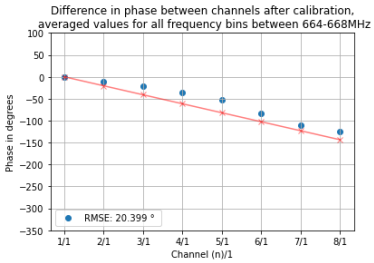

(c) Calibration with w_{cal} from 642 MHz

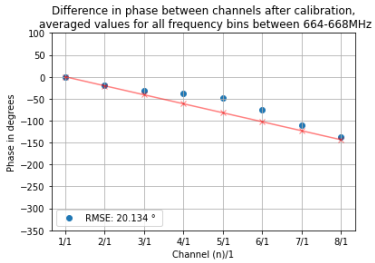

(d) Calibration with w_{cal} from 666 MHz

Figure 55 Experiment 3, Measurement 5: Phase difference between each channel and channel 1, compared with theoretical expected values. Frequency f = 666, azimuth α = 20.

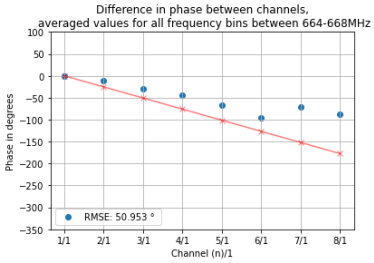

(a) No calibration

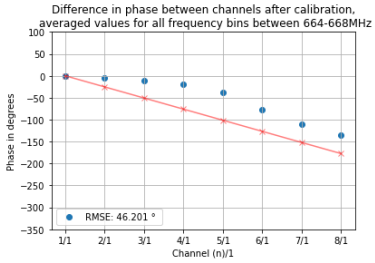

(b) Calibration with w_{cal} from 618 MHz

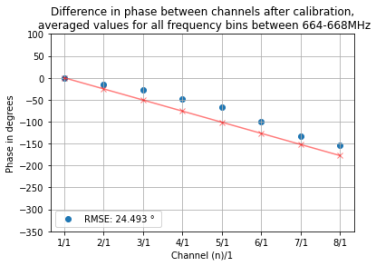

(c) Calibration with w_{cal} from 642 MHz

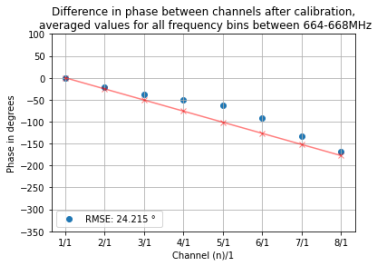

(d) Calibration with w_{cal} from 666 MHz

Figure 56 Experiment 3, Measurement 6: Phase difference between each channel and channel 1, compared with theoretical expected values. Frequency f = 666, azimuth α = 25.

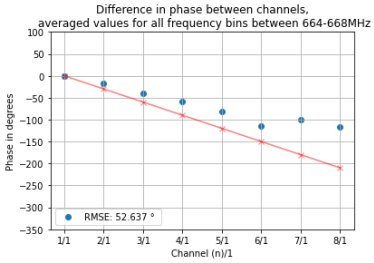

(a) No calibration

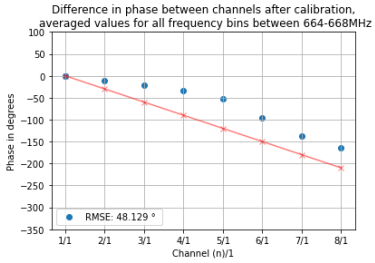

(b) Calibration with w_{cal} from 618 MHz

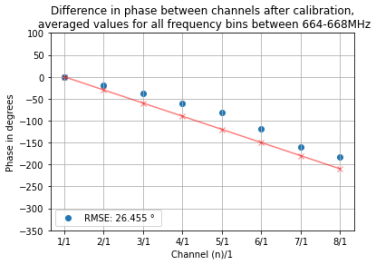

(c) Calibration with w_{cal} from 642 MHz

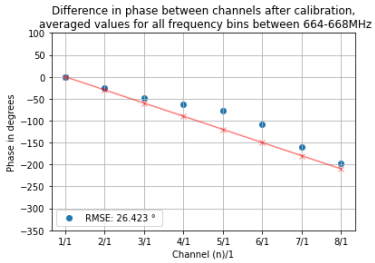

(d) Calibration with w_{cal} from 666 MHz

Figure 57 Experiment 3, Measurement 7: Phase difference between each channel and channel 1, compared with theoretical expected values. Frequency f = 666, azimuth α = 30.

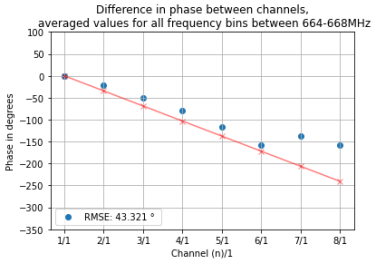

(a) No calibration

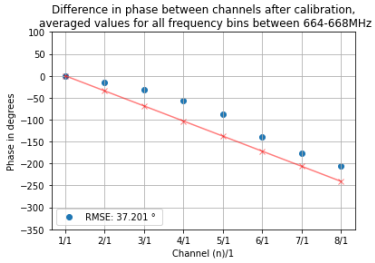

(b) Calibration with w_{cal} from 618 MHz

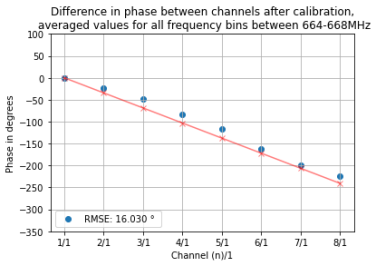

(c) Calibration with w_{cal} from 642 MHz

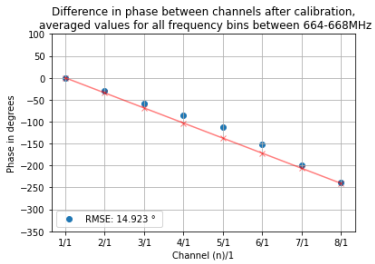

(d) Calibration with w_{cal} from 666 MHz

Figure 58 Experiment 3, Measurement 8: Phase difference between each channel and channel 1, compared with theoretical expected values. Frequency f = 666, azimuth α = 35.

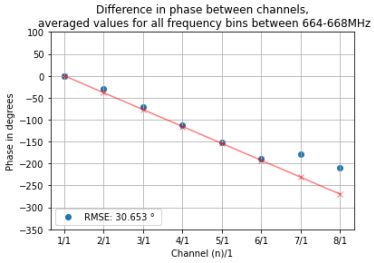

(a) No calibration

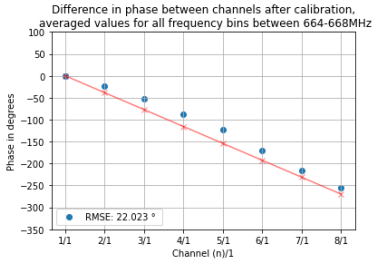

(b) Calibration with w_{cal} from 618 MHz

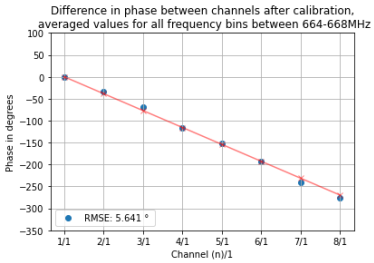

(c) Calibration with w_{cal} from 642 MHz

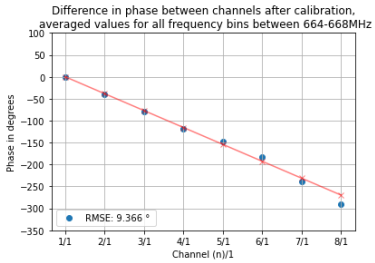

(d) Calibration with w_{cal} from 666 MHz

Figure 59 Experiment 3, Measurement 9: Phase difference between each channel and channel 1, compared with theoretical expected values. Frequency f = 666, azimuth α = 40.

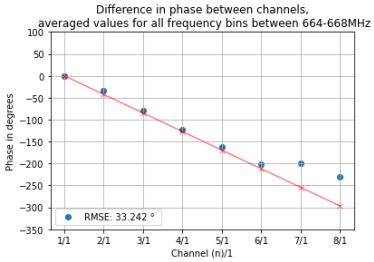

(a) No calibration

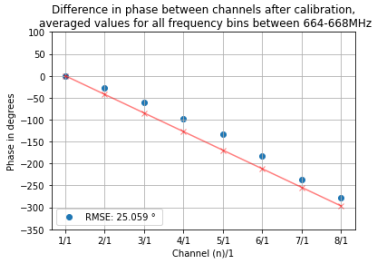

(b) Calibration with w_{cal} from 618 MHz

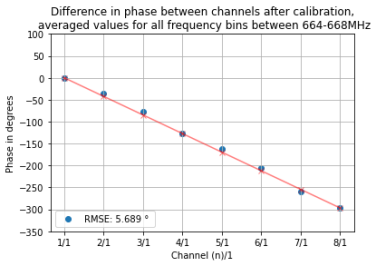

(c) Calibration with w_{cal} from 642 MHz

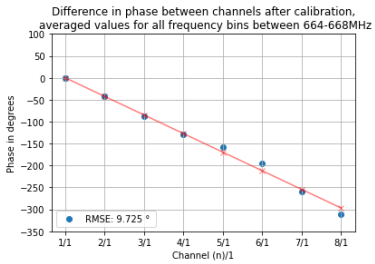

(d) Calibration with w_{cal} from 666 MHz

Figure 60 Experiment 3, Measurement 10: Phase difference between each channel and channel 1, compared with theoretical expected values. Frequency f = 666, azimuth α = 45.

B.1.4 Experiment 2, Phase: Figures before and after calibration

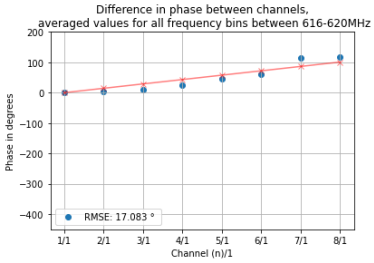

(a) No calibration

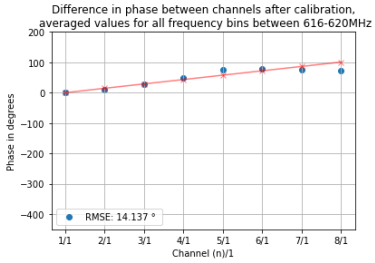

(b) Calibration with w_{cal} from 618 MHz

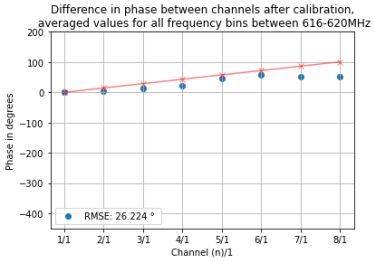

(c) Calibration with w_{cal} from 642 MHz

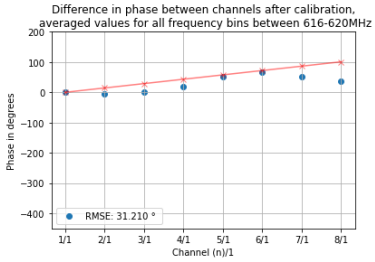

(d) Calibration with w_{cal} from 666 MHz

Figure 61 Experiment 2, Measurement 1: Phase difference between each channel and channel 1, compared with theoretical expected values. Frequency f = 618, azimuth α = -15.

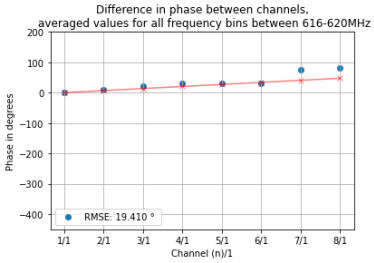

(a) No calibration

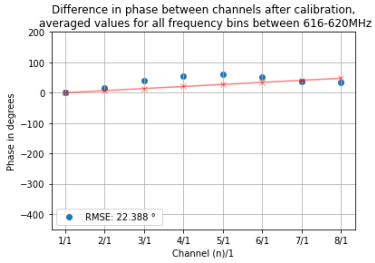

(b) Calibration with w_{cal} from 618 MHz

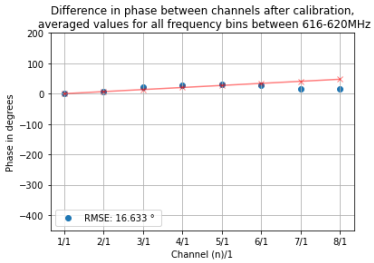

(c) Calibration with w_{cal} from 642 MHz

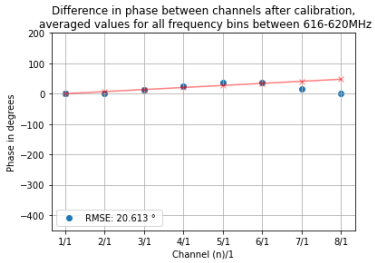

(d) Calibration with w_{cal} from 666 MHz

Figure 62 Experiment 2, Measurement 8: Phase difference between each channel and channel 1, compared with theoretical expected values. Frequency f = 618, azimuth α = -7.

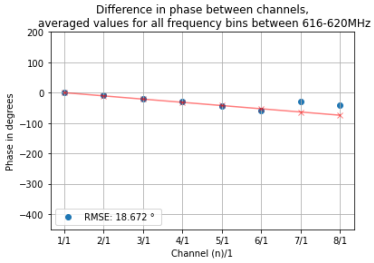

(a) No calibration

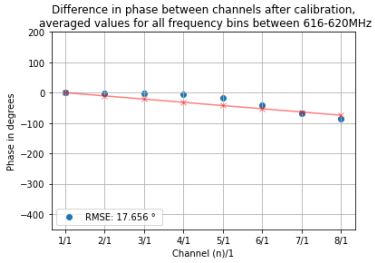

(b) Calibration with w_{cal} from 618 MHz

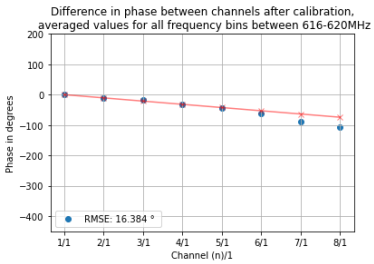

(c) Calibration with w_{cal} from 642 MHz

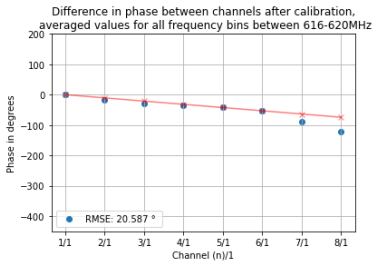

(d) Calibration with w_{cal} from 666 MHz

Figure 63 Experiment 2, Measurement 10: Phase difference between each channel and channel 1, compared with theoretical expected values. Frequency f = 618, azimuth α = 11.

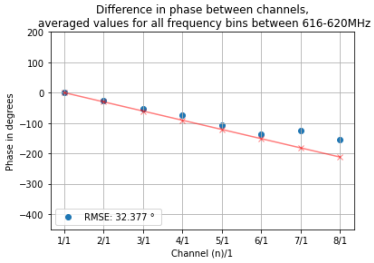

(a) No calibration

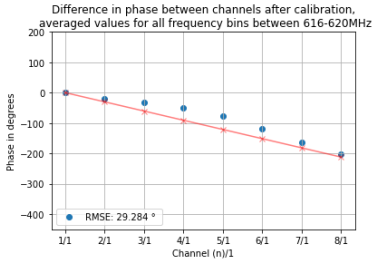

(b) Calibration with w_{cal} from 618 MHz

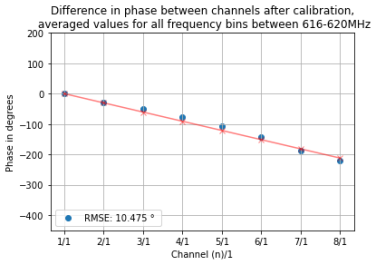

(c) Calibration with w_{cal} from 642 MHz

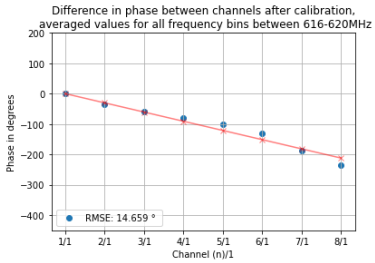

(d) Calibration with w_{cal} from 666 MHz

Figure 64 Experiment 2, Measurement 12: Phase difference between each channel and channel 1, compared with theoretical expected values. Frequency f = 618, azimuth α = 33.

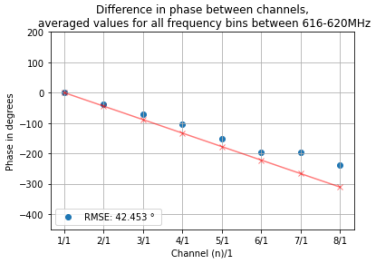

(a) No calibration

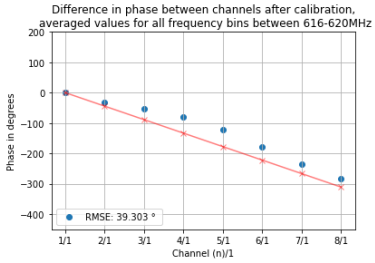

(b) Calibration with w_{cal} from 618 MHz

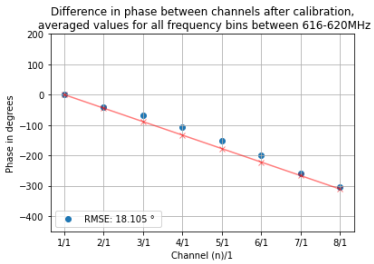

(c) Calibration with w_{cal} from 642 MHz

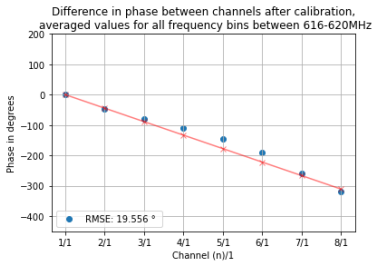

(d) Calibration with w_{cal} from 666 MHz

Figure 65 Experiment 2, Measurement 14: Phase difference between each channel and channel 1, compared with theoretical expected values. Frequency f = 618, azimuth α = 53.

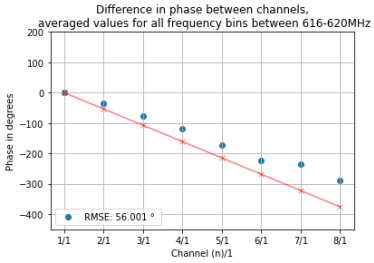

(a) No calibration

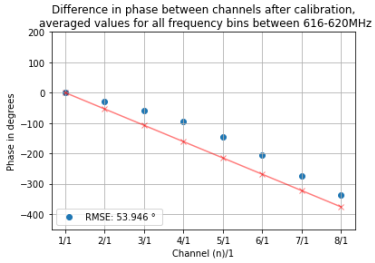

(b) Calibration with w_{cal} from 618 MHz

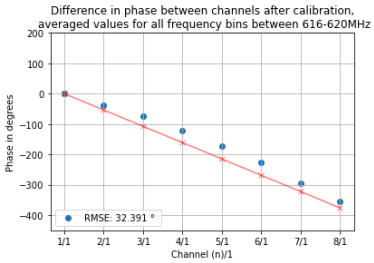

(c) Calibration with w_{cal} from 642 MHz

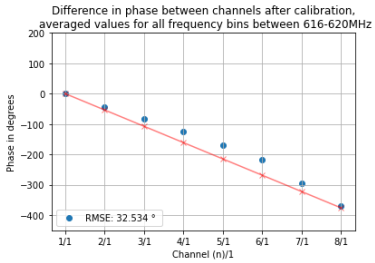

(d) Calibration with w_{cal} from 666 MHz

Figure 66 Experiment 2, Measurement 17: Phase difference between each channel and channel 1, compared with theoretical expected values. Frequency f = 618, azimuth α = 73.

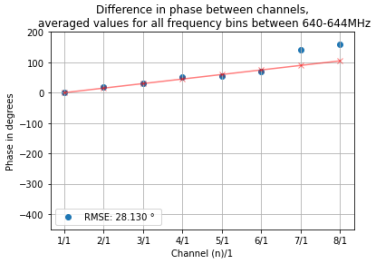

(a) No calibration

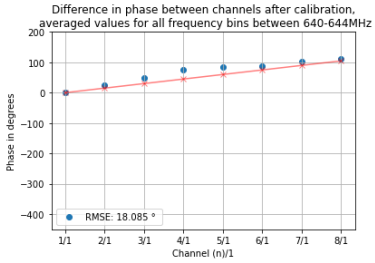

(b) Calibration with w_{cal} from 618 MHz

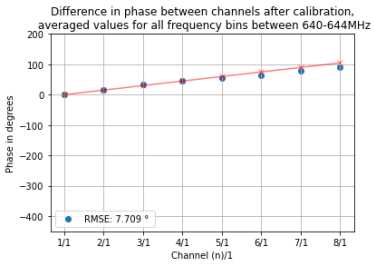

(c) Calibration with w_{cal} from 642 MHz

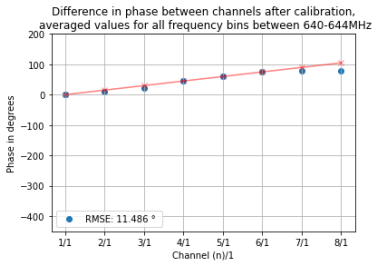

(d) Calibration with w_{cal} from 666 MHz

Figure 67 Experiment 2, Measurement 1: Phase difference between each channel and channel 1, compared with theoretical expected values. Frequency f = 642, azimuth α = -15.

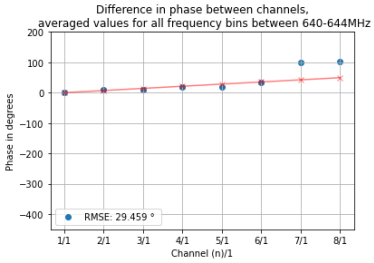

(a) No calibration

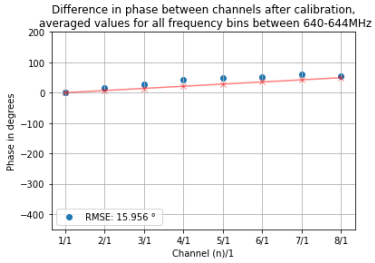

(b) Calibration with w_{cal} from 618 MHz

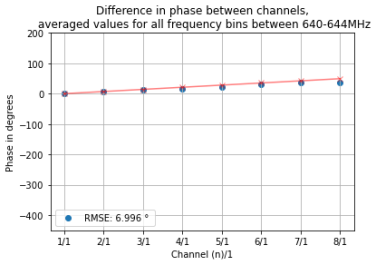

(c) Calibration with w_{cal} from 642 MHz

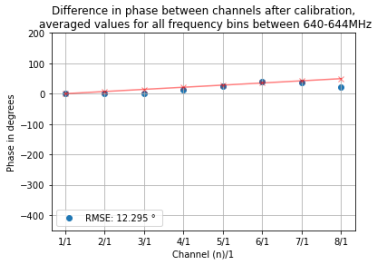

(d) Calibration with w_{cal} from 666 MHz

Figure 68 Experiment 2, Measurement 8: Phase difference between each channel and channel 1, compared with theoretical expected values. Frequency f = 642, azimuth α = -7.

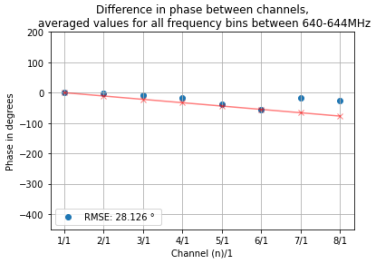

(a) No calibration

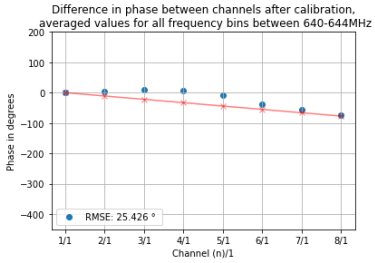

(b) Calibration with w_{cal} from 618 MHz

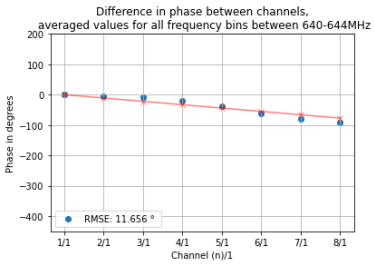

(c) Calibration with w_{cal} from 642 MHz

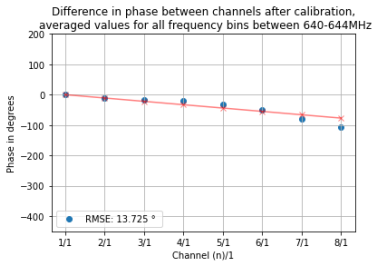

(d) Calibration with w_{cal} from 666 MHz

Figure 69 Experiment 2, Measurement 10: Phase difference between each channel and channel 1, compared with theoretical expected values. Frequency f = 642, azimuth α = 11.

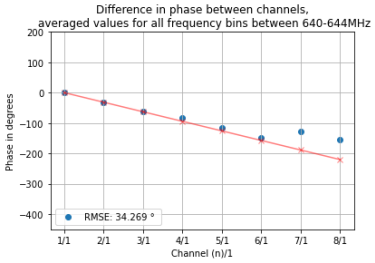

(a) No calibration

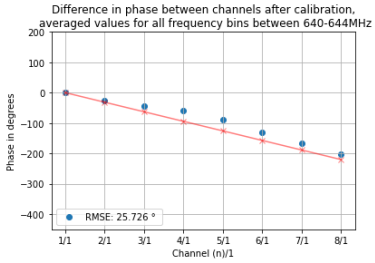

(b) Calibration with w_{cal} from 618 MHz

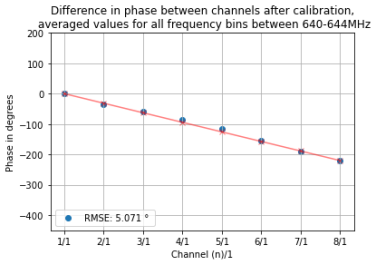

(c) Calibration with w_{cal} from 642 MHz

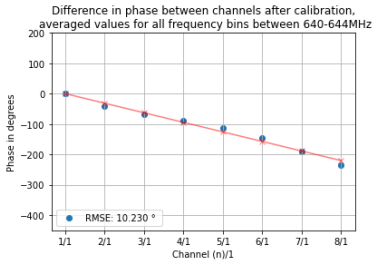

(d) Calibration with w_{cal} from 666 MHz

Figure 70 Experiment 2, Measurement 12: Phase difference between each channel and channel 1, compared with theoretical expected values. Frequency f = 642, azimuth α = 33.

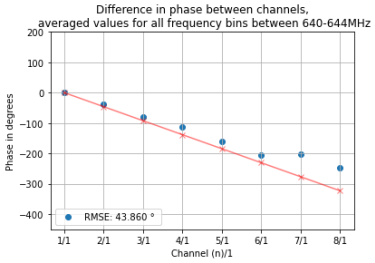

(a) No calibration

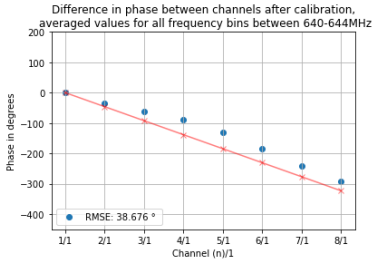

(b) Calibration with w_{cal} from 618 MHz

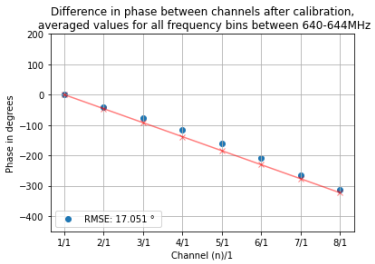

(c) Calibration with w_{cal} from 642 MHz

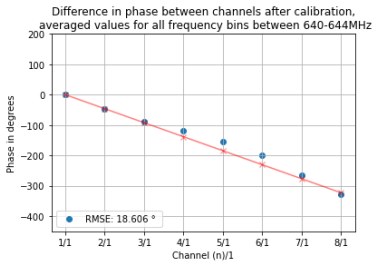

(d) Calibration with w_{cal} from 666 MHz

Figure 71 Experiment 2, Measurement 14: Phase difference between each channel and channel 1, compared with theoretical expected values. Frequency f = 642, azimuth α = 53.

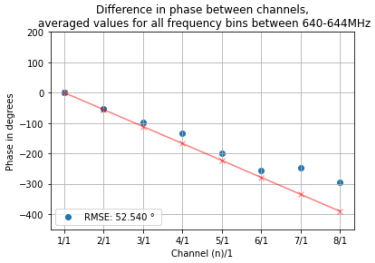

(a) No calibration

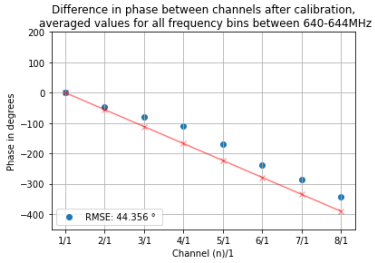

(b) Calibration with w_{cal} from 618 MHz

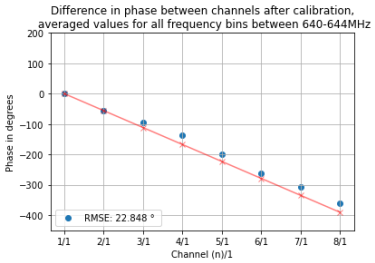

(c) Calibration with w_{cal} from 642 MHz

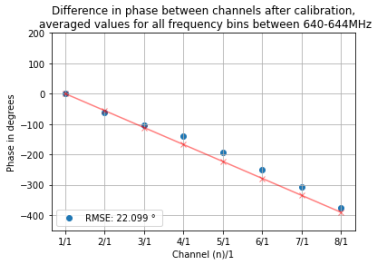

(d) Calibration with w_{cal} from 666 MHz

Figure 72 Experiment 2, Measurement 17: Phase difference between each channel and channel 1, compared with theoretical expected values. Frequency f = 642, azimuth α = 73.

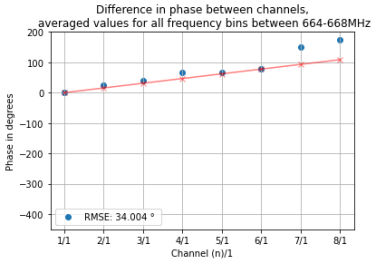

(a) No calibration

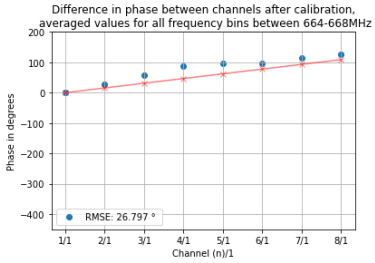

(b) Calibration with w_{cal} from 618 MHz

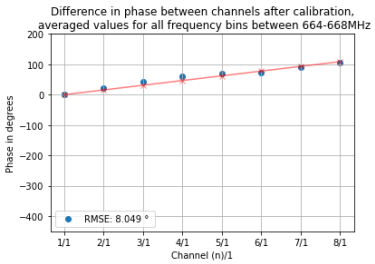

(c) Calibration with w_{cal} from 642 MHz

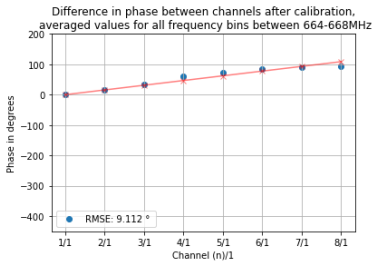

(d) Calibration with w_{cal} from 666 MHz

Figure 73 Experiment 2, Measurement 1: Phase difference between each channel and channel 1, compared with theoretical expected values. Frequency f = 666, azimuth α = -15.

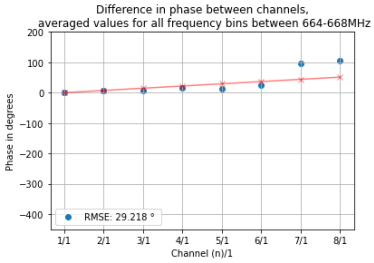

(a) No calibration

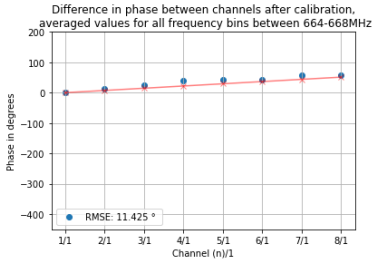

(b) Calibration with w_{cal} from 618 MHz

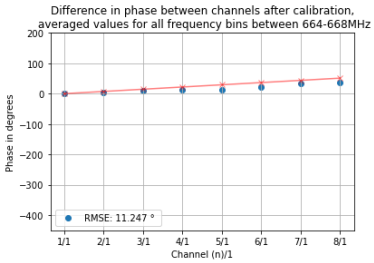

(c) Calibration with w_{cal} from 642 MHz

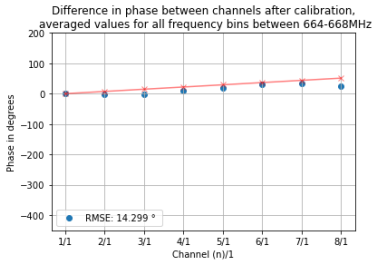

(d) Calibration with w_{cal} from 666 MHz

Figure 74 Experiment 2, Measurement 8: Phase difference between each channel and channel 1, compared with theoretical expected values. Frequency f = 666, azimuth α = -7.

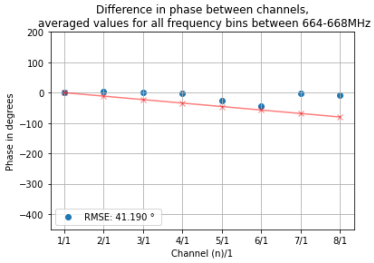

(a) No calibration

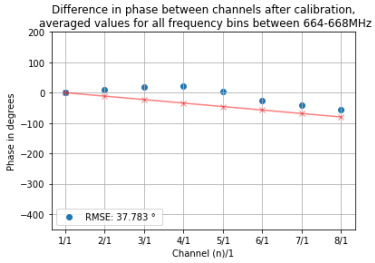

(b) Calibration with w_{cal} from 618 MHz

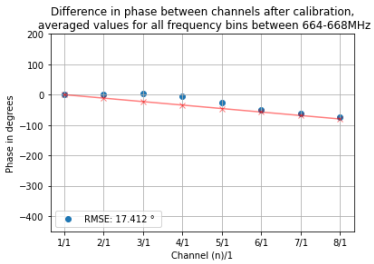

(c) Calibration with w_{cal} from 642 MHz

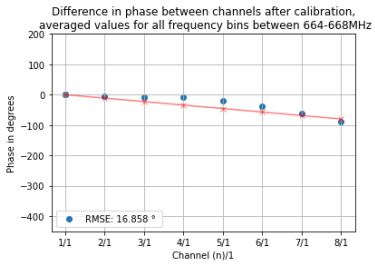

(d) Calibration with w_{cal} from 666 MHz

Figure 75 Experiment 2, Measurement 10: Phase difference between each channel and channel 1, compared with theoretical expected values. Frequency f = 666, azimuth α = 11.

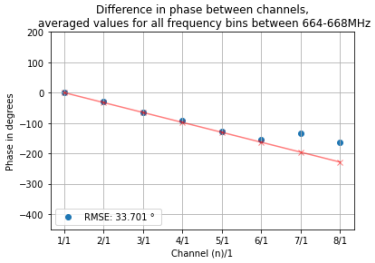

(a) No calibration

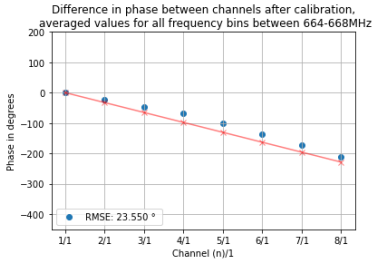

(b) Calibration with w_{cal} from 618 MHz

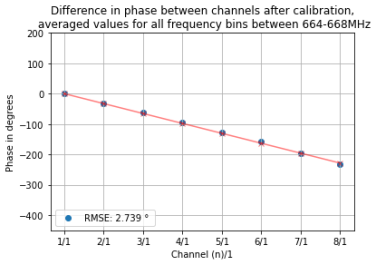

(c) Calibration with w_{cal} from 642 MHz

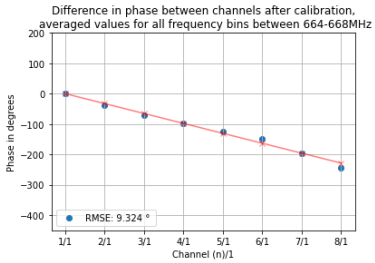

(d) Calibration with w_{cal} from 666 MHz

Figure 76 Experiment 2, Measurement 12: Phase difference between each channel and channel 1, compared with theoretical expected values. Frequency f = 666, azimuth α = 33.

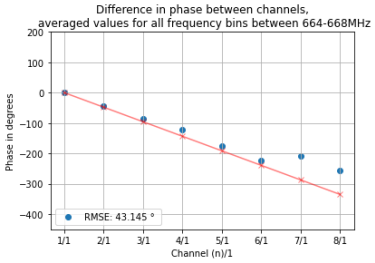

(a) No calibration

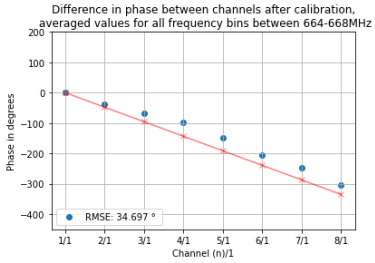

(b) Calibration with w_{cal} from 618 MHz

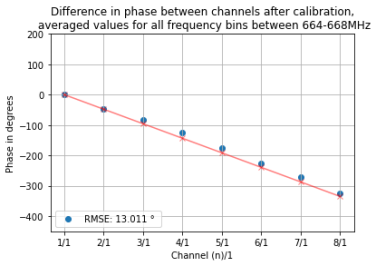

(c) Calibration with w_{cal} from 642 MHz

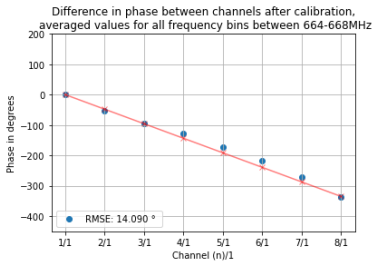

(d) Calibration with w_{cal} from 666 MHz

Figure 77 Experiment 2, Measurement 14: Phase difference between each channel and channel 1, compared with theoretical expected values. Frequency f = 666, azimuth α = 53.

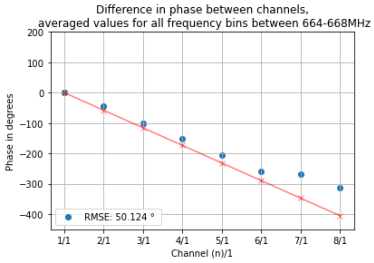

(a) No calibration

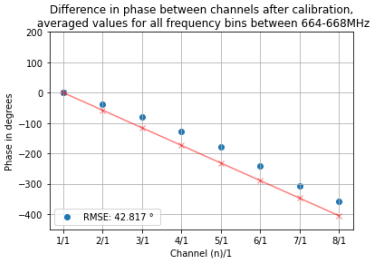

(b) Calibration with w_{cal} from 618 MHz

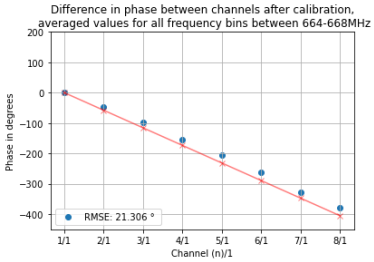

(c) Calibration with w_{cal} from 642 MHz

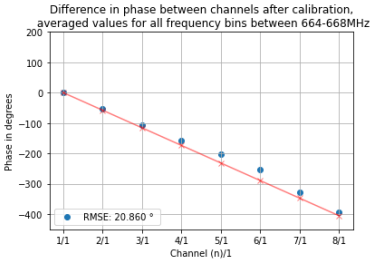

(d) Calibration with w_{cal} from 666 MHz

Figure 78 Experiment 2, Measurement 17: Phase difference between each channel and channel 1, compared with theoretical expected values. Frequency f = 666, azimuth α = 73.

B.2 Magnitude calibration

B.2.1 Experiment 3: Tables with RMSE before and after calibration

Table 16: Experiment 3: Comparison of RMSE regarding magnitude for frequency 618 MHz without calibration and with calibration

Measurement	Azimuth	Without calibration	w_{cal} from 618 MHz	w_{cal} from 642 MHz	w_{cal} from 666 MHz
	α	RMSE dB	RMSE dB	RMSE dB	RMSE dB
1	0°	2.713	0.044	1.657	1.103
2	5°	3.898	1.605	2.629	2.288
3	10°	4.381	2.490	3.115	2.911
4	15°	3.314	1.911	2.098	1.957
5	20°	2.361	1.619	1.325	1.163
6	25°	1.269	1.896	0.974	0.850
7	30°	1.203	1.788	0.870	0.714
8	35°	0.737	2.174	1.295	1.197
9	40°	1.068	1.921	1.358	1.062
10	45°	0.770	2.378	1.555	1.456

Table 17: Experiment 3: Comparison of RMSE regarding magnitude for frequency 642 MHz without calibration and with calibration

Measurement	Azimuth	Without calibration	w_{cal} from 618 MHz	w_{cal} from 642 MHz	w_{cal} from 666 MHz
	α	RMSE dB	RMSE dB	RMSE dB	RMSE dB
1	0°	1.834	1.437	0.439	0.675
2	5°	2.280	1.024	0.901	0.813
3	10°	2.547	0.628	1.259	0.940
4	15°	3.338	0.914	2.030	1.689
5	20°	3.676	1.171	2.362	2.022
6	25°	3.719	1.202	2.454	2.049
7	30°	3.461	1.042	2.257	1.805
8	35°	2.546	0.478	1.435	0.882
9	40°	1.539	1.270	0.885	0.353
10	45°	1.017	2.022	1.201	1.082

Table 18: Experiment 3: Comparison of RMSE regarding magnitude for frequency 666 MHz without calibration and with calibration

Measurement	Azimuth	Without calibration	w_{cal} from 618 MHz	w_{cal} from 642 MHz	w_{cal} from 666 MHz
	α	RMSE dB	RMSE dB	RMSE dB	RMSE dB
1	$0°$	1.675	1.137	0.794	0.052
2	$5°$	2.348	0.645	1.330	0.703
3	$10°$	2.551	0.514	1.540	0.907
4	$15°$	2.398	0.712	1.516	0.808
5	$20°$	2.600	0.760	1.626	0.991
6	$25°$	2.625	0.852	1.541	1.016
7	$30°$	2.624	1.000	1.664	1.106
8	$35°$	0.869	2.079	1.299	1.091
9	$40°$	1.747	1.225	1.121	0.694
10	$45°$	1.810	1.319	1.315	0.862

B.2.2 Experiment 2: Magnitude RMSE before and after calibration

Table 19: Experiment 2: Comparison of RMSE regarding magnitude for frequency 618 MHz without calibration and with calibration

Measurement	Azimuth	Without calibration	w_{cal} from 618 MHz	w_{cal} from 642 MHz	w_{cal} from 666 MHz
	α	RMSE dB	RMSE dB	RMSE dB	RMSE dB
1	$-15°$	3.682	2.002	2.386	2.279
8	$-7°$	3.373	1.952	1.927	2.086
10	$11°$	4.005	1.722	2.610	2.446
12	$33°$	2.344	0.969	1.069	0.878
14	$53°$	0.875	3.264	2.213	2.324
17	$75°$	4.679	2.287	3.310	3.098

Table 20: Experiment 2: Comparison of RMSE regarding magnitude for frequency 642 MHz without calibration and with calibration

Measurement	Azimuth	Without calibration	w_{cal} from 618 MHz	w_{cal} from 642 MHz	w_{cal} from 666 MHz
	α	RMSE dB	RMSE dB	RMSE dB	RMSE dB
1	$-15°$	1.876	1.397	0.959	1.030
8	$-7°$	3.041	0.867	1.812	1.563
10	$11°$	3.540	1.499	2.114	2.032
12	$33°$	2.961	0.781	1.645	1.413
14	$53°$	1.716	1.198	0.853	0.696
17	$75°$	3.889	1.692	2.479	2.387

Table 21: Experiment 2: Comparison of RMSE regarding magnitude for frequency 666 MHz without calibration and with calibration

Measurement	Azimuth	Without calibration	w_{cal} from 618 MHz	w_{cal} from 642 MHz	w_{cal} from 666 MHz
	α	RMSE dB	RMSE dB	RMSE dB	RMSE dB
1	$-15°$	2.343	1.331	0.994	1.185
8	$-7°$	3.131	0.913	1.969	1.612
10	$11°$	1.747	1.591	0.360	0.842
12	$33°$	2.962	1.068	1.638	1.559
14	$53°$	2.106	1.329	1.067	1.141
17	$75°$	4.191	1.901	2.854	2.613

B.2.3 Experiment 3, Magnitude: Figures before and after calibration

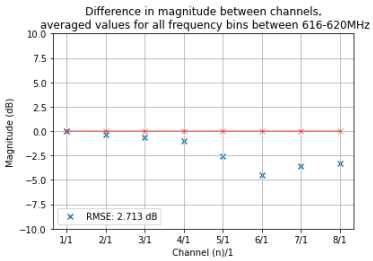

(a) No calibration

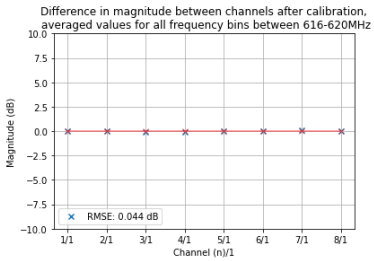

(b) Calibration with w_{cal} from 618 MHz

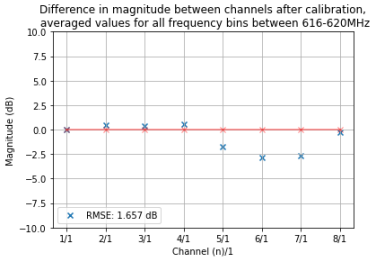

(c) Calibration with w_{cal} from 642 MHz

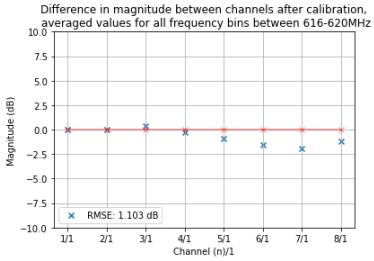

(d) Calibration with w_{cal} from 666 MHz

Figure 79 Experiment 3, Measurement 1: Magnitude difference between each channel and channel 1, compared with theoretical expected values. Frequency f = 618, azimuth α = 0.

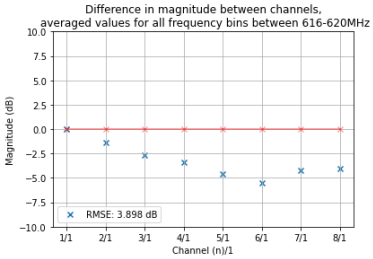

(a) No calibration

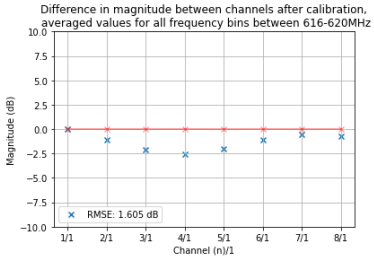

(b) Calibration with w_{cal} from 618 MHz

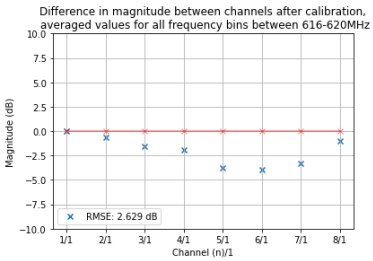

(c) Calibration with w_{cal} from 642 MHz

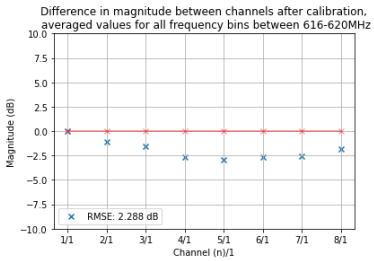

(d) Calibration with w_{cal} from 666 MHz

Figure 80 Experiment 3, Measurement 2: Magnitude difference between each channel and channel 1, compared with theoretical expected values. Frequency $f = 618$, azimuth $\alpha = 5$.

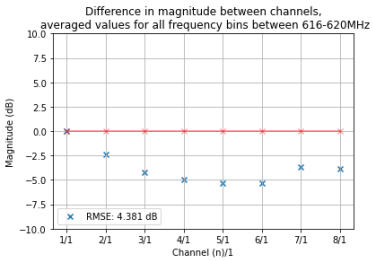

(a) No calibration

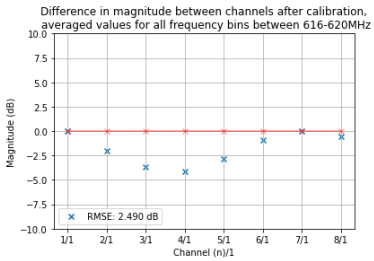

(b) Calibration with w_{cal} from 618 MHz

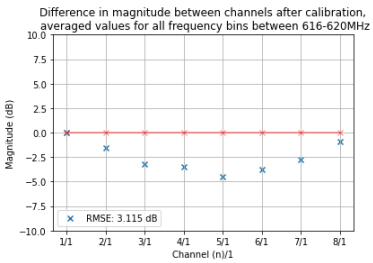

(c) Calibration with w_{cal} from 642 MHz

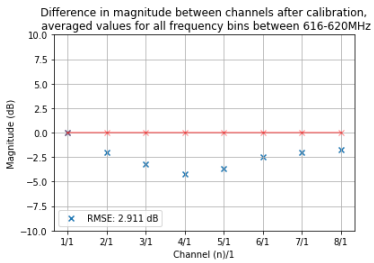

(d) Calibration with w_{cal} from 666 MHz

Figure 81 Experiment 3, Measurement 3: Magnitude difference between each channel and channel 1, compared with theoretical expected values. Frequency $f = 618$, azimuth $\alpha = 10$.

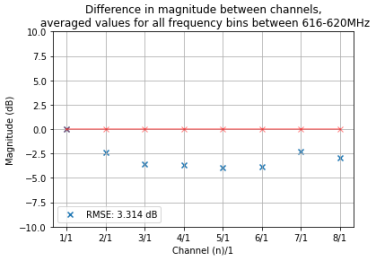

(a) No calibration

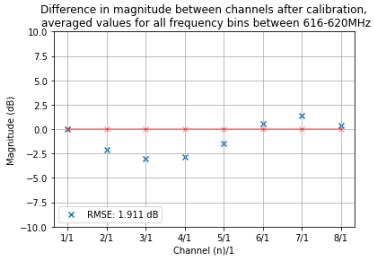

(b) Calibration with w_{cal} from 618 MHz

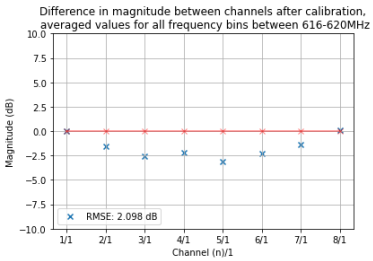

(c) Calibration with w_{cal} from 642 MHz

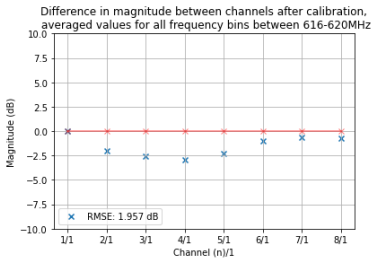

(d) Calibration with w_{cal} from 666 MHz

Figure 82 Experiment 3, Measurement 4: Magnitude difference between each channel and channel 1, compared with theoretical expected values. Frequency $f = 618$, azimuth $\alpha = 15$.

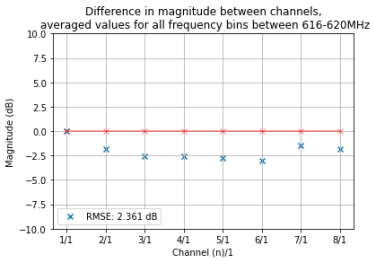

(a) No calibration

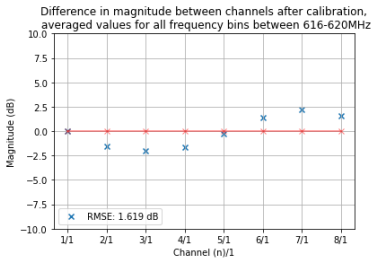

(b) Calibration with w_{cal} from 618 MHz

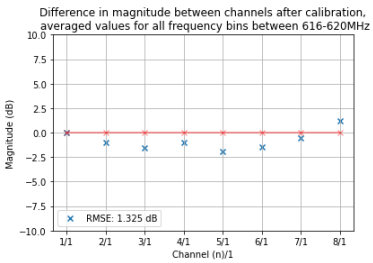

(c) Calibration with w_{cal} from 642 MHz

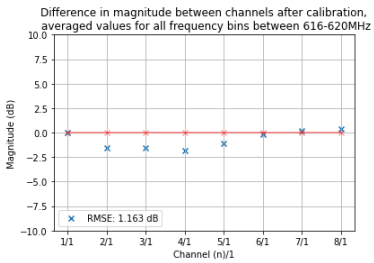

(d) Calibration with w_{cal} from 666 MHz

Figure 83 Experiment 3, Measurement 5: Magnitude difference between each channel and channel 1, compared with theoretical expected values. Frequency $f = 618$, azimuth $\alpha = 20$.

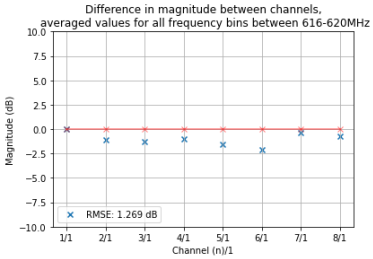

(a) No calibration

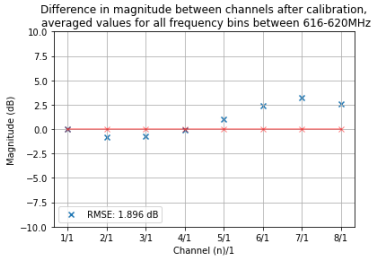

(b) Calibration with w_{cal} from 618 MHz

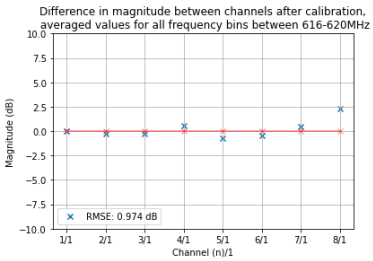

(c) Calibration with w_{cal} from 642 MHz

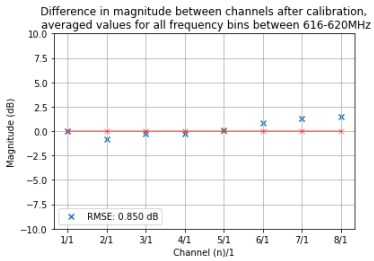

(d) Calibration with w_{cal} from 666 MHz

Figure 84 Experiment 3, Measurement 6: Magnitude difference between each channel and channel 1, compared with theoretical expected values. Frequency $f = 618$, azimuth $\alpha = 25$.

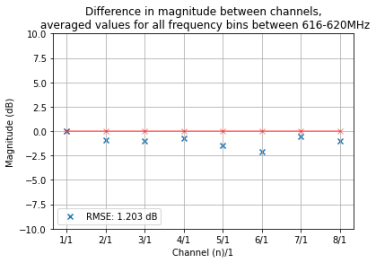

(a) No calibration

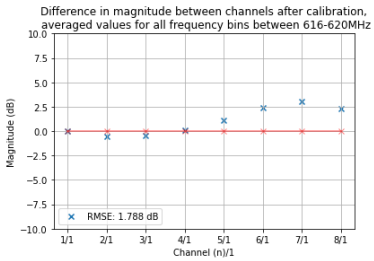

(b) Calibration with w_{cal} from 618 MHz

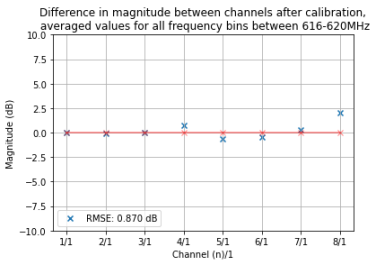

(c) Calibration with w_{cal} from 642 MHz

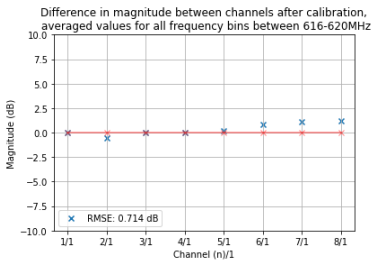

(d) Calibration with w_{cal} from 666 MHz

Figure 85 Experiment 3, Measurement 7: Magnitude difference between each channel and channel 1, compared with theoretical expected values. Frequency $f = 618$, azimuth $\alpha = 30$.

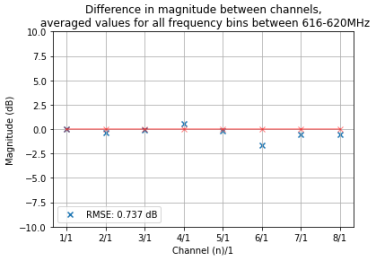

(a) No calibration

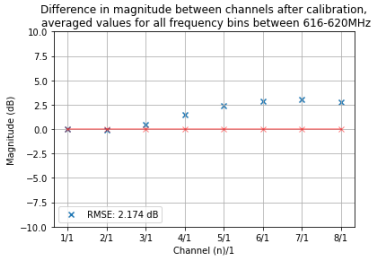

(b) Calibration with w_{cal} from 618 MHz

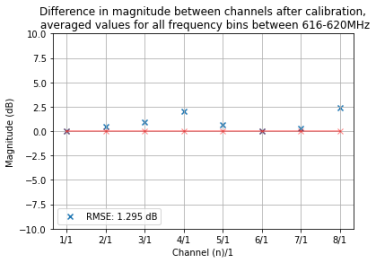

(c) Calibration with w_{cal} from 642 MHz

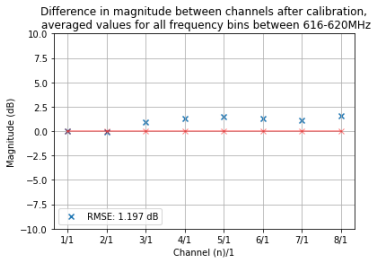

(d) Calibration with w_{cal} from 666 MHz

Figure 86 Experiment 3, Measurement 8: Magnitude difference between each channel and channel 1, compared with theoretical expected values. Frequency $f = 618$, azimuth $\alpha = 35$.

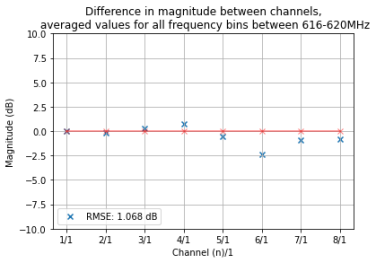

(a) No calibration

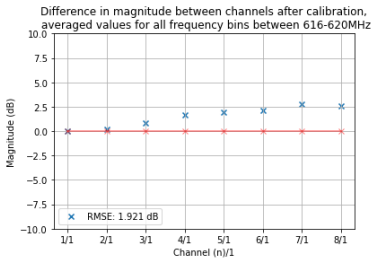

(b) Calibration with w_{cal} from 618 MHz

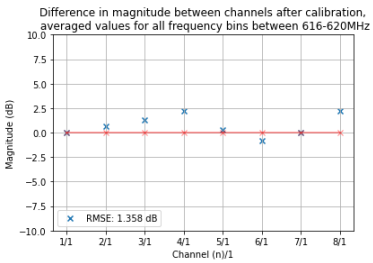

(c) Calibration with w_{cal} from 642 MHz

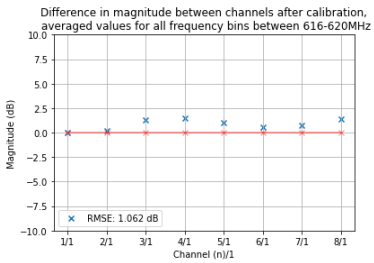

(d) Calibration with w_{cal} from 666 MHz

Figure 87 Experiment 3, Measurement 9: Magnitude difference between each channel and channel 1, compared with theoretical expected values. Frequency $f = 618$, azimuth $\alpha = 40$.

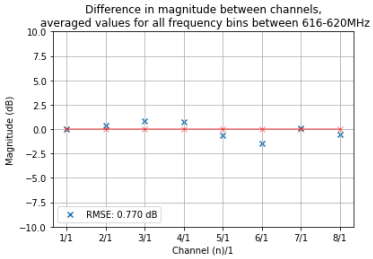

(a) No calibration

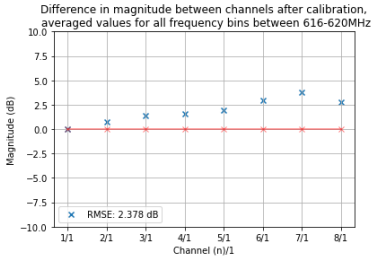

(b) Calibration with w_{cal} from 618 MHz

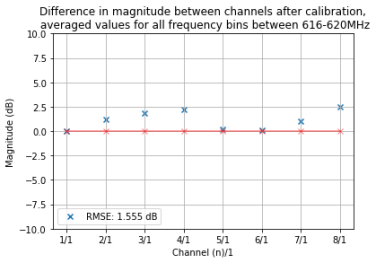

(c) Calibration with w_{cal} from 642 MHz

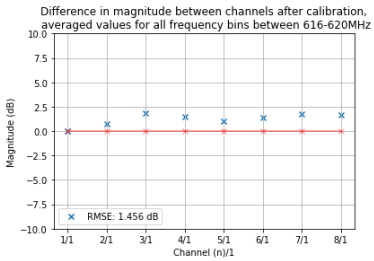

(d) Calibration with w_{cal} from 666 MHz

Figure 88 Experiment 3, Measurement 10: Magnitude difference between each channel and channel 1, compared with theoretical expected values. Frequency $f = 618$, azimuth $\alpha = 45$.

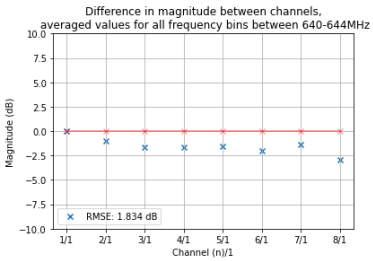

(a) No calibration

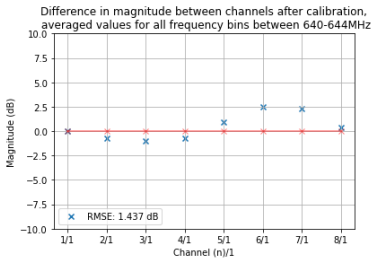

(b) Calibration with w_{cal} from 618 MHz

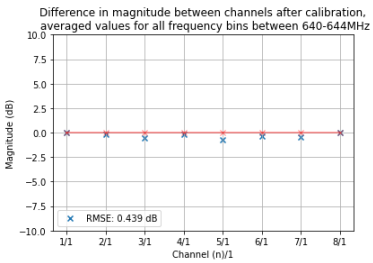

(c) Calibration with w_{cal} from 642 MHz

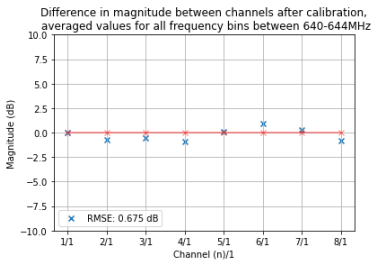

(d) Calibration with w_{cal} from 666 MHz

Figure 89 Experiment 3, Measurement 1: Magnitude difference between each channel and channel 1, compared with theoretical expected values. Frequency $f = 642$, azimuth $\alpha = 0$.

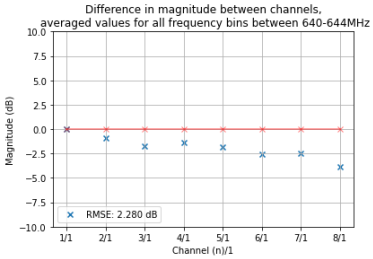

(a) No calibration

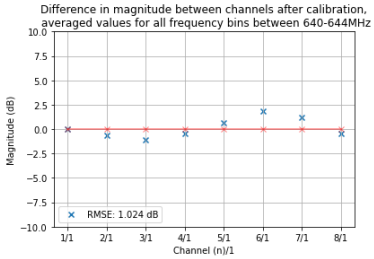

(b) Calibration with w_{cal} from 618 MHz

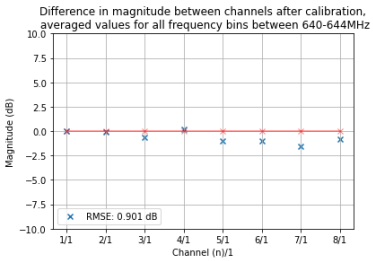

(c) Calibration with w_{cal} from 642 MHz

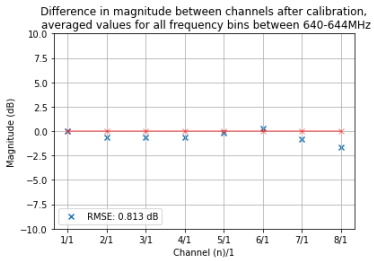

(d) Calibration with w_{cal} from 666 MHz

Figure 90 Experiment 3, Measurement 2: Magnitude difference between each channel and channel 1, compared with theoretical expected values. Frequency $f = 642$, azimuth $\alpha = 5$.

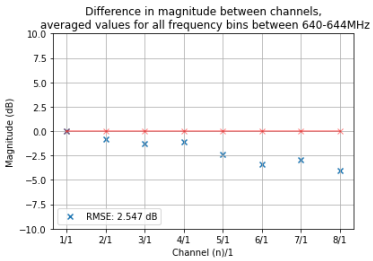

(a) No calibration

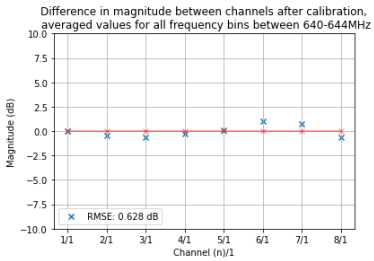

(b) Calibration with w_{cal} from 618 MHz

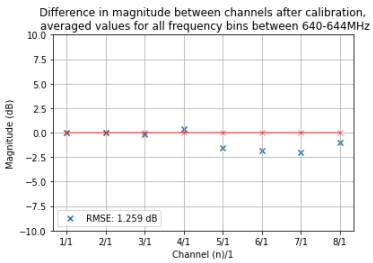

(c) Calibration with w_{cal} from 642 MHz

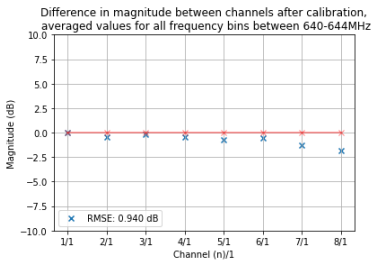

(d) Calibration with w_{cal} from 666 MHz

Figure 91 Experiment 3, Measurement 3: Magnitude difference between each channel and channel 1, compared with theoretical expected values. Frequency $f = 642$, azimuth $\alpha = 10$.

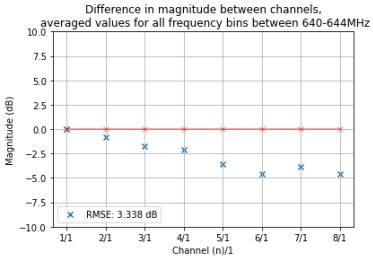

(a) No calibration

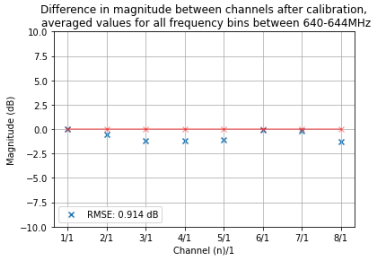

(b) Calibration with w_{cal} from 618 MHz

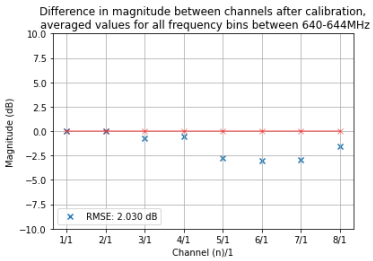

(c) Calibration with w_{cal} from 642 MHz

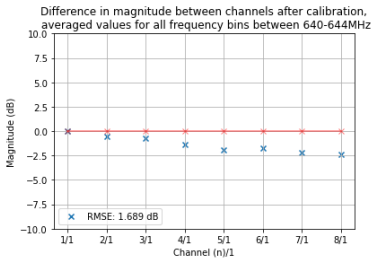

(d) Calibration with w_{cal} from 666 MHz

Figure 92 Experiment 3, Measurement 4: Magnitude difference between each channel and channel 1, compared with theoretical expected values. Frequency $f = 642$, azimuth $\alpha = 15$.

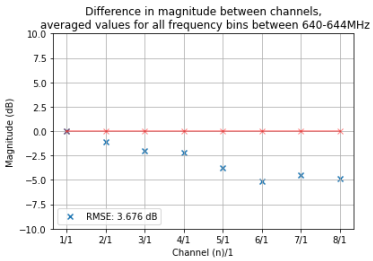

(a) No calibration

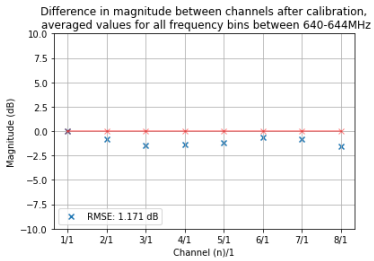

(b) Calibration with w_{cal} from 618 MHz

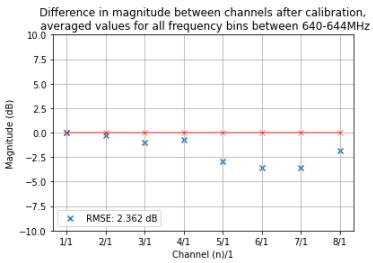

(c) Calibration with w_{cal} from 642 MHz

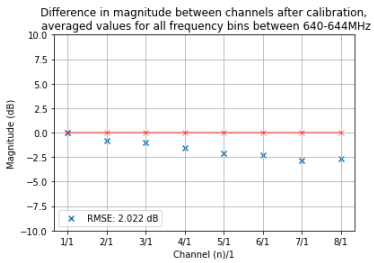

(d) Calibration with w_{cal} from 666 MHz

Figure 93 Experiment 3, Measurement 5: Magnitude difference between each channel and channel 1, compared with theoretical expected values. Frequency $f = 642$, azimuth $\alpha = 20$.

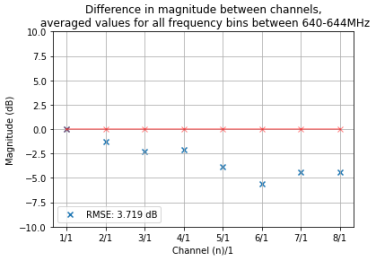

(a) No calibration

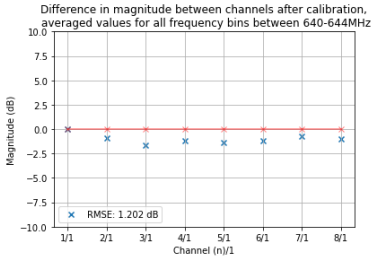

(b) Calibration with w_{cal} from 618 MHz

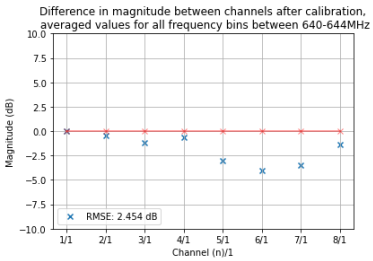

(c) Calibration with w_{cal} from 642 MHz

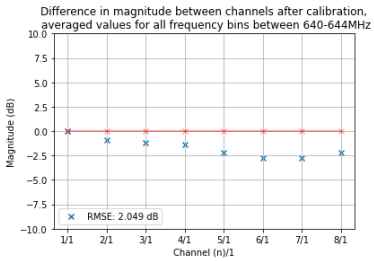

(d) Calibration with w_{cal} from 666 MHz

Figure 94 Experiment 3, Measurement 6: Magnitude difference between each channel and channel 1, compared with theoretical expected values. Frequency $f = 642$, azimuth $\alpha = 25$.

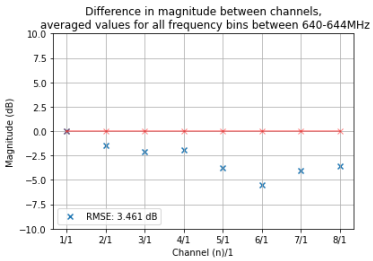

(a) No calibration

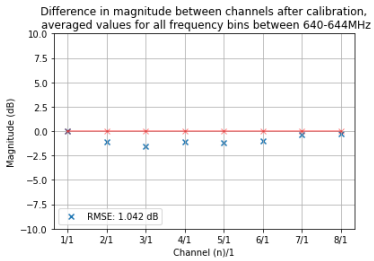

(b) Calibration with w_{cal} from 618 MHz

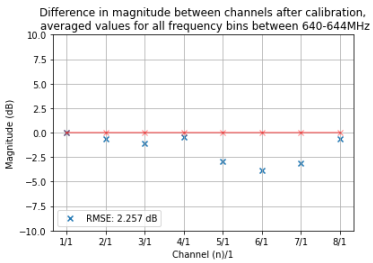

(c) Calibration with w_{cal} from 642 MHz

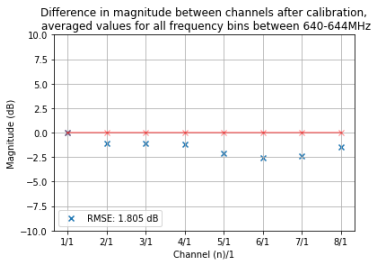

(d) Calibration with w_{cal} from 666 MHz

Figure 95 Experiment 3, Measurement 7: Magnitude difference between each channel and channel 1, compared with theoretical expected values. Frequency $f = 642$, azimuth $\alpha = 30$.

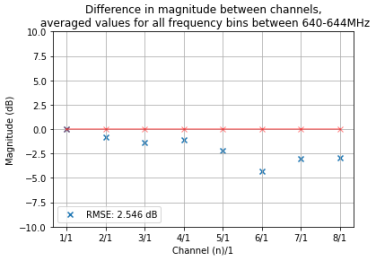

(a) No calibration

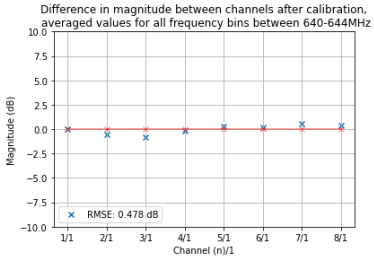

(b) Calibration with w_{cal} from 618 MHz

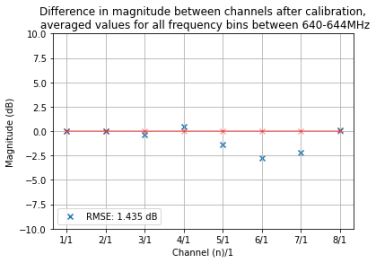

(c) Calibration with w_{cal} from 642 MHz

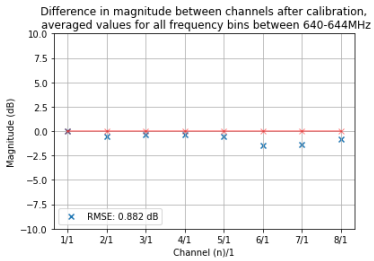

(d) Calibration with w_{cal} from 666 MHz

Figure 96 Experiment 3, Measurement 8: Magnitude difference between each channel and channel 1, compared with theoretical expected values. Frequency $f = 642$, azimuth $\alpha = 35$.

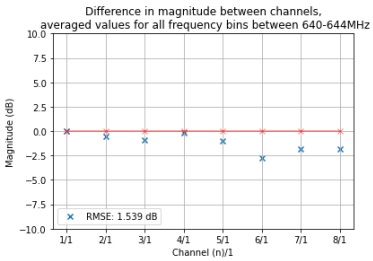

(a) No calibration

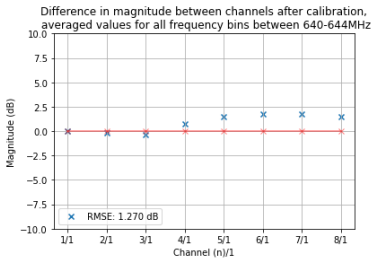

(b) Calibration with w_{cal} from 618 MHz

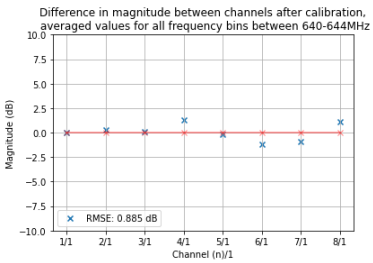

(c) Calibration with w_{cal} from 642 MHz

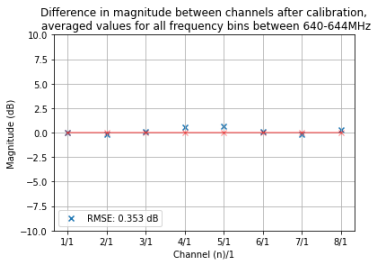

(d) Calibration with w_{cal} from 666 MHz

Figure 97 Experiment 3, Measurement 9: Magnitude difference between each channel and channel 1, compared with theoretical expected values. Frequency $f = 642$, azimuth $\alpha = 40$.

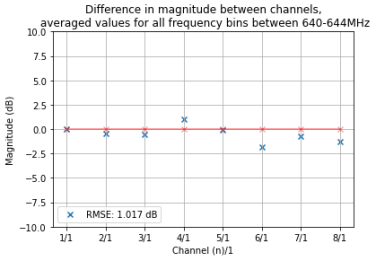

(a) No calibration

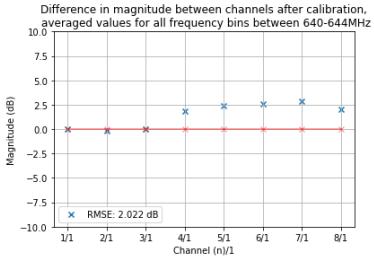

(b) Calibration with w_{cal} from 618 MHz

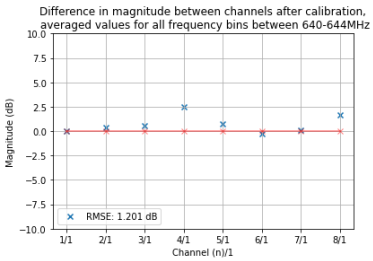

(c) Calibration with w_{cal} from 642 MHz

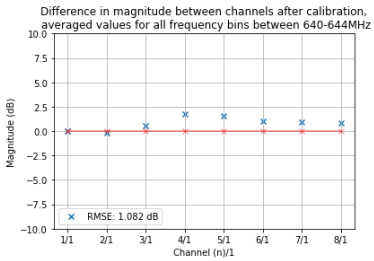

(d) Calibration with w_{cal} from 666 MHz

Figure 98 Experiment 3, Measurement 10: Magnitude difference between each channel and channel 1, compared with theoretical expected values. Frequency $f = 642$, azimuth $\alpha = 45$.

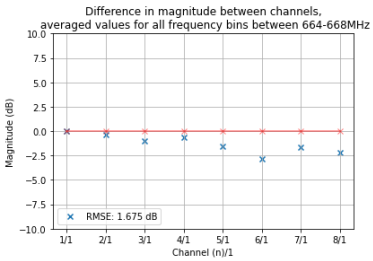

(a) No calibration

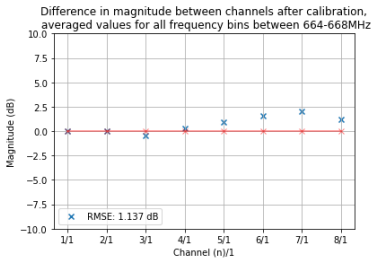

(b) Calibration with w_{cal} from 618 MHz

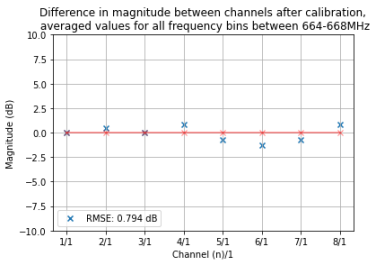

(c) Calibration with w_{cal} from 642 MHz

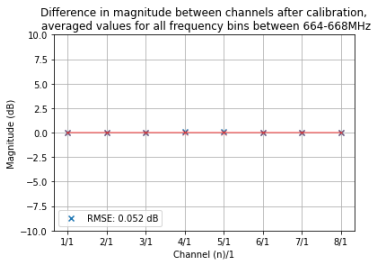

(d) Calibration with w_{cal} from 666 MHz

Figure 99 Experiment 3, Measurement 1: Magnitude difference between each channel and channel 1, compared with theoretical expected values. Frequency $f = 666$, azimuth $\alpha = 0$.

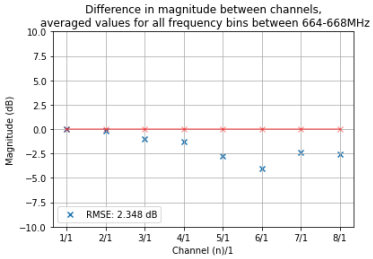

(a) No calibration

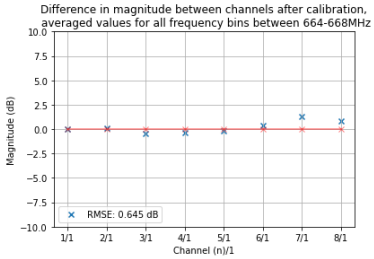

(b) Calibration with w_{cal} from 618 MHz

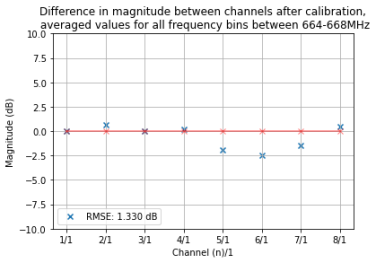

(c) Calibration with w_{cal} from 642 MHz

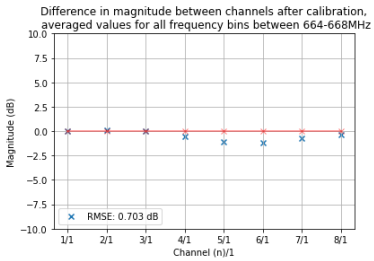

(d) Calibration with w_{cal} from 666 MHz

Figure 100 Experiment 3, Measurement 2: Magnitude difference between each channel and channel 1, compared with theoretical expected values. Frequency $f = 666$, azimuth $\alpha = 5$.

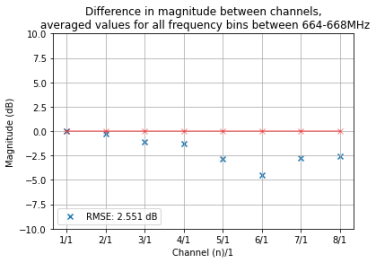

(a) No calibration

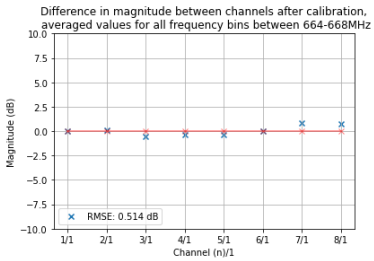

(b) Calibration with w_{cal} from 618 MHz

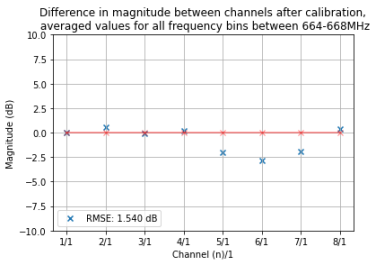

(c) Calibration with w_{cal} from 642 MHz

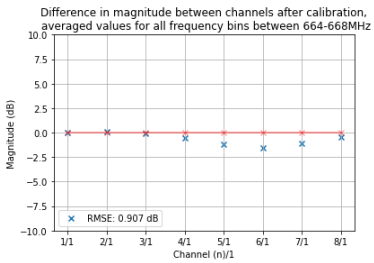

(d) Calibration with w_{cal} from 666 MHz

Figure 101 Experiment 3, Measurement 3: Magnitude difference between each channel and channel 1, compared with theoretical expected values. Frequency $f = 666$, azimuth $\alpha = 10$.

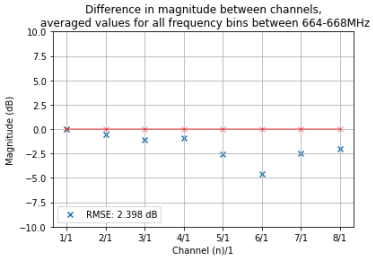

(a) No calibration

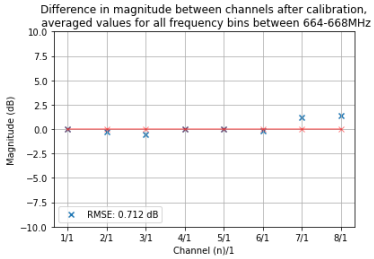

(b) Calibration with w_{cal} from 618 MHz

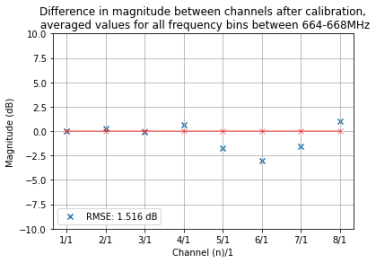

(c) Calibration with w_{cal} from 642 MHz

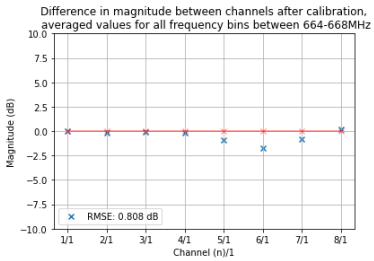

(d) Calibration with w_{cal} from 666 MHz

Figure 102 Experiment 3, Measurement 4: Magnitude difference between each channel and channel 1, compared with theoretical expected values. Frequency $f = 666$, azimuth $\alpha = 15$.

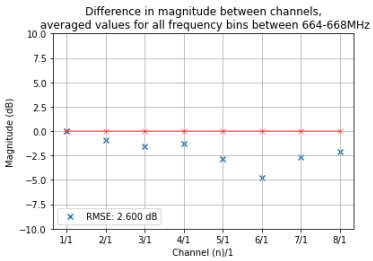

(a) No calibration

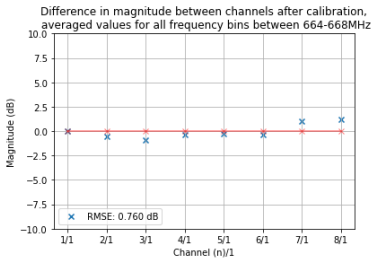

(b) Calibration with w_{cal} from 618 MHz

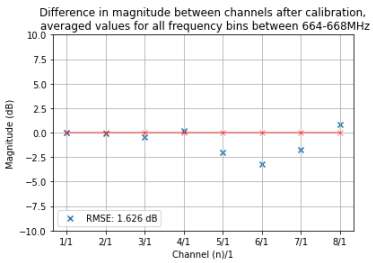

(c) Calibration with w_{cal} from 642 MHz

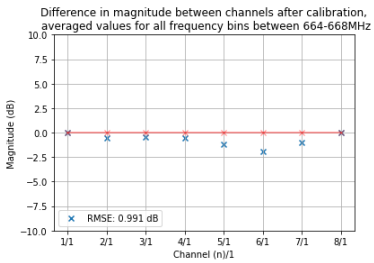

(d) Calibration with w_{cal} from 666 MHz

Figure 103 Experiment 3, Measurement 5: Magnitude difference between each channel and channel 1, compared with theoretical expected values. Frequency $f = 666$, azimuth $\alpha = 20$.

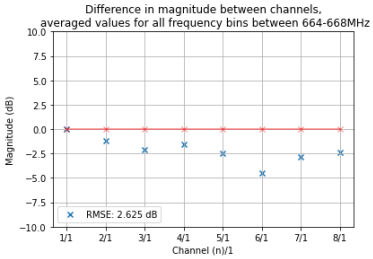

(a) No calibration

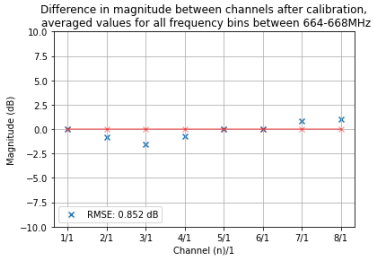

(b) Calibration with w_{cal} from 618 MHz

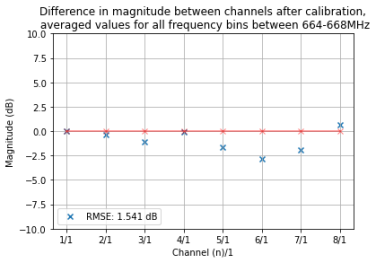

(c) Calibration with w_{cal} from 642 MHz

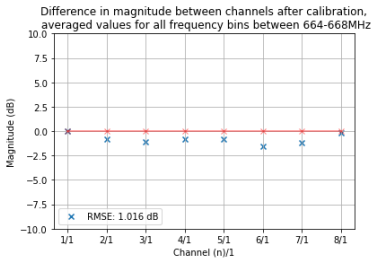

(d) Calibration with w_{cal} from 666 MHz

Figure 104 Experiment 3, Measurement 6: Magnitude difference between each channel and channel 1, compared with theoretical expected values. Frequency $f = 666$, azimuth $\alpha = 25$.

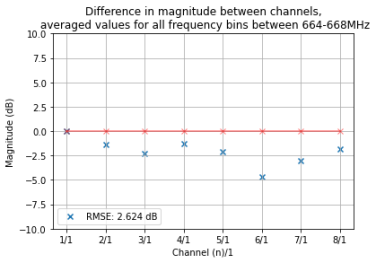

(a) No calibration

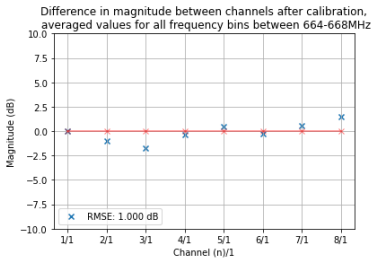

(b) Calibration with w_{cal} from 618 MHz

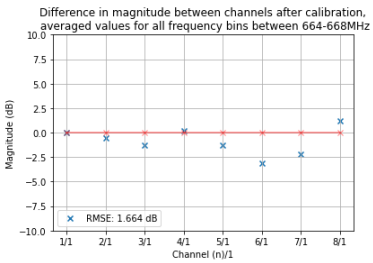

(c) Calibration with w_{cal} from 642 MHz

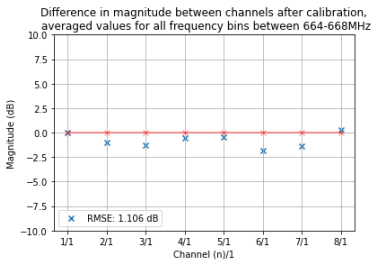

(d) Calibration with w_{cal} from 666 MHz

Figure 105 Experiment 3, Measurement 7: Magnitude difference between each channel and channel 1, compared with theoretical expected values. Frequency $f = 666$, azimuth $\alpha = 30$.

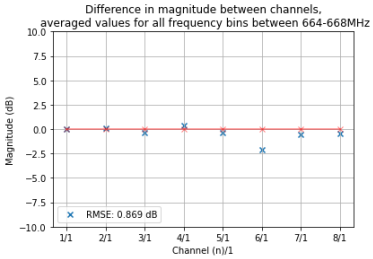

(a) No calibration

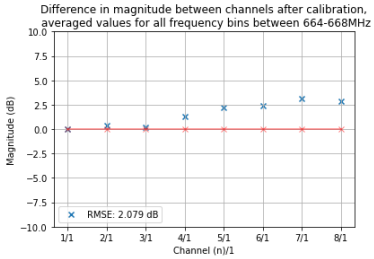

(b) Calibration with w_{cal} from 618 MHz

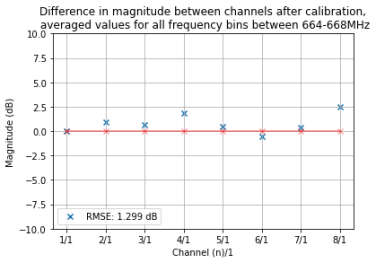

(c) Calibration with w_{cal} from 642 MHz

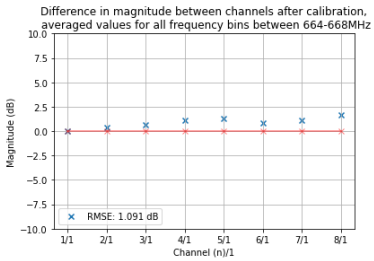

(d) Calibration with w_{cal} from 666 MHz

Figure 106 Experiment 3, Measurement 8: Magnitude difference between each channel and channel 1, compared with theoretical expected values. Frequency $f = 666$, azimuth $\alpha = 35$.

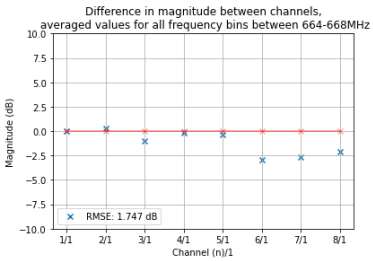

(a) No calibration

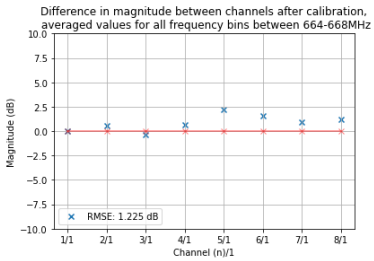

(b) Calibration with w_{cal} from 618 MHz

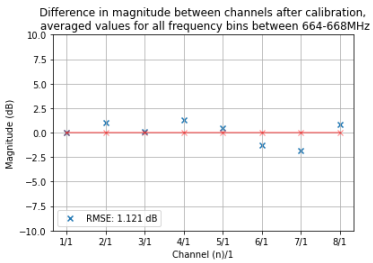

(c) Calibration with w_{cal} from 642 MHz

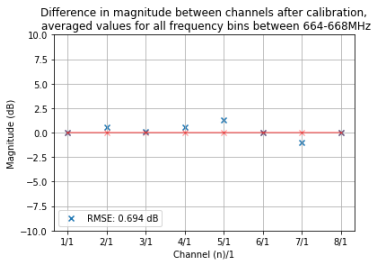

(d) Calibration with w_{cal} from 666 MHz

Figure 107 Experiment 3, Measurement 9: Magnitude difference between each channel and channel 1, compared with theoretical expected values. Frequency $f = 666$, azimuth $\alpha = 40$.

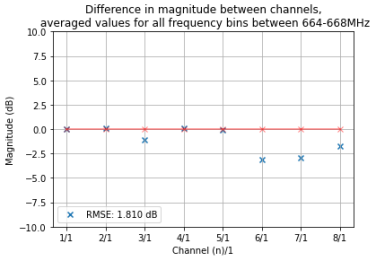

(a) No calibration

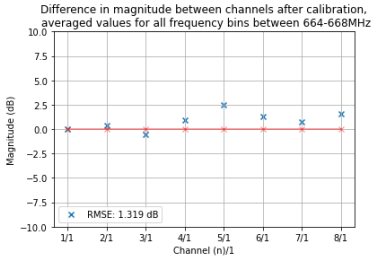

(b) Calibration with w_{cal} from 618 MHz

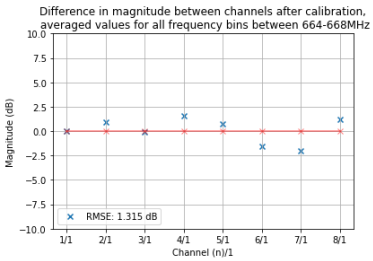

(c) Calibration with w_{cal} from 642 MHz

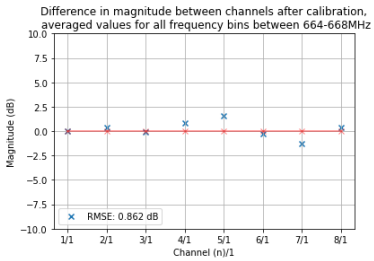

(d) Calibration with w_{cal} from 666 MHz

Figure 108 Experiment 3, Measurement 10: Magnitude difference between each channel and channel 1, compared with theoretical expected values. Frequency $f = 666$, azimuth $\alpha = 45$.

B.2.4 Experiment 2, Magnitude: Figures before and after calibration

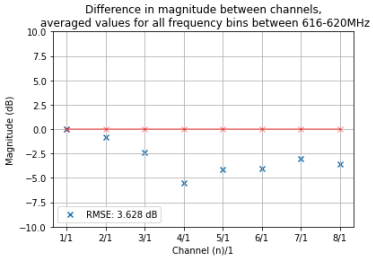

(a) No calibration

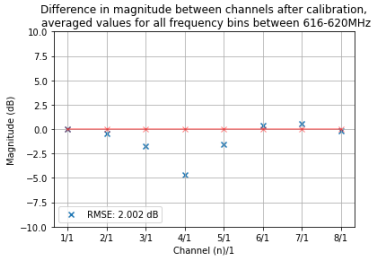

(b) Calibration with w_{cal} from 618 MHz

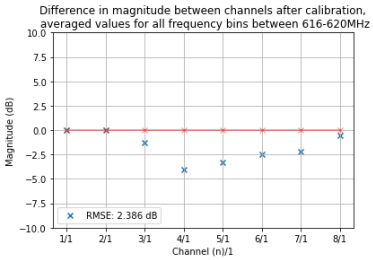

(c) Calibration with w_{cal} from 642 MHz

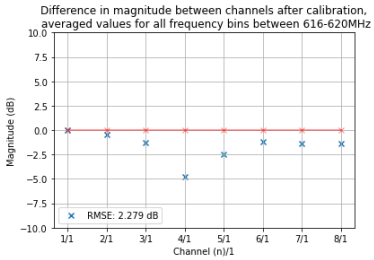

(d) Calibration with w_{cal} from 666 MHz

Figure 109 Experiment 2, Measurement 1: Magnitude difference between each channel and channel 1, compared with theoretical expected values. Frequency f = 618, azimuth α = -15.

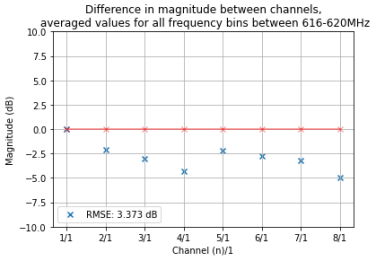

(a) No calibration

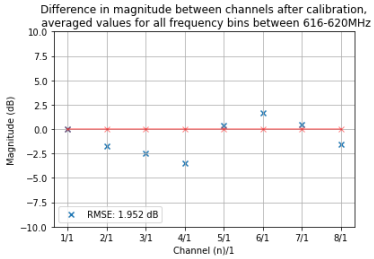

(b) Calibration with w_{cal} from 618 MHz

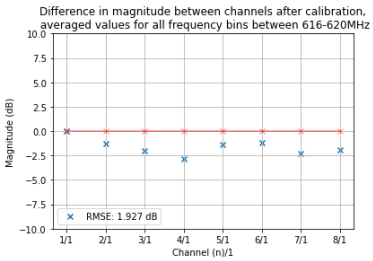

(c) Calibration with w_{cal} from 642 MHz

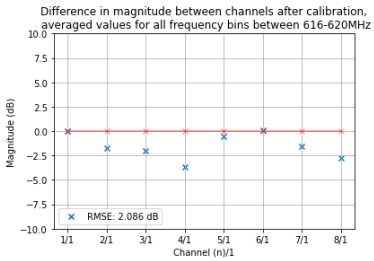

(d) Calibration with w_{cal} from 666 MHz

Figure 110 Experiment 2, Measurement 8: Magnitude difference between each channel and channel 1, compared with theoretical expected values. Frequency f = 618, azimuth α = -7.

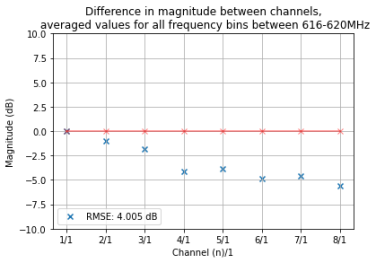

(a) No calibration

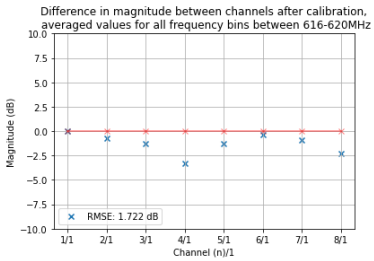

(b) Calibration with w_{cal} from 618 MHz

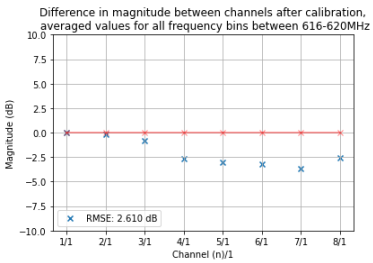

(c) Calibration with w_{cal} from 642 MHz

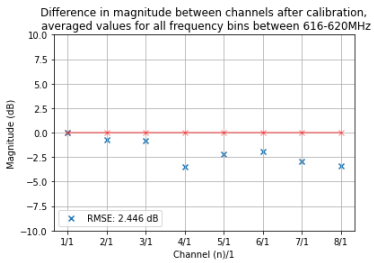

(d) Calibration with w_{cal} from 666 MHz

Figure 111 Experiment 2, Measurement 10: Magnitude difference between each channel and channel 1, compared with theoretical expected values. Frequency f = 618, azimuth α = 11.

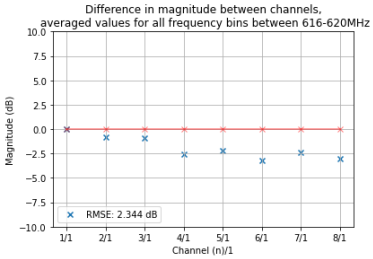

(a) No calibration

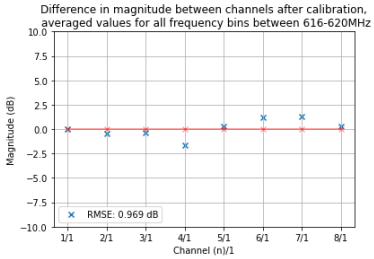

(b) Calibration with w_{cal} from 618 MHz

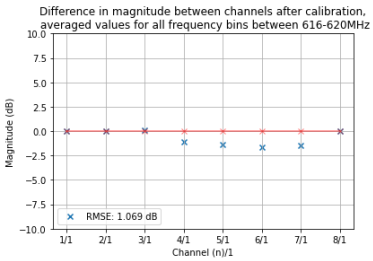

(c) Calibration with w_{cal} from 642 MHz

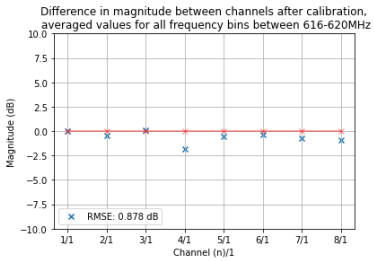

(d) Calibration with w_{cal} from 666 MHz

Figure 112 Experiment 2, Measurement 12: Magnitude difference between each channel and channel 1, compared with theoretical expected values. Frequency $f = 618$, azimuth $\alpha = 33$.

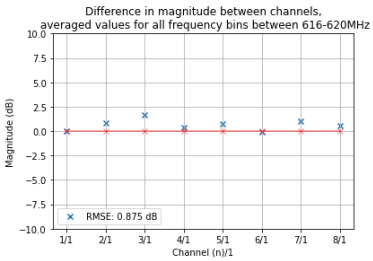

(a) No calibration

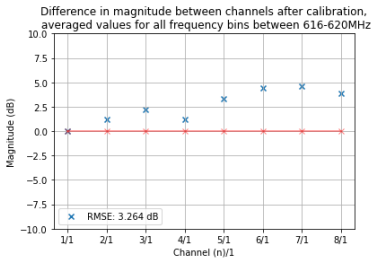

(b) Calibration with w_{cal} from 618 MHz

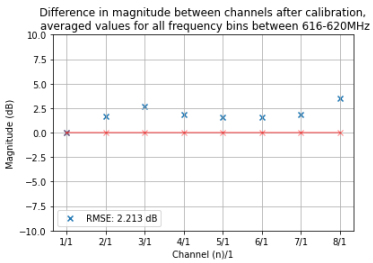

(c) Calibration with w_{cal} from 642 MHz

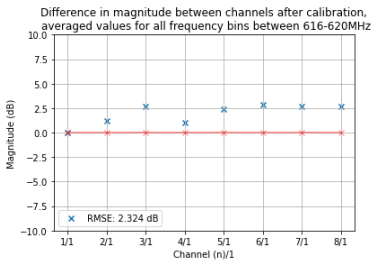

(d) Calibration with w_{cal} from 666 MHz

Figure 113 Experiment 2, Measurement 14: Magnitude difference between each channel and channel 1, compared with theoretical expected values. Frequency $f = 618$, azimuth $\alpha = 53$.

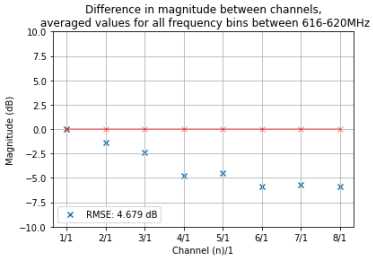

(a) No calibration

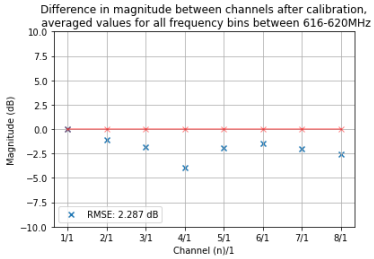

(b) Calibration with w_{cal} from 618 MHz

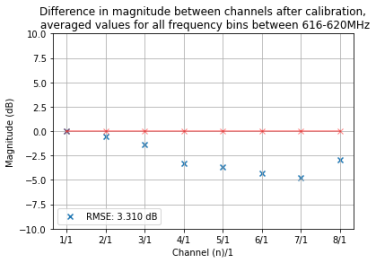

(c) Calibration with w_{cal} from 642 MHz

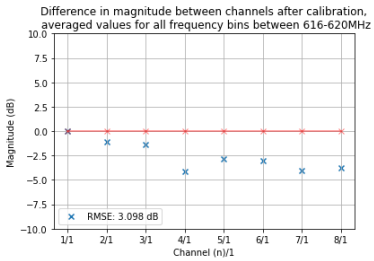

(d) Calibration with w_{cal} from 666 MHz

Figure 114 Experiment 2, Measurement 17: Magnitude difference between each channel and channel 1, compared with theoretical expected values. Frequency f = 618, azimuth α = 73.

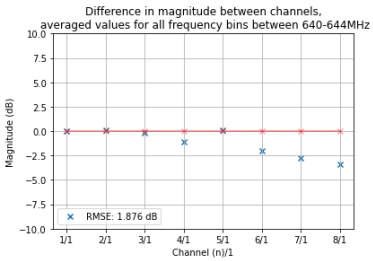

(a) No calibration

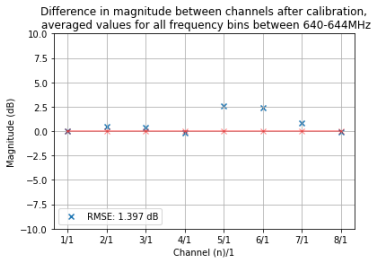

(b) Calibration with w_{cal} from 618 MHz

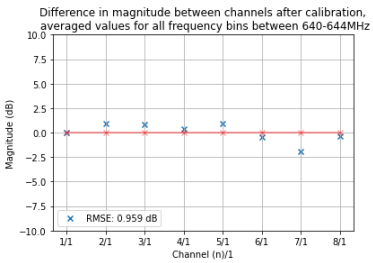

(c) Calibration with w_{cal} from 642 MHz

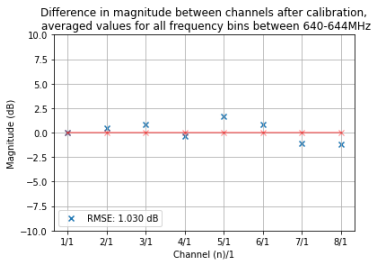

(d) Calibration with w_{cal} from 666 MHz

Figure 115 Experiment 2, Measurement 1: Magnitude difference between each channel and channel 1, compared with theoretical expected values. Frequency f = 642, azimuth α = -15.

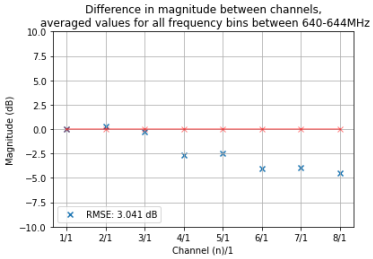

(a) No calibration

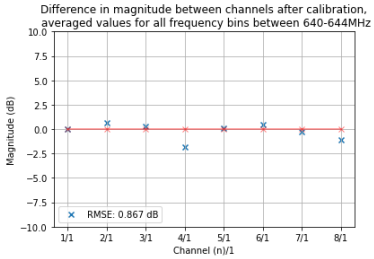

(b) Calibration with w_{cal} from 618 MHz

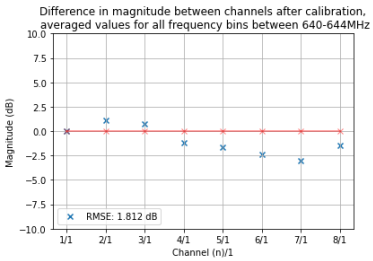

(c) Calibration with w_{cal} from 642 MHz

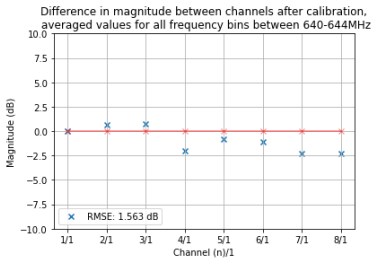

(d) Calibration with w_{cal} from 666 MHz

Figure 116 Experiment 2, Measurement 8: Magnitude difference between each channel and channel 1, compared with theoretical expected values. Frequency f = 642, azimuth α = -7.

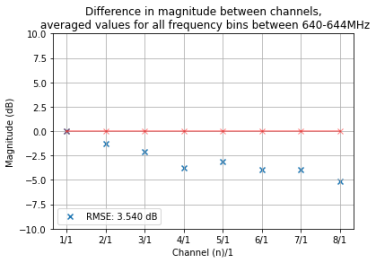

(a) No calibration

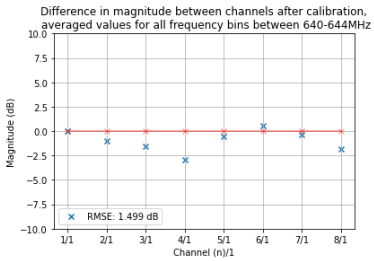

(b) Calibration with w_{cal} from 618 MHz

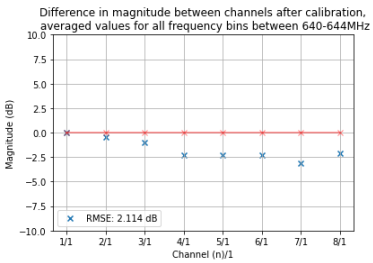

(c) Calibration with w_{cal} from 642 MHz

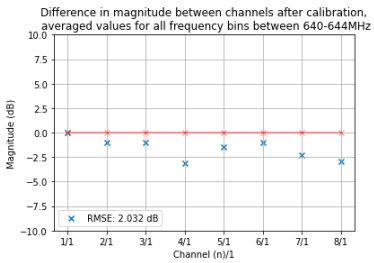

(d) Calibration with w_{cal} from 666 MHz

Figure 117 Experiment 2, Measurement 10: Magnitude difference between each channel and channel 1, compared with theoretical expected values. Frequency f = 642, azimuth α = 11.

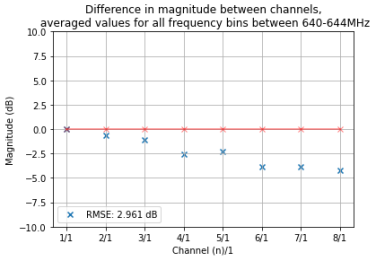

(a) No calibration

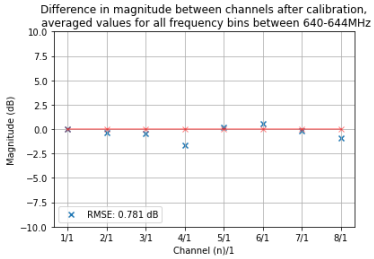

(b) Calibration with w_{cal} from 618 MHz

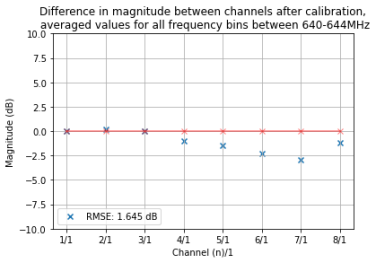

(c) Calibration with w_{cal} from 642 MHz

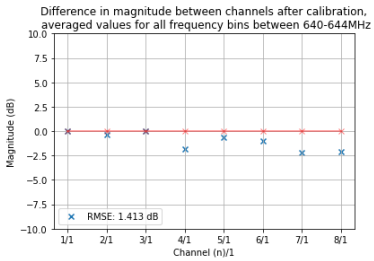

(d) Calibration with w_{cal} from 666 MHz

Figure 118 Experiment 2, Measurement 12: Magnitude difference between each channel and channel 1, compared with theoretical expected values. Frequency $f = 642$, azimuth $\alpha = 33$.

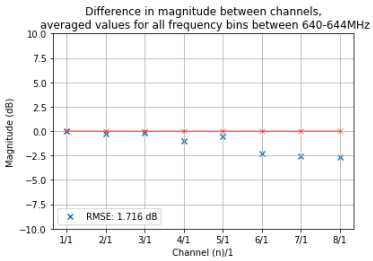

(a) No calibration

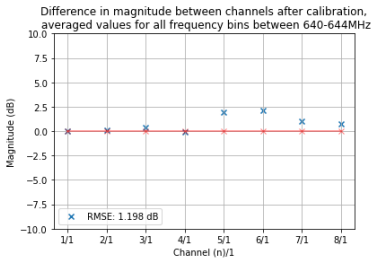

(b) Calibration with w_{cal} from 618 MHz

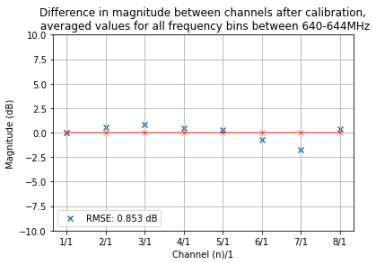

(c) Calibration with w_{cal} from 642 MHz

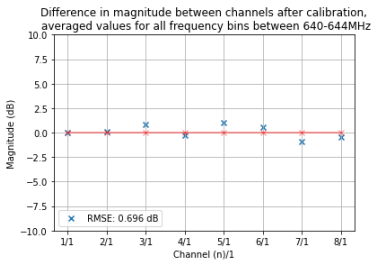

(d) Calibration with w_{cal} from 666 MHz

Figure 119 Experiment 2, Measurement 14: Magnitude difference between each channel and channel 1, compared with theoretical expected values. Frequency $f = 642$, azimuth $\alpha = 53$.

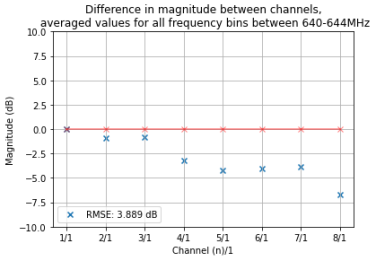

(a) No calibration

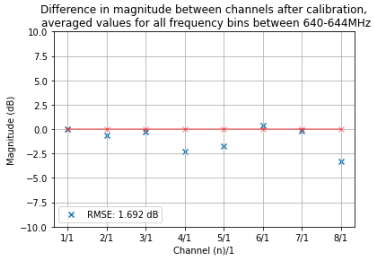

(b) Calibration with w_{cal} from 618 MHz

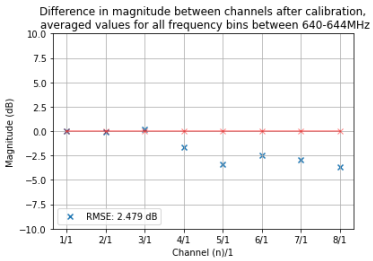

(c) Calibration with w_{cal} from 642 MHz

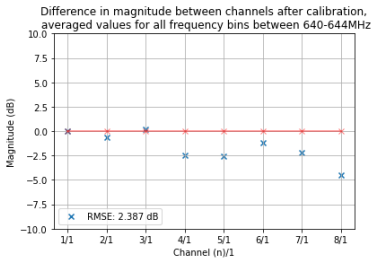

(d) Calibration with w_{cal} from 666 MHz

Figure 120 Experiment 2, Measurement 17: Magnitude difference between each channel and channel 1, compared with theoretical expected values. Frequency f = 642, azimuth α = 73.

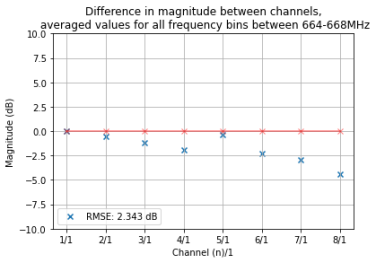

(a) No calibration

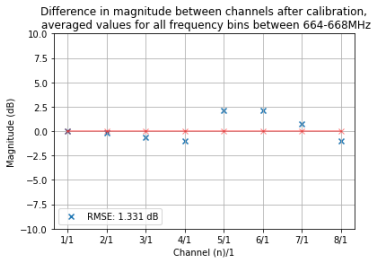

(b) Calibration with w_{cal} from 618 MHz

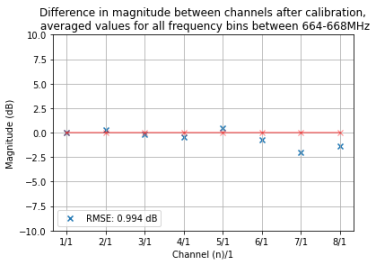

(c) Calibration with w_{cal} from 642 MHz

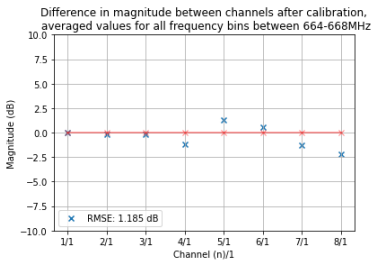

(d) Calibration with w_{cal} from 666 MHz

Figure 121 Experiment 2, Measurement 1: Magnitude difference between each channel and channel 1, compared with theoretical expected values. Frequency f = 666, azimuth α = -15.

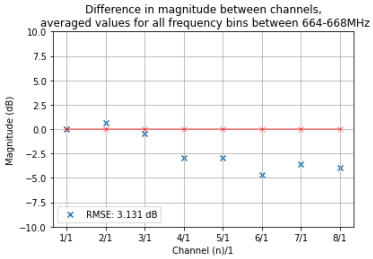

(a) No calibration

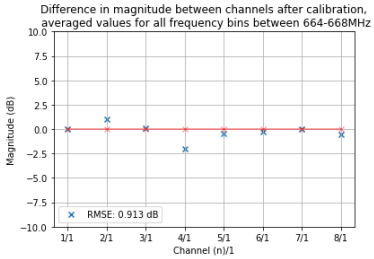

(b) Calibration with w_{cal} from 618 MHz

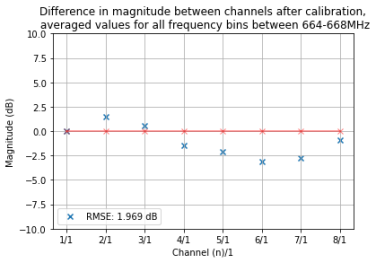

(c) Calibration with w_{cal} from 642 MHz

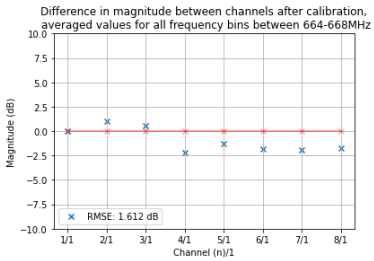

(d) Calibration with w_{cal} from 666 MHz

Figure 122 Experiment 2, Measurement 8: Magnitude difference between each channel and channel 1, compared with theoretical expected values. Frequency f = 666, azimuth α = -7.

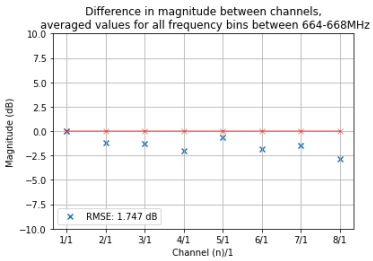

(a) No calibration

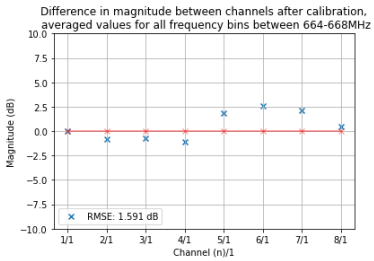

(b) Calibration with w_{cal} from 618 MHz

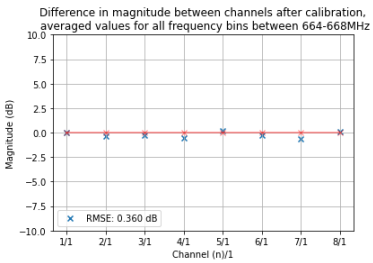

(c) Calibration with w_{cal} from 642 MHz

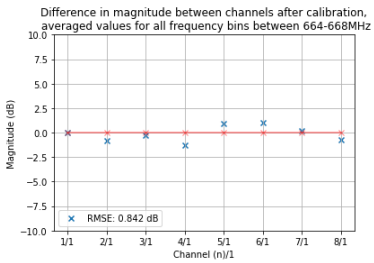

(d) Calibration with w_{cal} from 666 MHz

Figure 123 Experiment 2, Measurement 10: Magnitude difference between each channel and channel 1, compared with theoretical expected values. Frequency f = 666, azimuth α = 11.

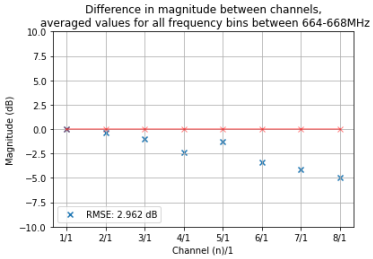

(a) No calibration

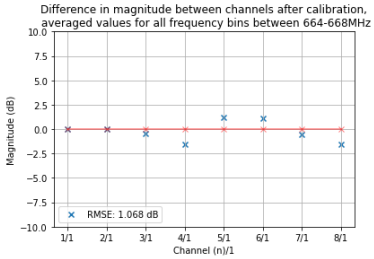

(b) Calibration with w_{cal} from 618 MHz

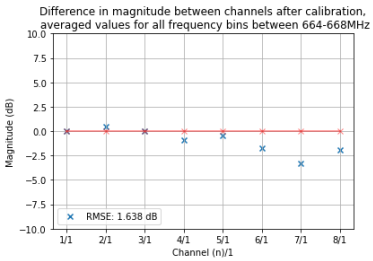

(c) Calibration with w_{cal} from 642 MHz

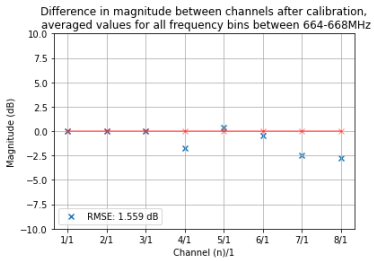

(d) Calibration with w_{cal} from 666 MHz

Figure 124 Experiment 2, Measurement 12: Magnitude difference between each channel and channel 1, compared with theoretical expected values. Frequency $f = 666$, azimuth $\alpha = 33$.

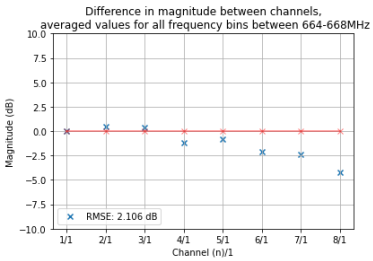

(a) No calibration

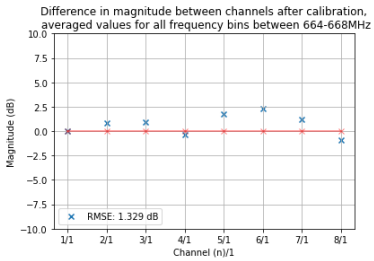

(b) Calibration with w_{cal} from 618 MHz

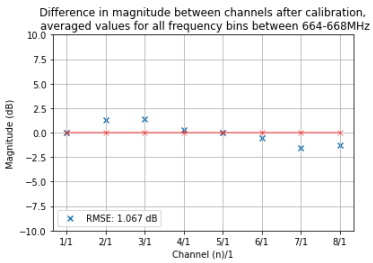

(c) Calibration with w_{cal} from 642 MHz

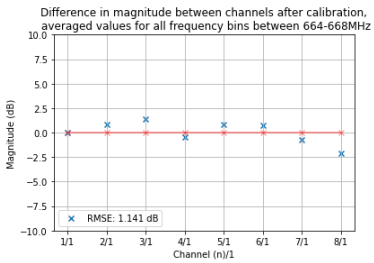

(d) Calibration with w_{cal} from 666 MHz

Figure 125 Experiment 2, Measurement 14: Magnitude difference between each channel and channel 1, compared with theoretical expected values. Frequency $f = 666$, azimuth $\alpha = 53$.

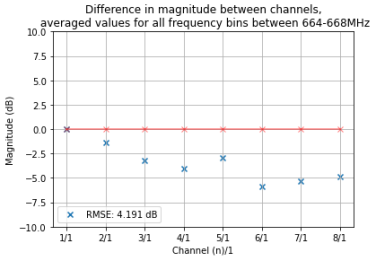

(a) No calibration

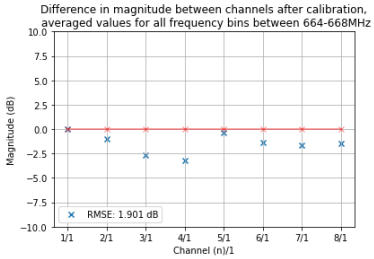

(b) Calibration with w_{cal} from 618 MHz

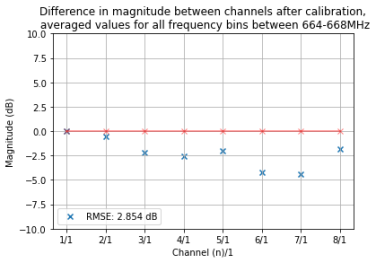

(c) Calibration with w_{cal} from 642 MHz

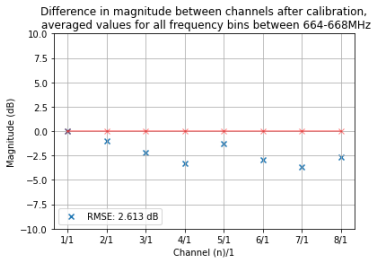

(d) Calibration with w_{cal} from 666 MHz

Figure 126 Experiment 2, Measurement 17: Magnitude difference between each channel and channel 1, compared with theoretical expected values. Frequency f = 666, azimuth α = 73.